AN ANALYSIS OF THE HYDRAULIC CONVEYING OF COARSE PARTICLE SLURRIES

A Thesis Submitted for the Degree

of

DOCTOR OF PHILOSOPHY

in the Faculty of Engineering

of the

University of London

by

SONIA IJADI-MAGHSOODI, B.Sc., M.Sc.

Department of Chemical Engineering and Chemical Technology

Imperial College

London

October 1987

To My Husband, Martin

ABSTRACT

Experiments have been performed to analyse the flow mechanism of coarse particle suspensions. The experiments were carried out with three different sizes of coal; coarse coal of size range 1 - 4mm and d_{50} = 3.25mm, mixed coal of size range 0.5 - 4mm and d_{50} = 1.9mm and fine coal of size range 0.5 - 2mm and d_{50} = 0.975mm. The hydraulic pressure gradient, the in-situ volumetric concentration and the delivered solid concentration were measured in a 26mm horizontal pipeline for mean slurry velocities of 0.2 - 4m/s, The experimental results were analysed using a two-layer model. The model defines two layer flow, i.e. the upper layer is free of particles and a moving bed of solids exists in the lower layer. This model was modified for the case of dense phase flow involving fine particles, by using the mean mixture density instead of clear fluid in the calculation of fluid shear stress at the pipe wall. The hydraulic pressure gradient predicted by this model for different particle sizes, densities and pipe diameter agrees very well with the experimental results.

The two-layer model was further improved to account for suspended particles in the upper layer. With this modification, the velocity at which the first particle starts to suspend, the threshold velocity, and also the velocity that complete suspension is attained could be predicted.

ACKNOWLEDGEMENTS

I would like to express my sincere gratitude to my research supervisor, Dr. M. Streat, for his patient and unfailing support throughout this work.

The willing assistance of Dr. N. Brown is gratefully acknowledged.

My thanks are also due to the members of the academic staff at Imperial College and the staff at the Departmental Workshop, Electronics and Glass Workshop.

I wish to thank the Science Research Council for a grant during the first two years of this work and British Petroleum for their financial support in the final six months. My thanks to the Brewing Research Foundation for their co-operation and understanding during the writing of this work.

I further wish to thank Mrs. Dianne Cole for her care and dedication in the typing of this manuscript.

Finally, I would like to thank my husband for his constant encouragement, patience and moral support, without which this work would not have been possible.

LIST OF CONTENTS

LIST OF FIGURES

LIST OF PLATES

LIST OF TABLES

CHAPTER 1

INTRODUCTION

Hydraulic conveying of solids in a pipeline is now widely used for transportation and handling of particulate material and possesses many advantages over conventional methods of materials handling.

In recent years there has been increasing interest in long distance hydraulic transportation and indeed there are many systems in successful operation (23). Hydraulic conveying is particularly suited to coal transportation, since massive deposits of coal are located in very remote regions where conventional methods of transportation are either impossible or extremely expensive.

All long distance pipelines operating to date pre-crush the solids to fine particles and then transport a coal-water slurry of relatively fine particle size as a homogeneous or heterogeneous suspension using custom designed pumps. The type of pump selected depends to a large extent upon the maximum particle size of the slurry and the pressure head that has to be developed. This slurry is normally of low concentration to prevent excessive wear and attrition to the moving parts.

More recently, the hydraulic transportation of high concentration coarse coal has been investigated (24). Coarse coal can be transported with much less elaborate preparation and offers considerable advantages over a fine coal slurry:

(i) less water would be needed;which is an advantage where water is in short supply

(ii) the higher concentration means that more coal is pumped per unit mass of slurry giving lower specific energy consumption

(iii) the pipeline could be safely shut down

(iv) dewatering can be performed using conventional draining, which is cheaper than mechanical dewatering and thermal drying

(v) the end product would be in the conventional dry size consistency so that it would be more easily transported, e.g. this type of slurry could be fed directly into a ship without dewatering and could be unloaded at the end of the voyage with conventional grab cranes.

High concentration transportation of coal over relatively short distances is particularly suitable for remote coal fields with access to the sea e.g. in Australia and South Africa. Here, dewatering prior to shipment will be easier and less expensive for coarse coal than for fine coal.

Pump attrition, however, is a major consideration for coarse coal pipelines and makes the operating cost less attractive in most cases. However, many of the problems associated with conventional pumps can be overcome by using a pressurized lock hopper feed system. Coal particles are fed to the pipeline at relatively high concentration and high pressure pumps are only used to handle the clear motive fluid. This technique is best suited for short distances, i.e. 1-2km, due to the practical limit of feed hopper volume. Other advantages of a high

concentration slurry are the reduction in the volume of motive fluid required and the lower transport velocity required compared to a low concentration slurry.

This thesis presents a set of experimental results for high concentration coarse coal transport. The experimental strategy adopted here is very similar to that previously presented by Televantos and Brown (40, 6).

A number of operating variables have been examined including the effect of size distribution, mean particle diameter, mean slurry velocity, in-situ and delivered solid concentration. Having obtained a set of reliable data it should be possible to develop a rational physically based model for the flow of such mixtures.

Mathematical analysis has been performed on the experimental data in order to find a rigorous model for predicting the operating velocity and pressure loss in the horizontal conveying of coal-water mixtures.

CHAPTER 2

LITERATURE SURVEY

2.1 Introduction

This chapter is a review of some of the important work published in the field of hydraulic conveying and provides the reader with some more detailed references. Particular attention has been given to the evaluation of the frictional energy losses. These frictional losses result from the forces exerted on individual particles by the fluid, the behaviour of particles and also the wall frictional forces on the particles and fluid. In horizontal flow of solid-liquid mixtures the evaluation of the frictional forces is very complicated, especially when taking into account the effect of turbulent eddies which constantly lift particles into the fluid stream.

There are many correlations available in the literature, though most of them are strictly empirical and based upon assumptions concerning the actual flow behaviour. Very few correlations attempt to develop rational relationships based on the frictional forces.

The purpose of this review is to provide a general background for hydraulic conveying of solid-liquid mixtures in horizontal pipes.

2.2 Flow Patterns

Solids may be transported in a pipeline either as a "non-settling" or as a "settling" mixture, depending upon the magnitude of the solid

terminal falling velocity and the size of the solid particles. Non-settling mixtures usually have a particle size of approximately 50μm or less and the sedimentation rate of a bulk slurry is not excessively fast. These suspensions can be treated as a single phase fluid, frequently behaving as a non-Newtonian fluid and at high concentration generally approaching Bingham plastic behaviour.

"Settling" mixtures usually contain fine particles at low concentration or coarse particles at any concentration and can not be treated as a single phase system except under conditions of high turbulence. As the mixture velocity is decreased from an initially high value the solids settle more and more freely until eventually the pipe blocks.

The flow regimes in this case have generally been classified as illustrated in figure 2.1 and defined as follows:-

(a) fully suspended flow or symmetric suspension.

(b) heterogeneous or asymmetric suspension.

(c) moving bed (often accompanied by saltation and suspension).

(d) stationary bed (often accompanied by saltation and suspension).

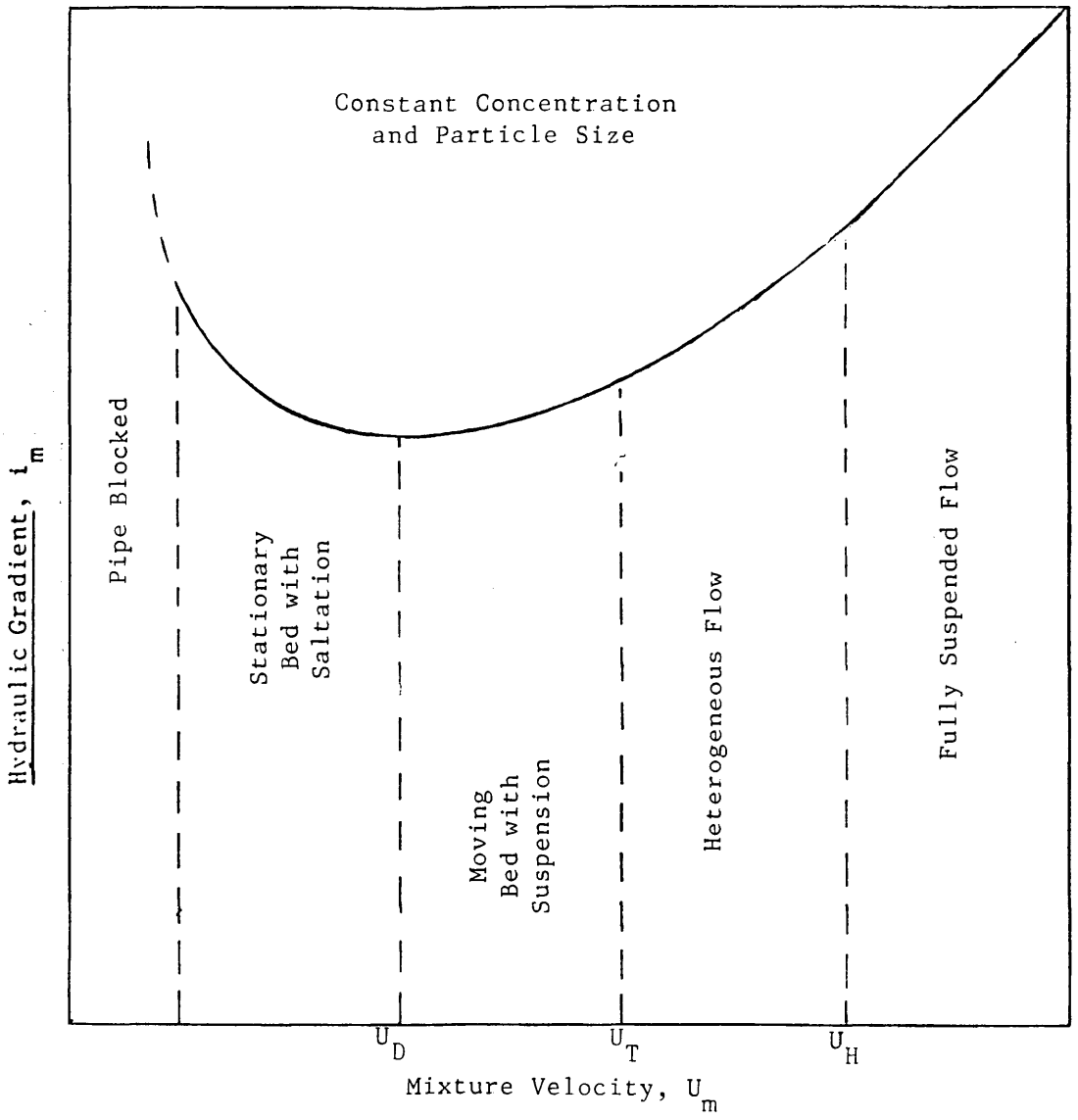

Figure 2.1 Schematic Representation of Pressure Gradient Curve

2.3 Pressure Gradient Prediction

2.3.1 Introduction

Prediction of the pressure gradient for each flow regime depends on many variables: size, shape and density of the particles, viscosity, density and the mean velocity of the fluid, pipe size, and concentration of solids.

Blatch (5) was the first person to represent the total hydraulic gradient (i_m) as a sum of the head loss due to water alone (i_w) and that attributed to the presence of solids (i_s):

$$i_m = i_s + i_w \qquad 2.1$$

and from her experimental results, she also found that:

$$i_s/i_w = k\ C_s \qquad 2.2$$

so that $$i_m = i_w + k\ C_s\ i_w \qquad 2.3$$

where k is a constant.

The contributions of the solid and the liquid to the pressure gradient prediction are not independent. Nevertheless, this simple additive relationship is still in use today for rule-of-thumb head loss calculations of solid-water two phase flow.

2.3.2 Homogeneous Suspension

Homogeneous suspensions can be subdivided into two categories:

(a) suspension of fine particles (less than about 100μm) where the particles are fully suspended and for which the concentration profile is symmetrical and the slurry behaves

as one single phase.

(b) suspension of coarse particles in a slurry of fine particles.

Fine particle suspensions at high solid concentration may exhibit non-Newtonian behaviour and such slurries must be tested in a viscometer by measuring shear stress (τ) as a function of shear rate (du/dr). If non-Newtonian behaviour is found then the pressure gradient of the suspension can be calculated by methods suitable for these slurries (21).

For the Newtonian case with the assumption of pseudohomogeneity, the pressure gradient can be calculated using the concept of dimensionless excess hydraulic gradient or alternatively by a more rigorous mechanistic approach.

Newitt et al (35) derived a dimensionless equation by assuming that the friction factor, f_m, for suspension is equal to the friction factor, f_f, of the homogeneous Newtonian fluid.

$$i_m = i_w \ \rho_m/\rho_L \qquad 2.4$$

where $$\rho_m = C_s \rho_s + (1-C_s) \rho_L \qquad 2.5$$

substituting ρ_m in equation 2.4 and writing $S = \rho_s/\rho_L$

$$\frac{i_m - i_w}{C_s \, i_w} = (S-1) \qquad 2.6$$

In practice it is found that equation 2.6 gives a good general approximation but some significant deviations are observed.

Newitt et al (35) correlated a considerable amount of data obtained in a 1 in pipe as follows:

$$(i_m - i_w) \; / \; C_s \; i_w = k(S-1) \qquad 2.7$$

where k = 0.6

The reduction in the value of k from unity is apparently due to some turbulent suspension of the solids and the value may change from 0.6 to 1 depending on the nature of the solids. It was, however, found by Newitt that equation 2.7 gave a good prediction of the pressure gradient in the symmetrical concentration profile region.

Julian and Dukler (21) have developed an analysis for a dilute solids gas suspension by assuming a symmetric concentration profile and have suggested that the analysis should also be suitable for solid-liquid systems.

Shook and Daniel (38) developed a mechanistic approach by assuming non uniform distribution of the solids and treating the mixture as an equivalent fluid of variable density and viscosity. They derived a set

of equations for the prediction of the friction factor of the mixture. However, the authors proposed an approximate procedure for prediction of the pressure gradient.

2.3.3 Heterogeneous Suspension Flow

The heterogeneous suspension flow regime is the most important mode of transport of granular materials by pipeline, because the maximum amount of solids is transported per unit energy input.

Durand and Condolios (10) are the pioneers of this study and their empirical formula with various refinements is still in use for design and scale-up. Durand and his many co-workers obtained extensive data on water slurries of a variety of sands and gravels in horizontal pipes up to 560mm in diameter with solids up to 25mm in size and up to delivered concentrations of 22%. They also assumed that the relative increase in head loss above that of the carrier fluid alone is proportional to the volumetric solids concentration C_s, i.e.

$$\frac{i_m - i_w}{i_w} = \Phi C_s \qquad 2.8$$

They also proposed that the relative excess hydraulic gradient was independent of particle size when the solids were sufficiently large. This led to the inclusion of the particle drag coefficient C_D, with other independent variables into the term:

$$\Psi = \frac{U_m^2 C_D^{\frac{1}{2}}}{g D (S-1)} \qquad 2.9$$

Using the parameters Φ and Ψ they found that their experimental results could be correlated by the expression:

$$\Phi = K \Psi^n \qquad 2.10$$

where K = 150 and n = -1.5

Many investigators have proposed alternative values for K and n (3, 26, 51).

Newitt et al (30) derived a correlation based on their own data obtained in a 25mm pipe using various particle sizes of perspex, fine coal and sands at volume fractions of up to 37%. They subdivided the heterogeneous flow regime into "suspension" flow and "flow with a moving bed".

For suspension flow:

$$\frac{i_m - i_w}{C_s \, i_w} = 1100 \left(\frac{g D U_t}{U_m^3} \right) (S-1) \qquad 2.11$$

and for flow with a moving bed:

$$\frac{i_m - i_w}{C_s\, i_w} = 66 \left(\frac{g\, D}{U_m^2} \right) (S-1) \qquad 2.12$$

Rose and Duckworth (36) have developed the most systematically based general correlation for the prediction of the pressure gradient. Their correlation is applicable to vertical, inclined and horizontal flow of gas-solid and liquid-solids mixtures. Their correlation is based on the mechanical energy equation, and is confirmed for a variety of different materials in a range of pipe sizes, but the correlation deals with only suspensions and is not suitable when a moving bed of solids exists.

Gaessler (18) conducted a detailed analysis of solid liquid mixtures in horizontal pipes of 46mm, 125mm, 160mm diameter and 0-10mm coal particles. He derived a correlation based on the frictional forces between the solids, pipe wall and the carrier fluid. This correlation is not widely used due to the complexity of calculation of the variables involved even though it is suitable for all the flow regimes.

2.3.4 Moving and Stationary Bed Flow

As the mixture velocity decreases some or all of the solids deposit on the bottom of the pipe and gradually move as a sliding bed with some suspension and saltation.

Wicks (21) has made a semi-empirical analysis of some aspects of solids-liquid flow where a bed of solids is present. His analysis is

based upon the rolling and lifting mechanism of particles on the bed surface. He described the forces acting on a particle at the moment of lifting and using the fluid properties and particle geometry he developed a graphical correlation. Although this method is not extensively tested it provides a useful approach.

There are many other empirical correlations for prediction of pressure gradient in the moving bed flow region but the majority are of the form suggested by Newitt et al (30)

$$\frac{i_m - i_w}{C_s i_w} = K\,(S-1) \qquad 2.13$$

where K varies from 0.6 to 1.

Shook and Daniel (37) have derived a relationship for a stationary bed with saltation and suspension flow patterns in a rectangular duct. They used the Bagnold expression for dispersive force acting at the surface of the bed and the appropriate force balances and developed an equation very similar to that of Newitt et al

$$\frac{i_m - \left(\frac{2f\,U_m^2}{g\,D}\right)}{C_s} = 0.8\,(S-1) \qquad 2.14$$

Though they did not recommend their equation for pipeline design purposes it does lend support to the form of the Newitt equation. The

value of K in equation 2.13 is not constant but depends on the value of solids concentration in the moving bed, volumetric solidsconcentration, C_s, and angle of internal friction.

Graf and Acaroglu (21) studied hydraulic transport of solids in the presence of a settled bed in channels and pipes and they developed a dimensionless correlation useful for crude estimation of pressure gradient.

Numerous models have been presented to predict the behaviour of hydraulic transport of slurries but these often involve much mathematical manipulation and the outcome of this work is often difficult to apply to realistic problems.

The method suggested by Wilson (44) to describe the behaviour of settling slurries is considered to be very important and useful due to the physical mechanistic approach. His analysis was originally developed for contact load transport, but subsequent development of the model allows for the inclusion of turbulently suspended solids. This model is explained in detail in Chapter 5 .

2.4 Prediction of Slurry Velocity

The prediction of slurry velocity for different flow regimes is another important parameter in slurry pipeline design.

Several investigators have observed the slurry velocities corresponding to the transition from one flow pattern to another and correlated their observation with empirical equations. However, none of the available theories explain the mechanism of particle suspension.

In principle, turbulent suspension of a sediment is an advanced stage of saltation and moving bed flow and it should be possible to describe both by one theory or model.

The mechanism of suspension of particles denser than the carrier fluid is still inadequately explained. In simple terms the turbulent fluid should be capable of supporting a solid in suspension when the vertical eddy velocity component, V, exceeds the fall velocity, U_t, of the solids though this concept is affected by other parameters, such as the solid concentration, diameter of pipe, fluid rheology, solid density and particle size.

Pipelines are designed to operate with some safety margin above the anticipated deposition velocity, U_D i.e. the velocity below which the particles start to deposit at the bottom of a bed as the stationary bed flow regime is approached. No deposition velocity correlation has been proposed to date which is applicable to a full range of particle sizes. For coarse material the formula proposed by Durand (21) is widely used.

$$U_D = F_L \sqrt{2gD\,(S-1)} \qquad 2.15$$

Here F_L is expressed graphically as a function of solid concentration and particle diameter using data which was limited to solid concentrations up to 15% by volume and particle diameters from 100μm to 4mm. F_L increases with solid concentration for particle diameters below 1.5mm but is independent of the concentration above this value of particle diameter. Charles et al (33) analysed about 50 sets of deposit velocity data for coal, tailings, small to coarse sand and gravel with particle diameter ranging from 60μm to 19mm and delivered solid concentration ranging from 0.008% to 69% by volume. Overall they showed that the value of F_L, therefore U_D gradually decreases with increasing

solid concentration in the range 10% to 15% by volume of solids.

The transition velocity between moving bed and heterogeneous suspension is referred to as the threshold velocity i.e. the velocity at which the first particle starts to suspend in the moving bed flow regime.

Spells (39) used an empirical approach based on dimensional analysis and presented correlation for low concentration mixtures of 80-800 μm particles of the form :

$$U_T = 54.4\ C_D^{0.815}\ D^{0.65}\ U_t^{1.63} \qquad 2.16$$

Wilson (49) attempted to predict the threshold velocity, U_T, using mixing length theory of turbulence. He obtained an equation for U_T and determined the constants involved using available experimental data:

$$U_T = 200\ \frac{U_{to}\ d}{\sqrt{f'}\ D} \qquad 2.17$$

where f' is a reduced friction factor. To account for the effect of particle size, Wilson (45) modified his equation using statistical theory of turbulence. The model showed that the threshold velocity for turbulent suspension is a simple exponential function of the ratio of particle diameter to pipe diameter. He analysed experimental results from four different laboratories to determine the constant of the equation.

$$U_T = \frac{0.6U_t}{\sqrt{f'/2}} \exp(45d/D) \qquad 2.18$$

Unfortunately he only really considered the value of d/D from 0.01 to 0.03 which is not wide enough for general use.

The transition velocity between heterogeneous and homogeneous suspension is referred to as U_H. Newitt et al (21) obtained a semi-theoretical relationship for the prediction of this velocity.

$$U_H = 17\ U_t \qquad 2.19$$

Zandi and Govatos (51), define a dimensionless parameter for various flow regimes.

$$N_I = \frac{U_m^2 \sqrt{C_D}}{C_s\ Dg\ (S-1)} \qquad 2.20$$

$N_I = 40$ is said to relate to the transition from flow with moving bed to heterogeneous suspension. Chhabra and Richardson (7, 8) have transported gravel of size 3.5, 5.7, and 8.1mm in a 42mm pipe and have confirmed the validity of the above criteria with their experimental results.

Many correlations exist to predict the transition velocity between

the heterogeneous and homogeneous suspension flow. Govier and Charles (20) using Durand and Newitt's equations show that:

Durand equation ;

$$U_H = 11.9(U_t D)^{0.5}\, d^{-0.25} \qquad 2.21$$

Newitt equation ;

$$U_H = 8.7(U_t D)^{0.33} \qquad 2.22$$

but they only claim an order of magnitude accuracy.

In homogeneous suspension the particles are fully supported by fluid turbulence when the hold up ration, H_R, reaches unity. H_R is the ratio of the average true liquid velocity, U_L, to the average true solids velocity U_s. Govier and Charles (20) schematically show in Figure 2.2 the four principal flow regimes are related to the variation of hold up ratio with mixture velocity. Generally an increase in slurry concentration will result in a decrease in the settling tendency of a particle and this would be expected to result in a decrease in the transition velocity. Conversely, increasing the particle size will increase the mixture velocity at which the transition occurs due to increase in the settling tendency of the particle. Therefore slurry concentration and particle size have an overall effect on the fluid turbulence and thus the transition velocity.

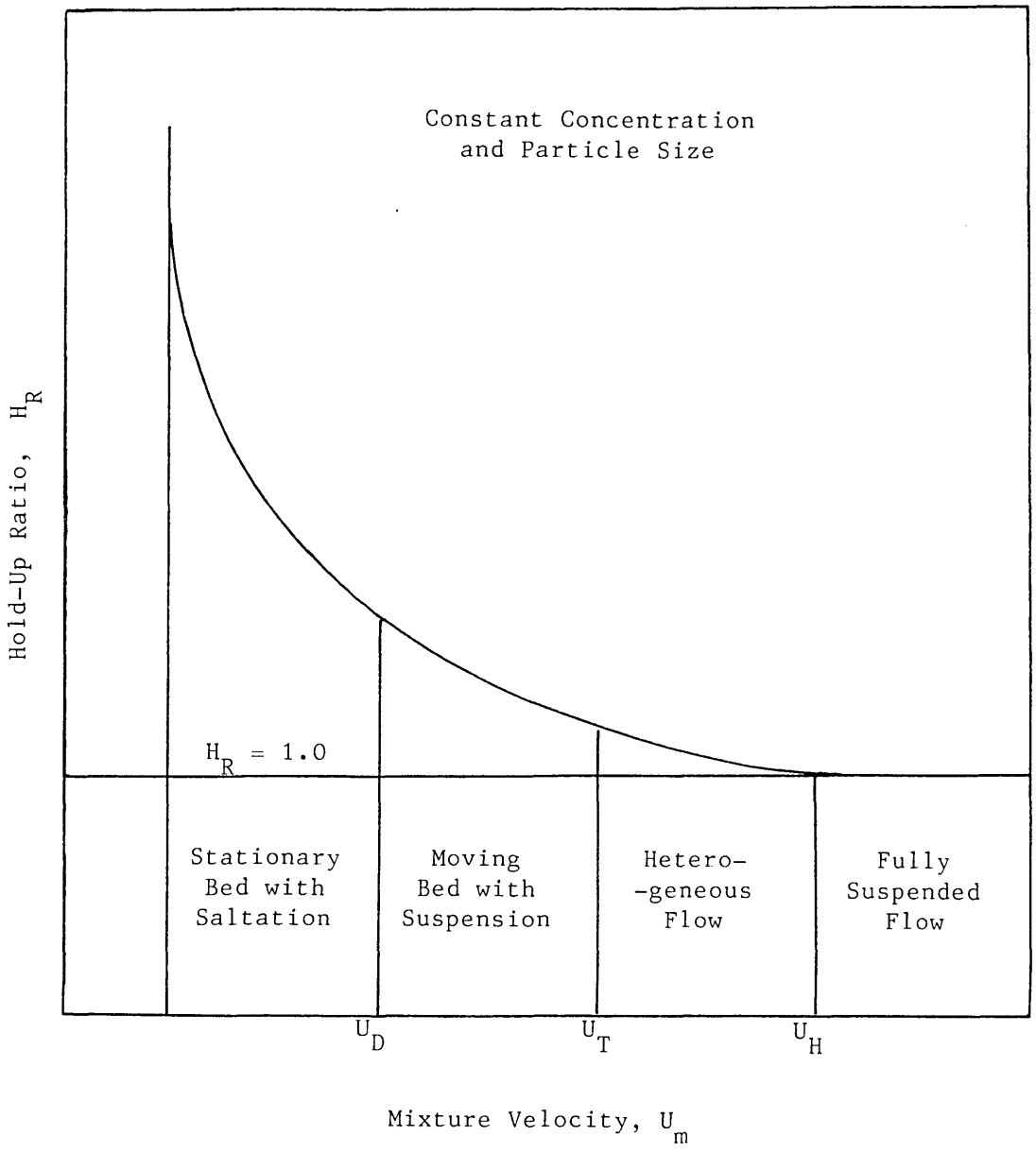

Figure 2.2 Schematic Representation of Variation of Hold-Up Ratio with Mixture Velocity

CHAPTER 3

PRELIMINARY COAL SLURRY WORK

3.1 Introduction

The hydraulic behaviour of coal particles in water was investigated in this work. During the hydraulic transportation of coal, some degradation inevitably occurs. The fine material produced increases the cost of dewatering and also affects the rheological properties of the slurry and this may affect the design of the pipeline.

The tendency of coal to fracture during handling is termed friability. This depends on the toughness, elasticity, physical characteristics and strength of the coal. The physical structure of coal is characterised by pores and fissures of varying sizes which influence physical and mechanical properties. Particle size distribution, density and degradation of coal particles should always be analysed and tested before transportation.

3.2 Degradation Test Method

The degree of friability and degradation of each coal sample was tested before transportation so that appropriate handling procedures could be developed.

Four samples of coal were supplied by British Petroleum (B.P.) for the hydraulic investigations. All samples were tested for degradation due to the contact load. These were: Bagworth, Littleton, Herrington Coking Coal and Australian Trading Steam Coal. The specifications supplied by B.P. are given in Tables 3.1 to 3.4.

For research purposes, particularly for the reproducibility of

experimental runs, the most suitable coal for the present work would possess a low Hardgrove grindability index (HGI) and a low degree of degradation due to attrition. For this purpose the following methods were applied.

A sample of coal was washed, wet sieved and air dried according to B.S.1017 Part 1 and any particles below 1mm in size were disregarded. A mixture of 50% by weight coal-water was then prepared. This mixture was placed in a milling container without a milling rod and agitated on a rotary mill for periods of one day to one week depending on the type of coal. The water was subsequently drained and the coal was air dried, weighed and sieved. The size degradation as well as total weight was measured.

The Herrington Coking Coal was extremely soft and was immediately disregarded.

The Australian (HGI = 54) and Littleton (HGI = 53) coals were degraded by about 55% and 20% below 1mm in size respectively after one day of milling. On the other hand Bagworth (HGI = 56) coal was agitated for one week and only 0.56% total weight was degraded below 1mm in particle size and the size distribution was not significantly affected. These results are shown on Figures 3.1-3.3 and Tables 3.5-3.7.

The degradation test showed that Bagworth coal, with a higher value of HGI, is the most suitable coal for the present study since it can be used in the pipeline repeatedly with very little particle size reduction.

3.3 Particle Size Distribution Analysis

Samples for particle size distribution were periodically obtained and analysed before and after experimental runs.

Samples were analysed by screening on Tyler sieves. The entire

batch of Bagworth coal was sieved prior to the experimental runs and all the particles greater than 4.00mm were discarded since over size particles blocked the slurry pipeline.

The following procedure was adopted:

1. The samples were air-dried according to B.S.1017 Part 1 and weighed.

2. The samples were re-slurried with tap water and passed through a wet sieving process. Any particles below 480μm were removed by washing.

3. Washed samples between the sieveswere again air-dried and weighed. The weight percent of the coal passing through each sieve was calculated and plotted against the sieve size or particle diameter. These are given for Bagworth coal during three sets of experimental runs in Figures 6.5-6.7 and Tables 6.5-6.7.

This procedure gives a reproducibility of better than ±1% for all the individual size fractions and was adopted after it became evident that dry screening of the complete sample underestimated the presence of fine particles due to their adherence to the larger particles. Throughout the computations d_{50} diameter has been used as representative of the sample size.

3.4 Density and Moisture Content Measurement Techniques

One of the important parameters in slurry transport is the density of the particles.

Coal particles contain pores and fissures and therefore they have a tendency to absorb air. Special procedures were used to measure the density of this material.

1. A sample of coal was ground to small size and wet sieved and particles between 1.00mm and 480μm were collected to give a narrow size distribution of coal.

2. A 50ml volumetric flask was weighed at 20°C.

3. This flask was filled with water and weighed at 20°C, giving the weight, volume and density of the water. This was repeated several times and an average was taken.

4. 20g of the above-mentioned coal sample was oven dried according to B.S.1016 Part 1, then placed in a flask and immediately weighed. Warm water was poured over and vacuum was applied until all air bubbles were removed. The removal of air bubbles is essential since the existence of contained air on the coal surface seriously affects the coal density measurement.

5. When all the trapped air was removed the flask plus deaerated water and coal particles were weighed at 20°C.

6. Coal density can be calculated from:

$$\text{Coal density} = \frac{(\text{Weight of Dry Coal + Flask}) - \text{Weight of Flask}}{\text{Volume of Flask} - (\text{Weight of Water} \times \text{Density of Water})}$$

This procedure was carried for several samples and the mean density of Bagworth coal was found to be $1325 \pm 20 kg/m^3$, i.e. very near to the value of $1350 kg/m^3$ as given in Table 3.1.

Surface moisture content and total moisture content were also measured for Bagworth coal. The former was measured using an air-drying procedure (given in B.S.1017 Part 1) at a temperature of 25^{o}-30^{o}C with free circulation of air above the sample for a period of 24 hours. Alternatively, the latter could be measured by two methods, (see B.S.1016 Part 1), i.e. drying at 105-110^{o}C in the oven or distillation with toluene. The former method is performed by heating the coal sample in the oven at 110^{o}C for a period of 5 hours and immediately weighing the hot sample to avoid absorption of moisture during cooling. Several samples were tested and the results of surface moisture content and total moisture content were 7% and 12% $\pm$1% respectively.

Table 3.1

COAL QUALITY DATA

Identification			Analytical Data	Air Dry WT%
Mine/Terminal	:	Bagworth	Moisture	: 10.1
District	:	South Midlands	Ash	: 7.1
Country	:	United Kingdom	Volatile Matter	: 34.8
			Fixed Carbon	: 48.0

Physical Properties			Maceral Analysis	
Relative Density	:	1.35	Vitrinite	: 64%
Hardgrove Gindability	:	56	Exinite	: 3%
Free Swelling Index	:	0.5	Inertinite	: 16%
			Mineral Matters	: 16%

Table 3.2

COAL QUALITY DATA

Identification			Analytical Data	Air Dry WT%
Mine/Terminal	:	Littleton	Moisture	: 2.0
District	:	Western	Ash	: 5.0
Country	:	United Kingdom	Volatile Matter	: 40.3
			Fixed Carbon	: 52.7

Physical Properties			Maceral Analysis	
Relative Density	:	1.4	Vitrinite	: n/s
Hardgrove Gindability	:	53	Exinite	: -
Free Swelling Index	:	0.5	Inertinite	: -
			Mineral Matters	: -

Table 3.3

COAL QUALITY DATA

Identification			Analytical Data	Air Dry WT%
Mine/Terminal	:	Herrington	Moisture	: 1.7
District	:	North East	Ash	: 9.0
Country	:	United Kingdom	Volatile Matter	: 27.2
			Fixed Carbon	: 62.1

Physical Properties			Maceral Analysis	
Relative Density	:	1.37	Vitrinite	: n/s
Hardgrove Gindability	:	74	Exinite	: -
Free Swelling Index	:	5.0	Inertinite	: -
			Mineral Matters	: -

Table 3.4

COAL QUALITY DATA

Identification			Analytical Data	Air Dry WT%
Mine/Terminal	:	Amsterdam	Moisture	: 8.1
District	:	Not Known	Ash	: 10.3
Country	:	Australia	Volatile Matter	: 30.1
			Fixed Carbon	: 51.5

Physical Properties			Maceral Analysis	
Relative Density	:	1.40	Vitrinite	: n/s
Hardgrove Gindability	:	54	Exinite	: -
Free Swelling Index	:	1.5	Inertinite	: -
			Mineral Matters	: -

Figure 3.1 Sieve Analysis of Bagworth Coal

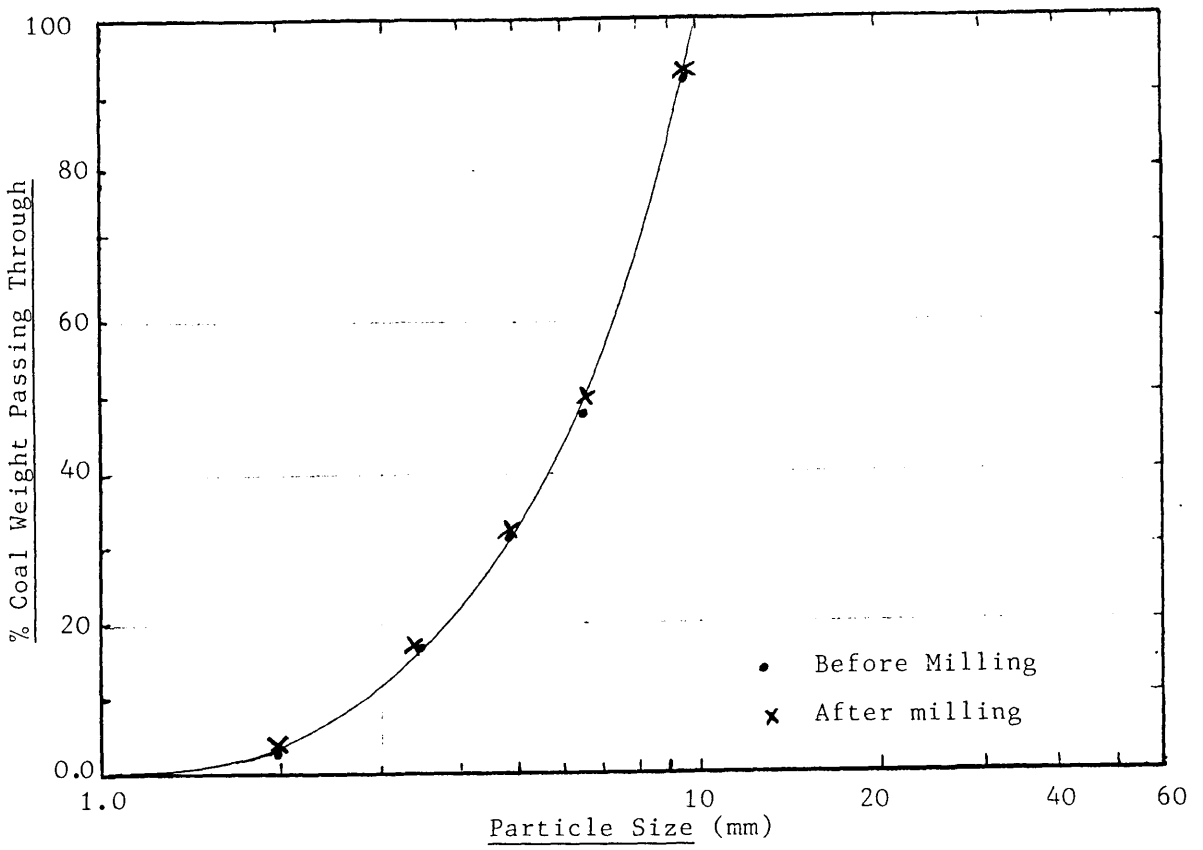

Aperture Size mm	% Coal Passing Through	
	Before Milling	After Milling
9.52	92	92.6
6.35	47	50.5
4.75	33	34.2
3.35	17	17.2
2.0	3	3.7
1.59	-	0.56
Total Weight (kg)	1426	1418

Table 3.5 Size Distribution of Bagworth Coal After One Week of Milling

Figure 3.2 Sieve Analysis of Littleton Coal

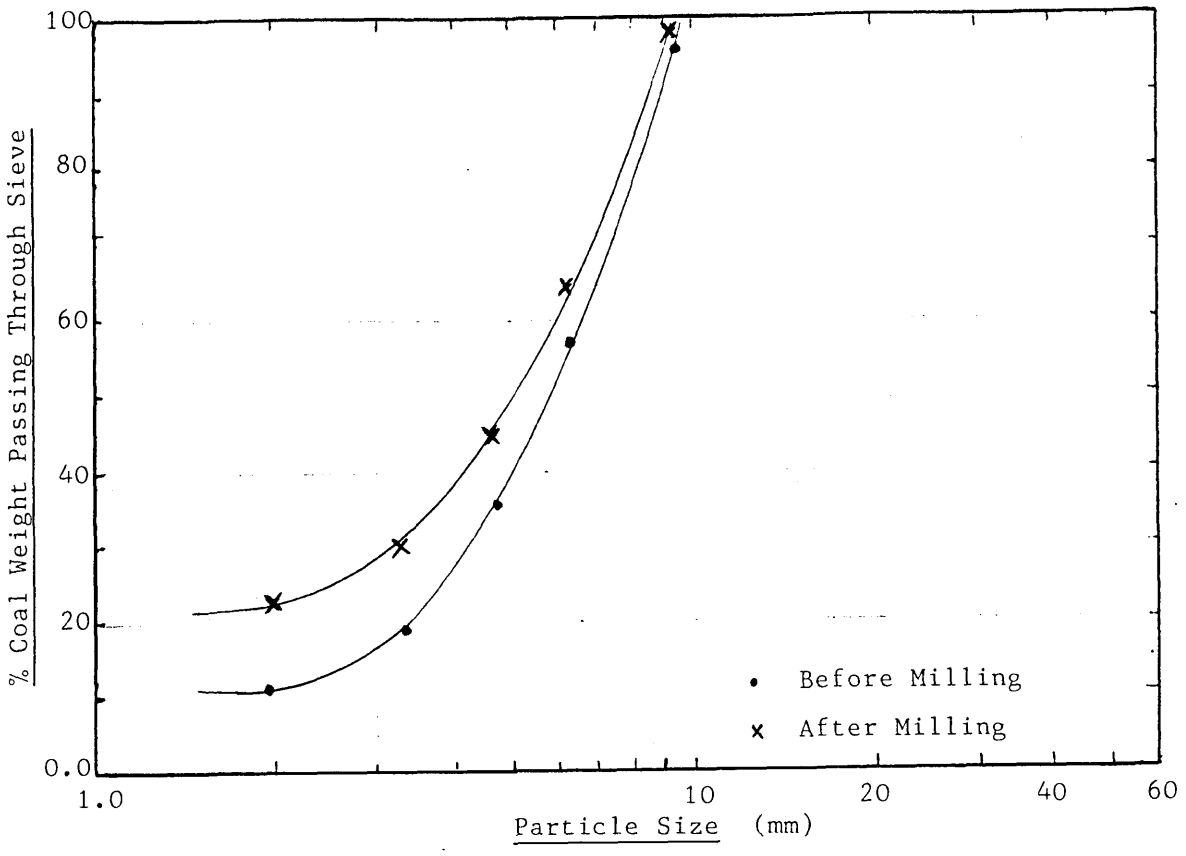

Aperture Size mm	% Coal Passing Through	
	Before Milling	After Milling
9.52	95.63	97
6.35	56.23	62.80
4.75	35.08	43.49
3.35	18.02	29.45
2.0	11.22	22.88
1.59	-	20.05
Total Weight (kg)	1766	1412

Table 3.6 Size Distribution of Littleton Coal After One Day of Milling

Figure 3.3 Sieve Analysis for Australian Trading Coal

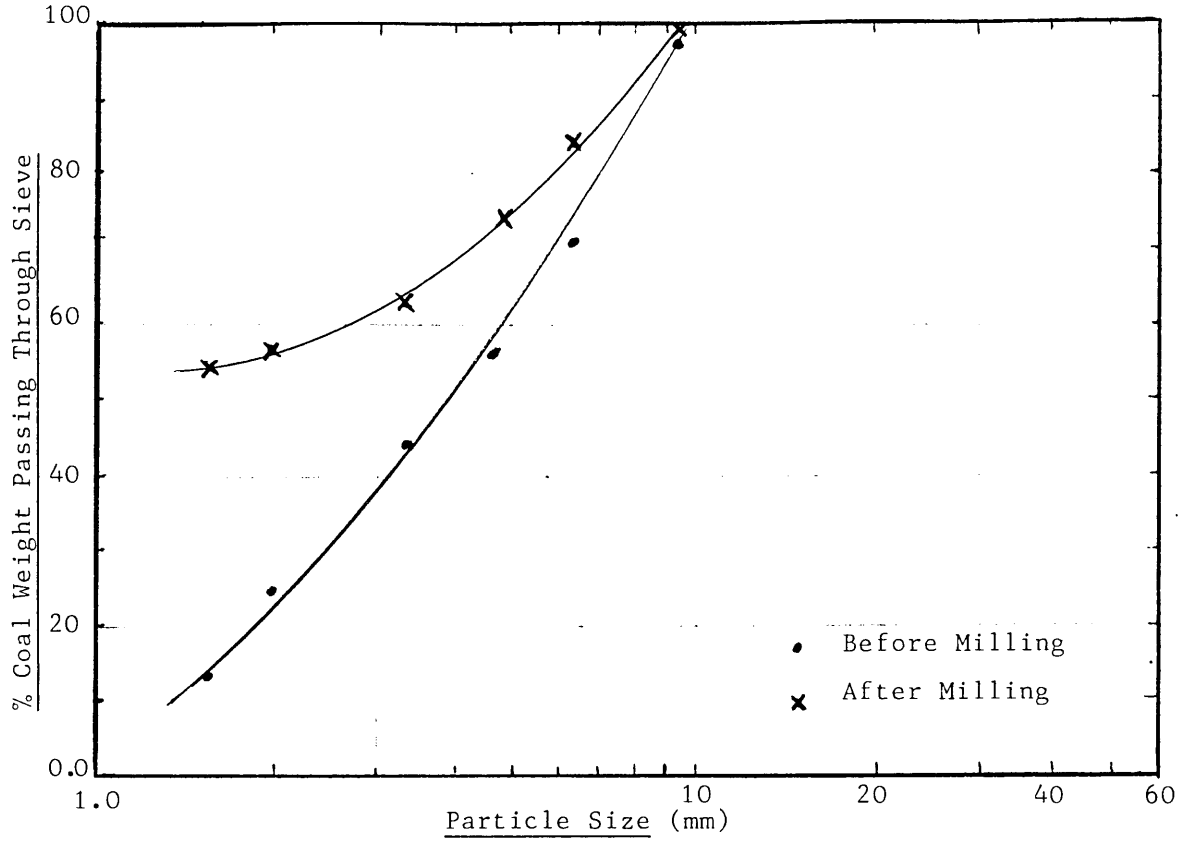

Aperture Size mm	% Coal Passing Through	
	Before Milling	After Milling
9.52	98	98.58
6.35	71.4	83.94
4.75	56.8	73.36
3.35	44	62.66
2.00	25.1	57.09
1.59	14.6	54.67
Total Weight (kg)	3177	1440

Table 3.7 Size Distribution of Australian Coal After One Day of Milling

CHAPTER 4

EXPERIMENTAL MEASUREMENTS AND PROCEDURE

4.1 Description of the Pilot Plant

The investigation of the hydraulic behaviour of coal particles of mean diameter 0.975mm, 1.9mm and 3.25mm has been carried out in a 26.15mm diameter mild steel pipeline incorporated into a pilot plant facility. This involved the measurement of the mean slurry velocity, U_m, in-situ volumetric solids concentration, C_s, delivered solids concentration, C_d, and hydraulic pressure gradient, i_m.

An overall view of the equipment is shown in Plate 4.1 and a flow diagram of the facility is presented in Figure 4.1. Figure 4.2 shows the detailed drawing of the transport line. The hydraulic transport pilot-plant was originally designed by Bantin and details of the major components are given elsewhere by Televantos (40).

The flow rig comprises 30m of pipeline, two pumps, two lock hopper pressure vessels and measuring devices. Coal particles were loaded to the receiving hopper and once loaded all the materials handling was performed hydraulically. The advantage of a lock hopper discharge system is that no special slurry pump is needed and degradation of solid particles is greatly reduced. Two pressure vessels were available each capable of withstanding a maximum pressure of 28 bar and their rather large size was needed in order to provide a reasonable run duration at velocities up to 4m/s. Both lock hoppers are of similar dimensions and each have a volume of $0.6m^3$, however their base cone angle is different so that the effect of hopper exit geometry could be studied. The feed hopper has an internal cone angle of 60^o and the receiving hopper has an

internal cone angle of 90^{o}.

Two Worthington Simpson vortex pumps were used; they were arranged in parallel to generate a pressure of 12 bar and give a maximum slurry velocity of just over 3.5m/s.

The clear water flow rate was controlled by using a valve situated in a by-pass line. The feed water was pumped from a 50 gallon plastic tank fitted with mechanically actuated level control.

The solids transport line has a total length of about 21m and consisted of standard one inch (25.4mm) nominal bore galvanised steel pipe section, with flange fittings. The pipework was designed to withstand a static pressure of 20 bar, which is well above the delivery pressure of the pumps. Standard 90^{o} radius bends were used throughout. The pipe roughness was measured by experiment using clear water and it was concluded that the pipe is essentially smooth. After the final pressure tapping a visible flow section of 700mm length was installed into the horizonal line (installation details are given by Brown (6)). This was not useful for coal slurry transportation.

4.2 Measurement Devices

In order to investigate the hydraulic transport behaviour of coal slurry, the mean slurry velocity, pressure gradient, in-situ solids concentration and delivered solids concentration were measured using the following devices.

4.2.1 Turbine Meter

4.2.1.1 Introduction

The turbine flow meter was supplied by Electonic Flow-Meters Limited (type B/S/15) with flow range of 0.2-3m/s for one-inch diameter pipeline.

Plate 4.1 Apparatus

Figure 4.1 Flow Diagram of The Hydraulic Pilot Plant

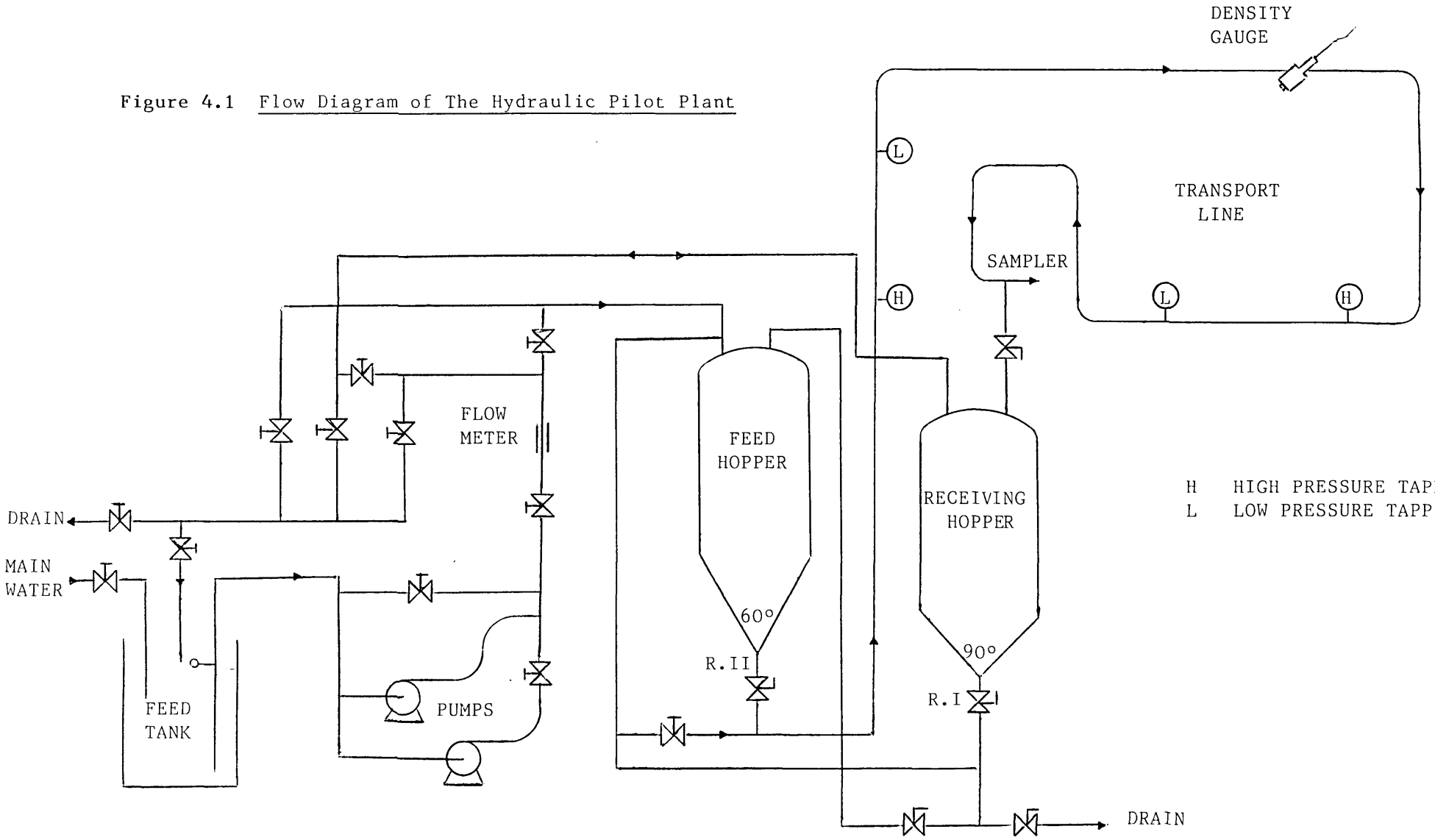

H HIGH PRESSURE TAPPING PLATE
L LOW PRESSURE TAPPING PLATE

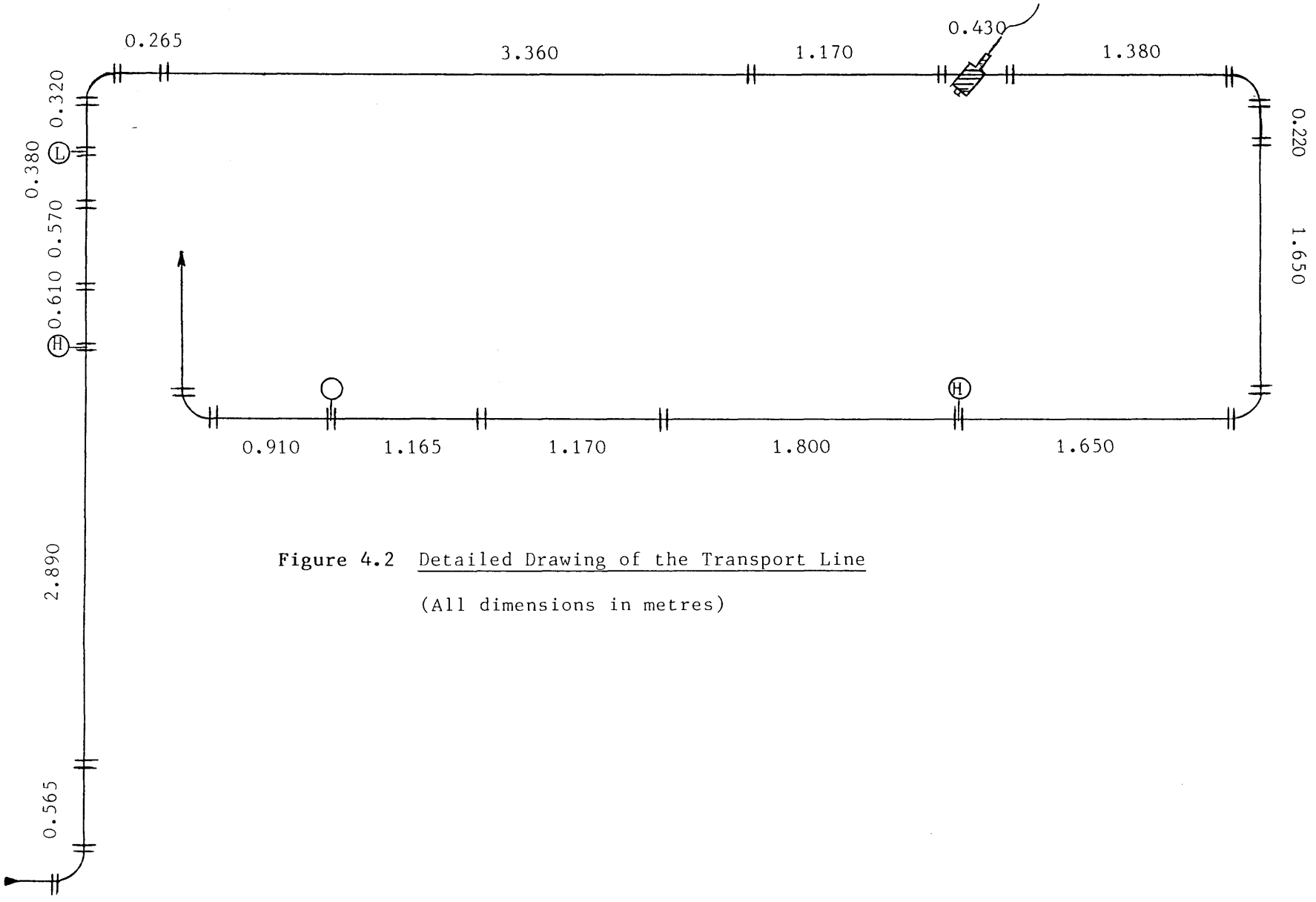

Figure 4.2 Detailed Drawing of the Transport Line

(All dimensions in metres)

This flow meter consists of an impeller and magnetic pick up; output pulses were amplified and counted, the count being proportional to the flow rate. The internal diameter of the flow meter is 1/2-inch therefore flow straightening sections were required to ensure that maximum accuracy could be achieved.

4.2.1.2 Calibration Procedure

Calibration of the flow meter was performed by pumping water through the flow meter and along the pipeline, the sliding plate before the receiving hopper was used to divert the water into the weighing tank. Pulses for each flow rate were counted using the BBC computer.

4.2.1.3 Result

The pulse rate was measured using BBC software. The averaged value of pulse rate was found to be directly proportional to the water flow rate and in excellent agreement with the calibration supplied by the manufacturer. The value of the calibration constant is given in Appendix A.

4.2.2 Differential Pressure Transducers

4.2.2.1 Introduction

Differential strain gauge transducers were used to obtain the pressure gradient along the horizontal pipe. These pressure transducers were of the type UP3 strain gauge with CP2 diaphragm isolators mounted under vacuum on the high pressure side and manufactured by Pidon Controls Limited. The specification of transducer range is critical for highest accuracy. The original transducers, having a range of $\pm$20psia, were

replaced with a new one of ±5psia. The original high range was unsuitable for the present study since pressure drop in coal slurry transport is much less than for sand slurries.

The position and method of back flushing of the transducers was also changed. The original position was far from the tapping point. To minimise inline pressure drop the transducers were moved much nearer to the tapping point. Also, due to the presence of the fine coal particles in the coal slurry, a modified backflushing method was used to prevent fine particles entering the transmission line.

The tapping points were located well downstream of any bends (greater than 50 pipe diameters) and in the region of linear pressure drop. A qualitative experimental investigation was undertaken to verify this. The horizontal tapping points were 4.253m apart and the vertical tapping points were 1.682m apart. Specially designed mild steel tapping plates with a perspex disc containing radial slots which acted as a membrane to prevent coal particles passing into the transmission lines were used to transmit the pressure signal. The tapping plate was incorporated into the pipe work between the two flanges. It is essential to align the flanges and tapping plate as accurately as possible to reduce local internal losses and to maintain liquid continuity. The pressure tappingswere originally designed by Bantin (4) and modified later; details of the modified system used in the present study are given by Brown (6).

The tapping points were connected to the transducers by water filled lines. The connection system is shown on Plate 4.2 and also drawn on Figure 4.3. The transmission water line and the tapping point could be backflushed with water from the feed tank located 2m above the system. After each run a centrifugal pump was used to backflush trapped air and

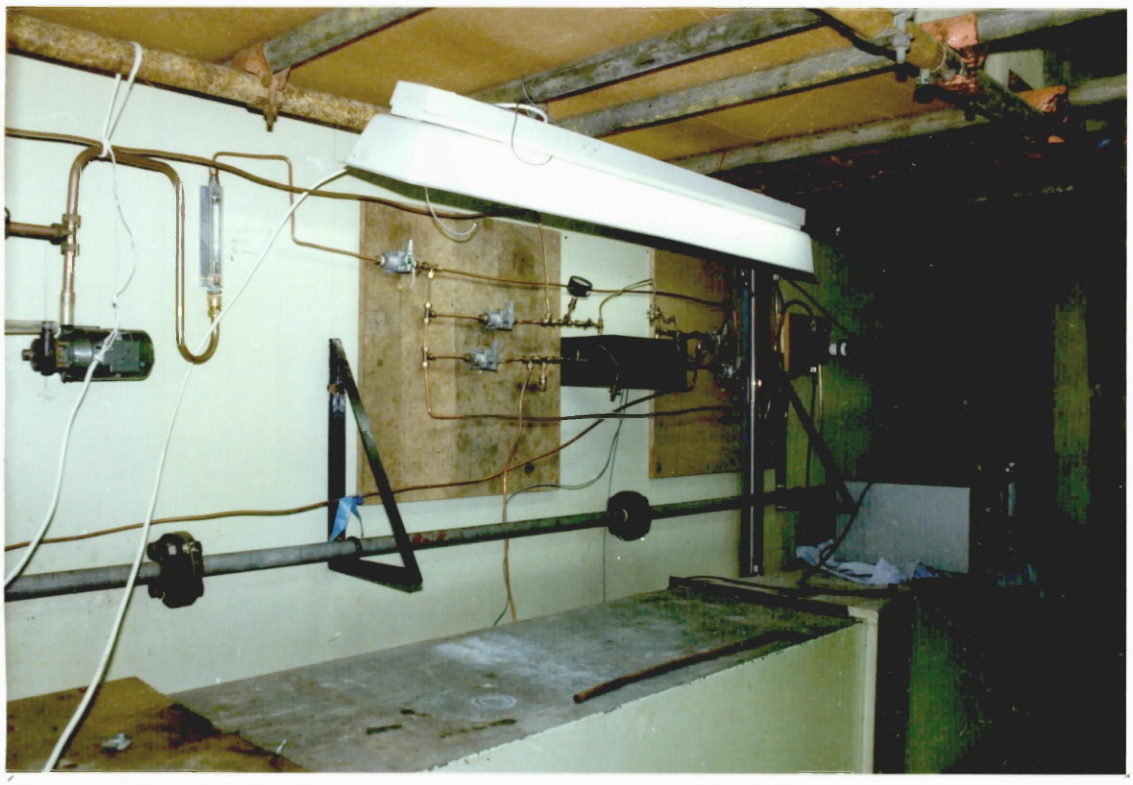

Plate 4.2 Pressure Tapping System

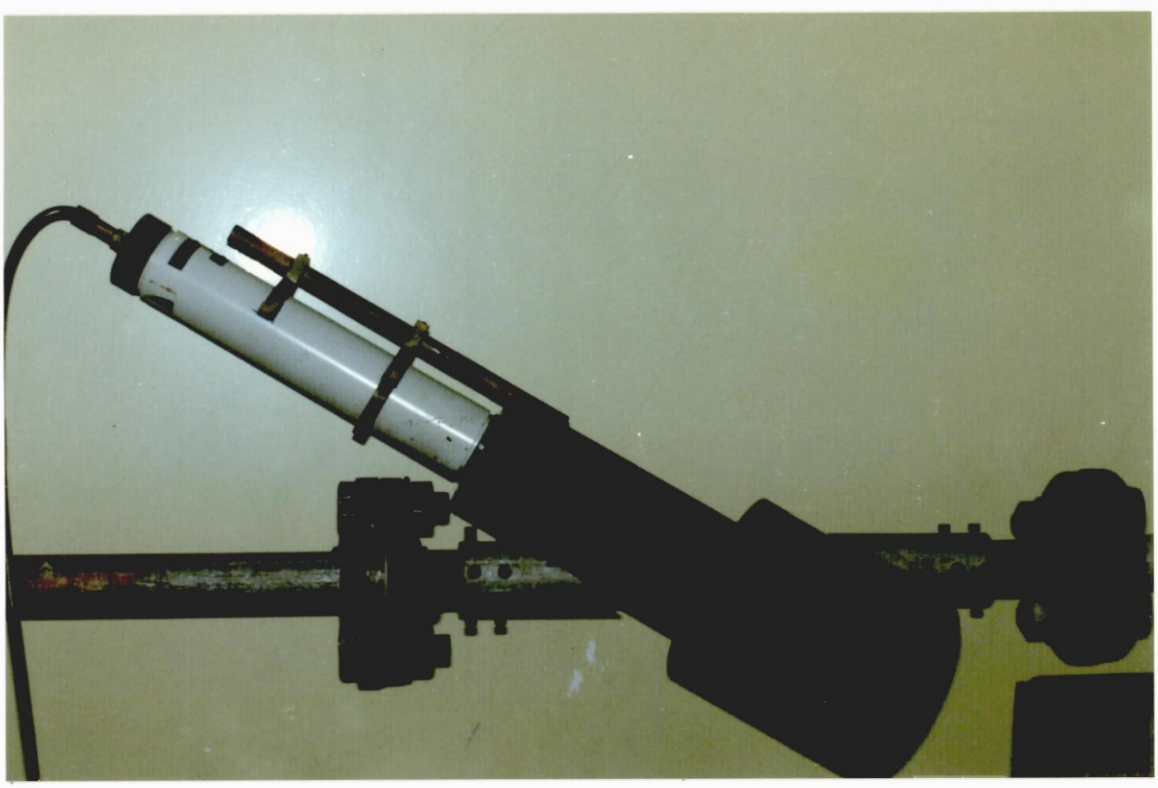

Plate 4.3 Density Gauge System

Figure 4.3 Diagram of Differential Pressure Transducers System

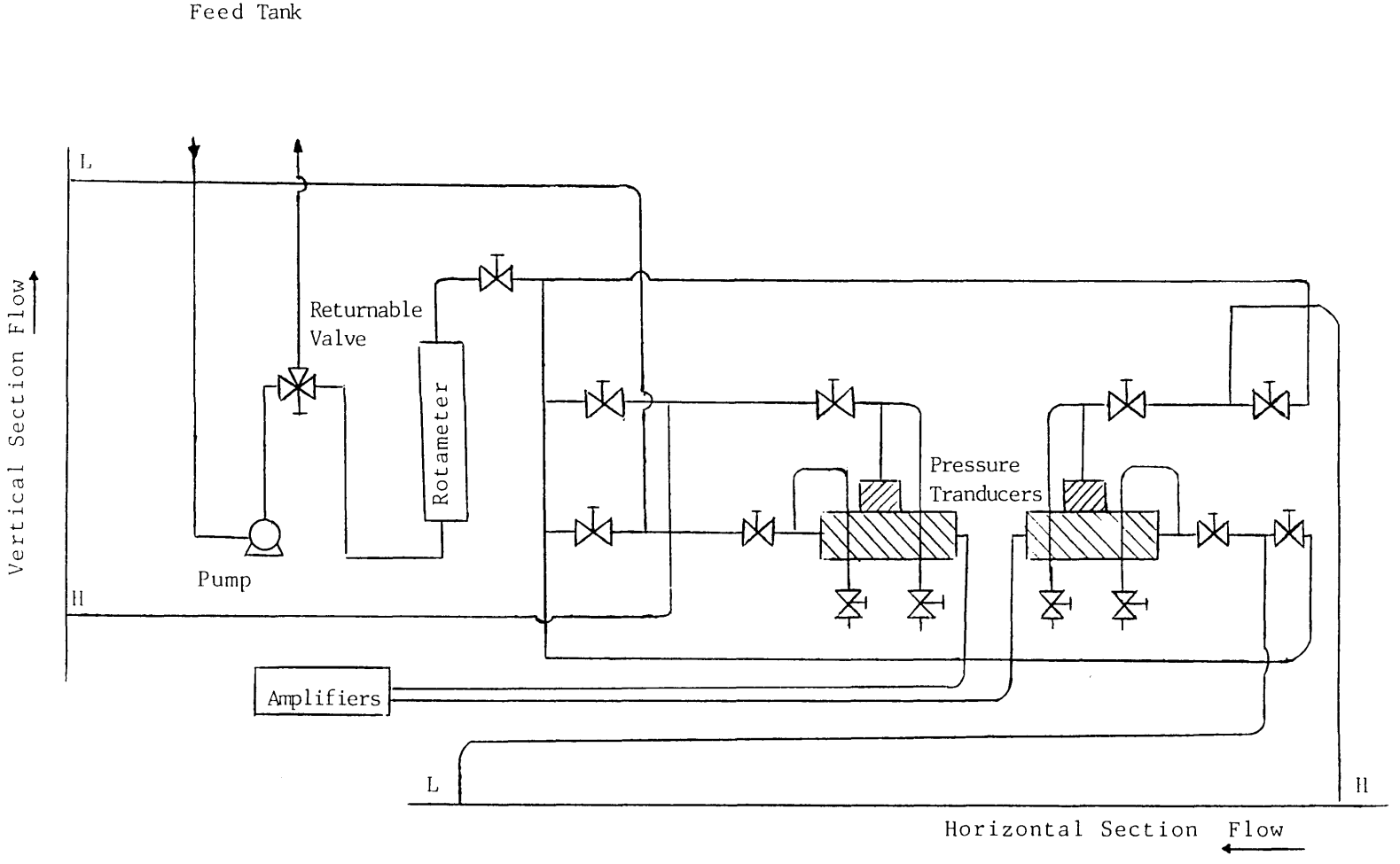

Figure 4.4 Apparatus for Pressure Transducer Calibration

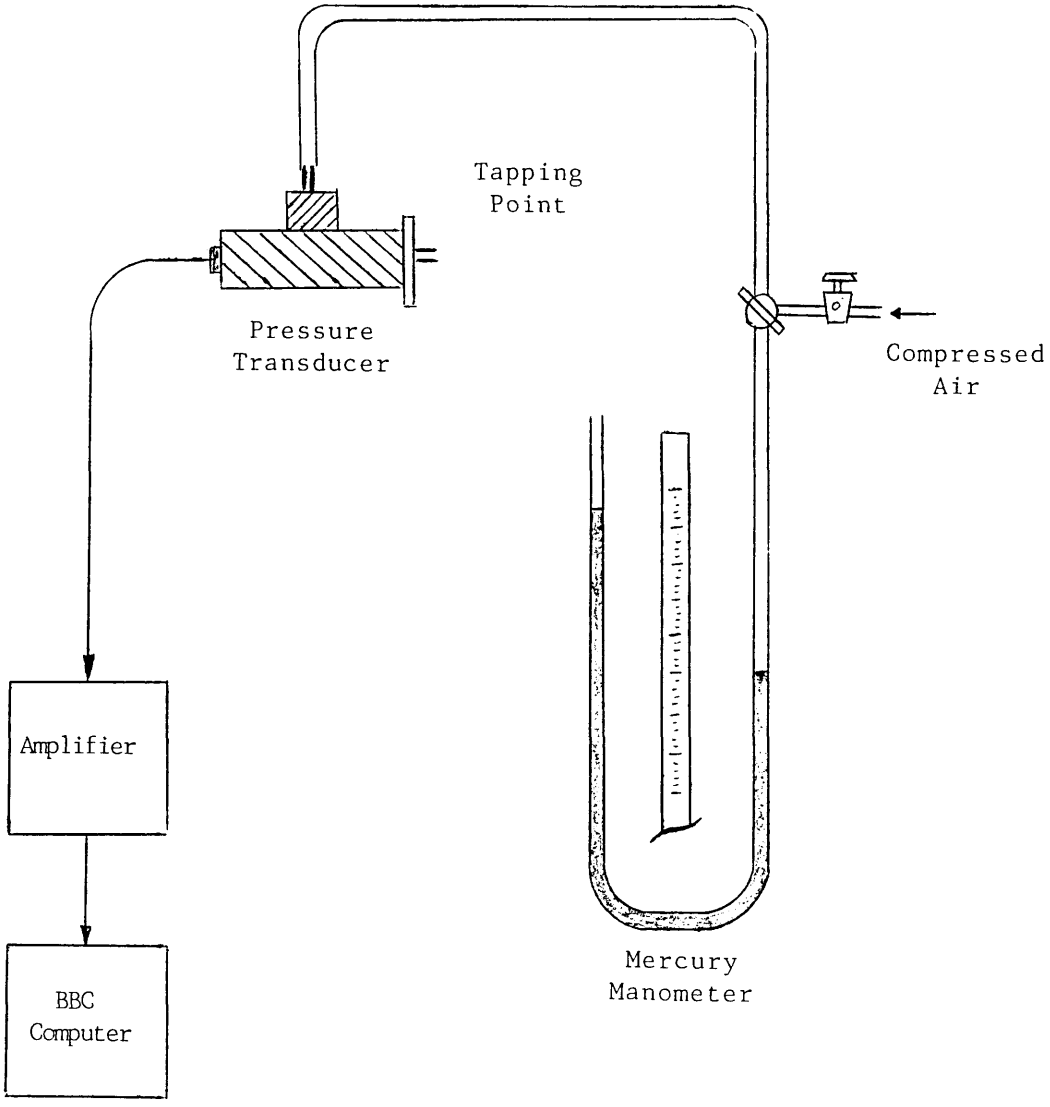

fine particles. During this operation the transducer was isolated with ball valves to prevent overloading.

The protection of the gauges against slight overload pressure is critical since they lose their linearity very quickly. During recommissioning of the pilot-plant the accuracy of the computer output was checked by connecting the transducers to a water-mercury manometer. The agreement of the hydraulic gradient was excellent.

4.2.2.2 Transducer Calibration Procedure

The calibration of each transducer was carried out as follows: the water transmission lines were disconnected, regulated compressed air was supplied to the high pressure side of the transducers while the other side was open to atmosphere (the high pressure side was selected so that increasing the pressure gave a positive analogue output). Known differential pressures were applied on the strain gauge and the reading shown on the mercury manometer was compared with the digital output of the transducer. The diagram of the set-up for calibration is given on Figure 4.4. The transducers all read zero differential pressure when the pipework contained water only.

4.2.2.3 Calibration Result

The electrical output signal of the pressure transducers was recorded and converted into a digital number via computer hardware, this digital value was counted over one second and averaged over 10 readings. The averaged value of the input signal was found to be directly proportional to the value of the pressure drop. The calibration line and details are given in Appendix A.

4.2.3 Gamma Ray Density Gauge

4.2.3.1 Introduction and Theory

Plate 4.3 shows the density gauge system. The in-situ volumetric solid concentration in the pipeline during slurry transport is measured by a gamma ray attenuation technique. This method relies on the fact that attenuation of a gamma ray beam is proportional to the density of the material for a given path length.

The half life of the caesium 137 isotope of approximately 100mCi strength used in the density gauges is 30 years, so that the count rate will only diminish by a few percent over the experimental period. The energy of the source is 0.662MeV which is high enough to enable a collimated beam to penetrate the metal walls of the pipe. However, the source strength is such that substantial protective shielding had to be used.

The detectors consist of a scintillation crystal optically coupled to the end window of a photo multiplier tube. The pulses are amplified and discriminated from noise before being counted. The photo-multiplier detector plateau was obtained by means of changing H T voltage and counting the pulses. The right value of H T voltage is chosen when the count rate is relatively independent of the applied voltage. The plateau for the present detector was found to be about 770$\pm$100V.

4.2.3.2 Theory of the Measurement

The theory is argued in detail in (40), however general theory used in the present work is repeated here.

The ratio of transmitted to incident radiation for a single absorbing medium of thickness X and density ρ is given by:

$$I/I_o = e^{-\mu\rho X} \qquad 4.1$$

where μ is the mass absorption coefficient of the material.

For a composite absorbing medium equation 4.1 can be generalised for n layers of material as:

$$I/I_o = \prod_{i=1}^{n} e^{-\mu_i \rho_i X_i} \qquad 4.2$$

Applying this directly to the case of slurry of concentration C_s in a parallel sided steel pipe of thickness X_p and internal diameter D, and using the path length, X_L, given by Bantin (4) as:

$$X_L = 2X_p + (1-C_s)D + C_sD \qquad 4.3$$

Equation 4.2 can be written for slurry in the form:

$$I_s/I_o = e^{-\mu_p\rho_p \cdot 2X_p} \cdot e^{-\mu_w\rho_w(1-C_s)D} \cdot e^{-\mu_s\rho_s C_s D} \qquad 4.4$$

For an empty steel pipe, attenuation in air is negligible in comparison to steel, so the transmitted radiation is given by:

$$I_E/I_o = e^{-\mu_p\rho_p 2X_p} \qquad 4.5$$

If the pipe is completely full of water, the transmitted radiation is given by:

$$I_w = I_o \, e^{-\mu_p \rho_p 2X_p} \cdot e^{-\mu_w \rho_w D} \qquad 4.6$$

Dividing 4.6 by 4.5 and taking natural logarithms we will have:

$$\ln (I_w/I_E) = -\mu_w \rho_w D \qquad 4.7$$

Similarly dividing 4.4 by 4.5 gives:

$$I_s/I_E = e^{-\mu_w \rho_w (1-C_s) D} \cdot e^{-\mu_s \rho_s D C_s} \qquad 4.8$$

Taking natural logarithms and substituting for the pipe diameter from equation 4.7 the final equation is obtained.

$$\ln (I_s/I_E) \Big/ \ln (I_w/I_E) = \left(\frac{\mu_s \rho_s}{\mu_w \rho_w} - 1 \right) C_s + 1 \qquad 4.9$$

The above relation is independent of X_p and D, since I_E, I_w, μ_s, ρ_s, μ_w ρ_w are all constant for the density gauge configuration and a given material. Equation 4.9 was used to relate the count rate, I_s, to the volumetric solid concentration, C_s, in the present study.

4.2.3.3 Calibration Procedure

The density gauge was calibrated for coal slurry using the system shown in Figure 4.5. The density gauge was coupled to a vertically mounted one inch diameter QVF pipe. A fine wire gauze was located in the lower section. A one meter long glass tube was connected to the top section of the density gauge to permit visual observation and this section was then connected to the drain and vacuum pump.

Transmitted radiation was estimated by taking a count-rate of the empty pipe. The column was then filled with water to measure I_w and finally the column was filled with a known amount of air dried coal particles. The air bubbles trapped in the pores of the coal particles were released by pouring a warm water over the coal and applying vacuum over the whole column. This was essential in order to obtain reproducible results. The bed was fluidised to give a uniform distribution of particles, flow was stopped and several readings of the freely settled bed concentration were obtained and the height of the bed was accurately measured with a cathetometer. The bed was gradually tapped down for different packed settled concentrations and this was repeated until no further compaction could be achieved. The bed level (cathetometer reading) and count-rate (computer output) were recorded at each stage. The column concentration was determined by knowing the dry weight of coal and the volume of the bed at each stage. The bed was fluidised again and the procedure repeated in order to reduce random errors.

The performance of the gamma-ray density gauge is based on the detection of the density difference between the particles and the carrier fluid. In the case of a coal slurry, this difference is not large and to improve the statistics of counting a long integration period of

Figure 4.5 Apparatus for Density Gauge Calibration

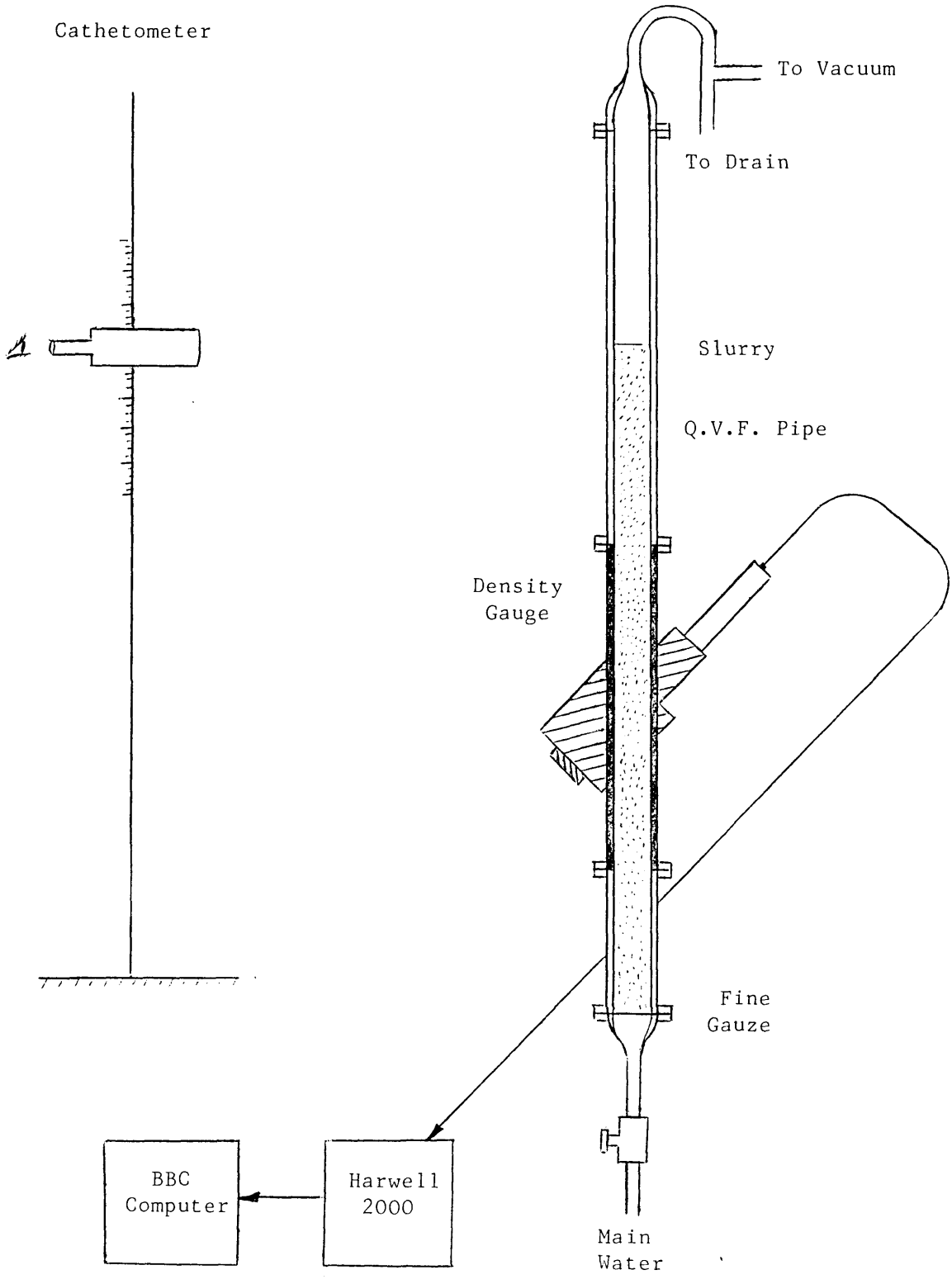

100 seconds is required.

4.2.3.4 Result

Figure 4.6 shows the calibration result for coal particles of size 0.5<d<1.0mm and linear regression of the points gives a straight line of the form

$$\ln(I_S/I_E)/\ln(I_W/I_E) = 0.34\ C_s + 0.996 \qquad 4.10$$

Since the slope of the line is fairly small the error in the reading of the in-situ concentration will be high. The average error was found to be about 5%.

The experimental value of the coal mass attenuation coefficient was checked with published data. The agreement is within 9%, and this could be due to the increasing difficulty of obtaining a reproducible result for different coal particles. The values of published data and experimental value for mass attenuation of coal are given in Table 4.1.

To decrease the error in reading in-situ concentration it is necessary to increase path length or decrease the energy of the source. Increasing the path length was considered by moving the source from its existing position to a bend, e.g. a right-angle bend, which would increase path length by a factor of about two and a half, therefore the attenuation of the gamma-ray will increase as given in equation 4.1. However, the generalised correlation (equation 4.9) used in the calibration of the density gauge indicates that the slope of the curve is independent of path length even though the attenuation is dependent on it. Decreasing the energy of the source was also considered, since the

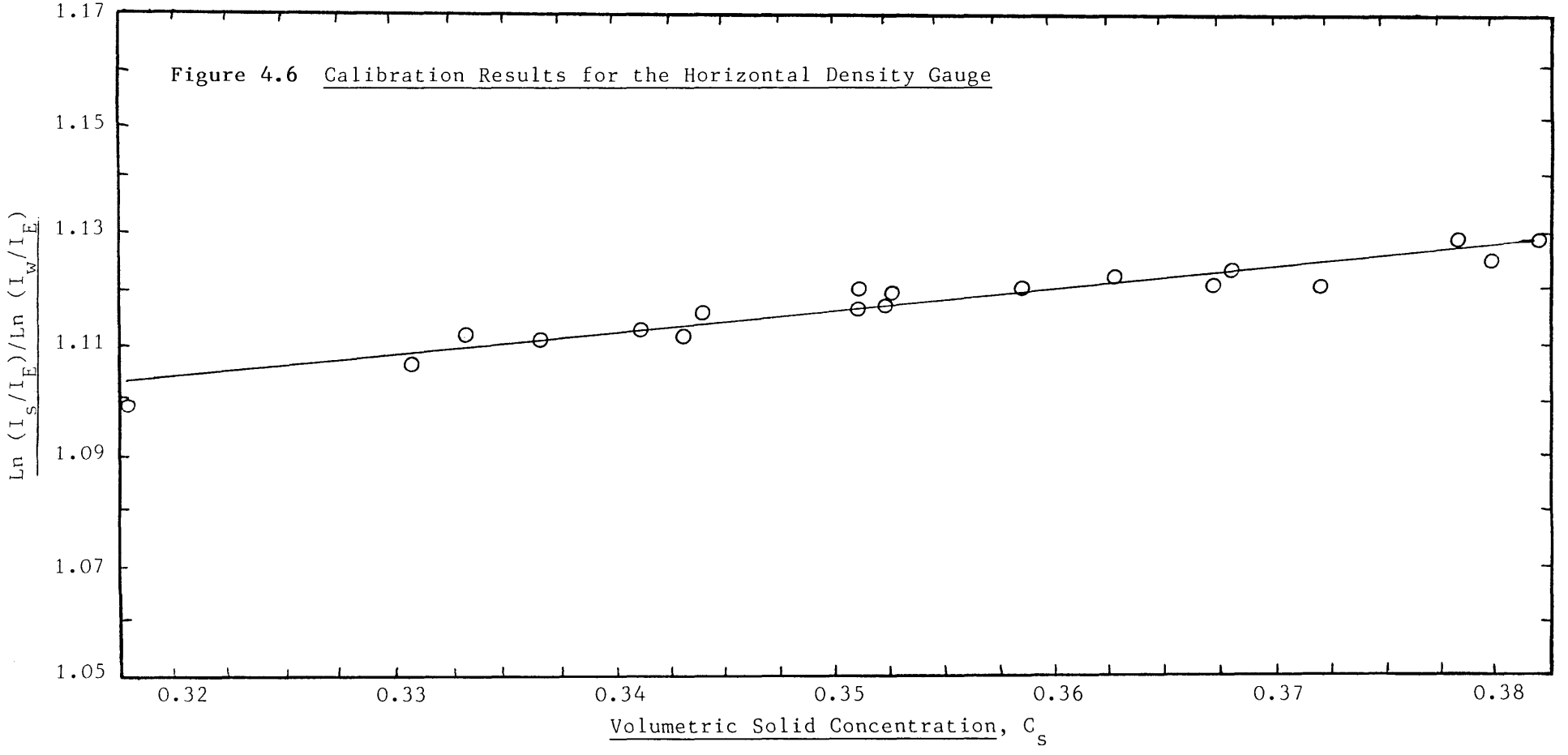

Figure 4.6 Calibration Results for the Horizontal Density Gauge

Table 4.1 Gamma Photon Attenuation Coefficients for Coal and Water

Material	Density (kg/m^3)	Mass Attenuation Coefficient Cm^2/g at Energy of $C_s137 = 0.662M_eV$	Reference No
Carbon	1.350	0.0788	27
Water	1.000	0.0876	27
Water	1.000	0.0759	25
Water	1.000	0.084	22
Coal	1.643	0.07304	22
Coal	1.307	0.0765	22
Coal	1.325	0.0834	Experimental

slope of the line is a function of μ_s, ρ_s, μ_w and ρ_w. Decreasing the source energy will increase the mass attenuation coefficient of the coal, μ_s, but the relative value of the mass attenuation of the coal (μ_s/μ_w) is found to be constant, therefore the term ($\mu_s \rho_s / \mu_w \rho_w$ - 1) is fixed.

It is concluded that the calibration line obtained is correct and there is no way of increasing the slope using the existing apparatus and poor resolution of coal concentration is inevitable, though the use of long integration times could improve the resolution.

It should be mentioned here that the calibration of a coal slurry can be easily affected by the presence of air bubbles at the surface of the particles.

The same calibration line was used for all three size-ranges of coal since the mass attenuation coefficient, μ_s, is dependent on the type of the material not the size of the particle. The use of large coal particles produces a lot of scatter in the line due to the difficulty of producing a uniform concentration in the bed.

4.2.4 Delivered Solids Concentration

4.2.4.1 Introduction

Delivered solids concentration was measured after each run by means of using a sliding plate sampling device.

4.2.4.2 Sampling Device

Plate 4.4 shows the sliding plate sampler. This was mounted on the top of the receiver hopper at the slurry entrance. When a sample is required the pneumatic ram diverts the total flow of the slurry to the sampling point without disturbing the flow. Samples were collected in a

$2000cm^3$ plastic measuring cylinder.

The delivered solids concentration, C_d, can be evaluated from the total mass, W_s, and volume, V_s, of the sample using this equation:

$$C_d = \left(\frac{W_s}{V_s} - \rho\right)/(\rho_s - \rho) \qquad 4.11$$

4.2.5 Instrumentation and Interfacing to the BBC Digital Computer

A suitable data logging system is required to make simultaneous measurement of the flow rate, pressure gradient, in-situ solid concentration and delivered solids concentration. A BBC microcomputer was used for this purpose.

The instrumentation block layout is shown in Figure 4.7 and also in Plate 4.5. Two types of signal were sent to the computer; analogue signals to the analogue input channel and pulse signals to 1MHz bus. The output signals from all the measurement devices were amplified before being interfaced to the BBC.

The horizontal differential pressure transducers have a full range output of 4.66 mv/v and this was amplified to 1.8v using an amplifier and conditioner of the type 2100 series manufactured by Pioden Controls Limited. The transducer analogue output signals were amplified and sent to one of the analogue channel inputs of the BBC and converted into digital signals using a BBC A/D convertor. The transducer output signals were taken every 10msec and the final reading was the average of 10 of these readings. This was done to compensate for noise. The amplifier output should be set to zero when the differential pressure on the strain gauge is zero. This was repeated before the start of the run to prevent

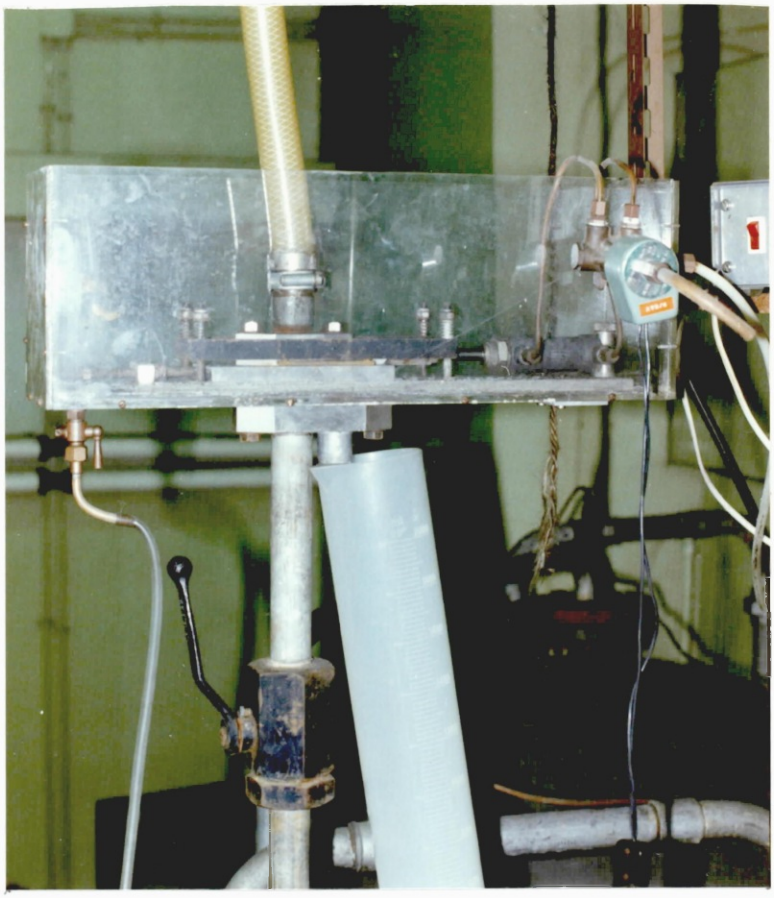

Plate 4.4 Sliding Plate Sampler

Plate 4.5 Electronics and Control Facility

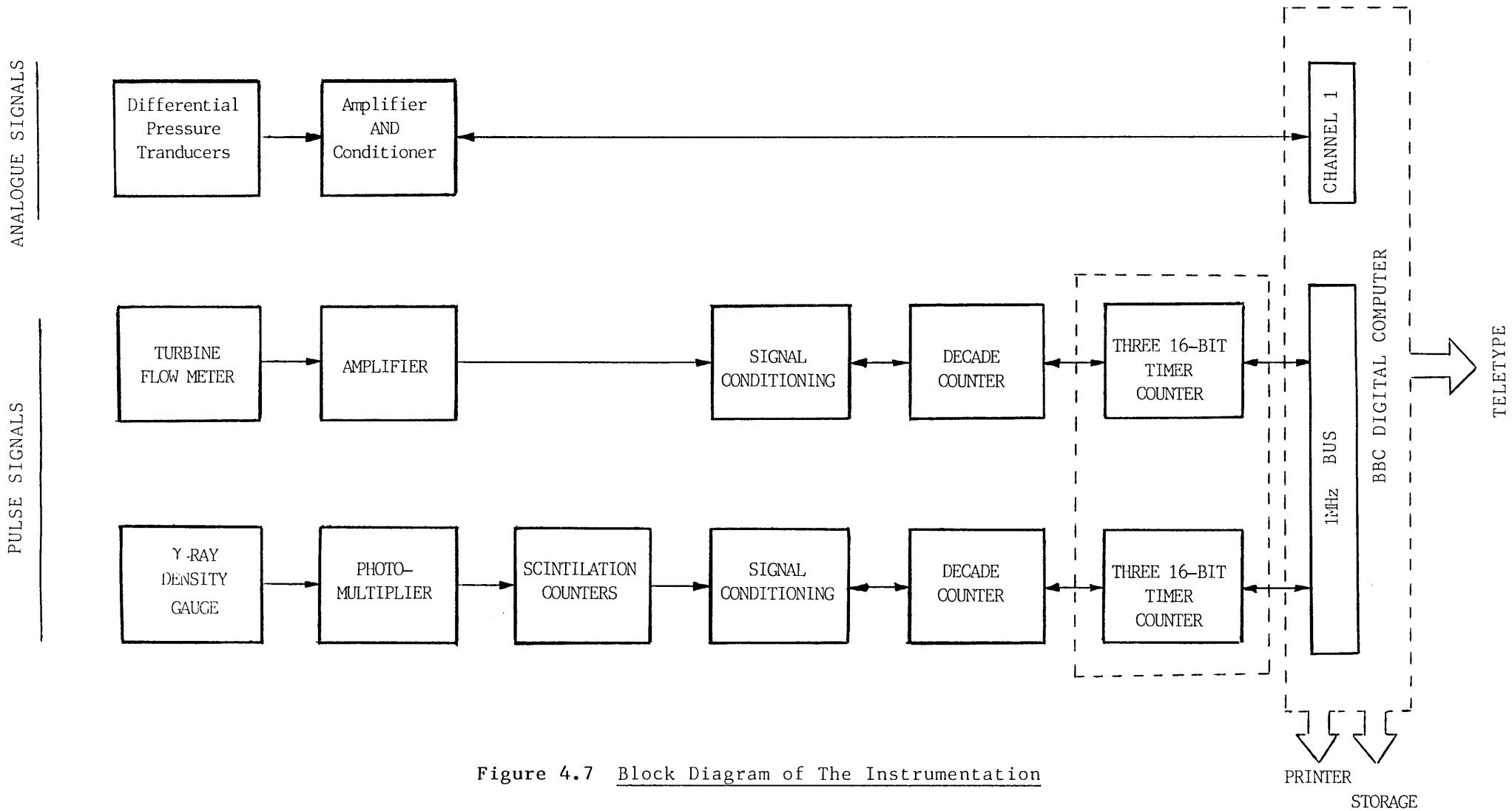

Figure 4.7 Block Diagram of The Instrumentation

any drift of zero balance with temperature. The full range output (F.R.O.) of the amplifier is set to 1.8v for a maximum output differential pressure (5 psia) by using the calibration figure given in the strain gauge test certificate, calibration figure being 56.8% of F.R.O. The amplifier span was adjusted to read 1.8 x 0.568.

The turbine flow meter and gamma-ray density gauge both have pulse electrical signals. Special hardware was designed so that these pulses could be interfaced to the BBC computer 1MHZ Bus. The turbine flow meter has a maximum frequency of 400 counts per second and the density gauge has a very high frequency of 1MHZ.

Gamma-rays are detected by a thallium activated sodium iodide crystal coupled to a photomultiplier tube (type DM1-1/9524A) manufactured by Nuclear Enterprises Limited. The scintillation tube is driven by a Harwell 2000 series scintillation counter (Adapter type 95/2179-1/6), powered by a high voltage power supply (type 95/2015-4/6). The scintillation counts have a maximum operating voltage of about 1100v, but the optimum voltage was found to be about 770v. This equipment is interfaced via hardware to the BBC. The counting period for both of these devices, i.e. flow meter and density gauge, is controlled by computer software. The optimum integration time was found to be 1 second for the former and 100 seconds for the latter.

4.3 Experimental Technique for Operating the Hydraulic Plant Rig

4.3.1 Hopper Loading Procedure

For convenience, coal was first loaded into the receiving hopper and then transferred to the feed hopper. The receiving hopper was half filled with water and about 400kg coal was loaded each time.

After loading, the hopper was fluidised with water using pump

pressure at the bottom of the hopper and connecting the outlet via a screen of size 0.5mm diameter. Fluidisation washes the coal dust from the load and also dispels trapped air between the particles. The load was left in the hopper overnight to allow coal particles to soak in the water.

The load was transferred to the feed hopper by applying pump pressure to the top of the receiving hopper and then opening valve (R.1) and using the transfer line to the feed hopper. The existence of any trapped air below valve R.1 will stop the transfer. This was overcome by ensuring that the transfer line was full of water.

The coal particles transferred freely to the feed hopper except when the coal sizes were above 4.0mm.

Coal was discharged from the pipeline by diverting the flow just before the receiving hopper by using the sliding plate to the specially made collecting tank.

4.3.2 Pre-Run Preparation

The following procedure was carried out before any experimental runs:

1. The power supply to all the electrical instruments and data logging system was activated half an hour prior to a run. This was found to be the time required for all the electronic equipment to stabilise at the ambient temperature, and thus give reproducible results.

2. The pressure tapping line and slotted plate were back flushed with filtered water to clear them of any fine coal and rust particles by isolating the pressure gauges and using pump pressure. This method was found very effective for unblocking a tapping system. The tapping plates were not replaced during the entire experimental campaign.

3. The pipeline was pumped full of water. With the pipeline full of water, the gamma-ray density gauge was adjusted for any drift by making a slight adjustment to the count rate to agree with the calibration count for clear water. This was done by making a fine adjustment to the scintillation tube voltage. Also drift in the zero balance of the differential pressure transducer amplifier was checked and corrected with no flow in the transport line.

4. The system was operated with clear water to remove any trapped air in the system.

4.3.3 Operation Method

Water was pumped from the feed tank to the top of the feed hopper using both pumps. This pressurises the feed hopper which initially contains a settled bed of solids and water. Initial pressures as high as 10-14 bar are needed to force the slurry into the transport line. However, this initial surge was always higher than the pressure needed to maintain steady flow. When the required pressure was reached, the ball valve at the base of the feed hopper was fully opened and coal-water slurry was transported by pipeline to the receiving hopper. This was initially full of water and during a run the incoming slurry displaces an equal volume of water to the drain. It was customary in earlier work to recycle some waste water to the feed tank during high velocity runs but this was avoided due to the presence of fine coal particles. Also a separate inlet of clear water was installed to overcome the low level of feed tank water. As a large over pressure was needed it was found better to commence at high velocity and make measurements by decreasing the velocity for each successive run, noting the position of the valve to avoid repetition. The discharge velocity from the hopper was observed to

be independent of the solids head in the hopper, except when the hopper was very nearly empty. It was often possible to obtain 10 runs at different velocities from one discharge of the hopper. An effort was made to get the runs for the whole velocity range for each hopper load to avoid any experimental measurement error due to the degradation of the coal particles, even though the degradation of the coal was observed to be very small.

Steady slurry flow was obtained by pumping clear water at steady throughput to the top of the discharge hopper. The data logging system was used to check for steady flow before any data storage. The data were taken in a period of 120 seconds. The sample of slurry was taken immediately after computer data logging to minimise any disturbances to the flow. At high velocity up to $2000cm^3$ of slurry was removed but at lower velocity below 1m/s this sampling was restricted to $500cm^3$ to minimise the effect on the flow.

When all the solids had been transferred to the receiving hopper the pumps were stopped and feed hopper ball valve was immediately closed to ensure that the hopper remains full of water. At the end of an experimental run it was necessary to transfer the coal back to the feed hopper.

Before shut down, the pipeline was flushed with clear water and also the pressure tapping system was back-flushed again.

CHAPTER 5

THEORETICAL INTERPRETATION OF HORIZONTAL FLOW

5.1 Introduction

Chapter 2 introduces the available literature on slurry transportation; though little mention was made of coarse slurry transport in dense phase flow which is the prime object of the present study.

In this chapter, a review of dense phase flow will be given and an attempt will be made to develop a physically based mechanism for slurry pressure gradient prediction in different flow regimes.

Most of the correlations available are either empirical or semi-empirical and as such are only valid under the experimental conditions applicable to the work. However, a mechanistic approach to the prediction of hydraulic gradient will be free of these drawbacks and more generally useful.

5.2 Dense Phase Theoretical Model

One approach that has been proposed for coarse coal transportation is the use of a carrier fluid with an effective density close to that of coal so that the large particles do not settle and therefore the flow regime is laminar rather than turbulent.

Elliot and Gliddon (17) showed experimentally that coarse coal having a top size of 13mm behaved as a Bingham plastic. Coal slurry was transported under laminar flow conditions and at relatively low specific energy consumption provided that,

1) the concentration by weight was about 60%
2) the size distribution corresponded to that of the maximum packing density
3) the proportion of fine coal ($d<150\mu m$) was 25% and of coarse coal ($1mm<d<13mm$) was 60%.

Their work showed that the yield stress of the above coal-water suspension ensured that the coarse material did not settle out, and thus the restarting of pipelines conveying such materials is likely to present little difficulty after shut-down. They also suggested that the presence of different clays and variation in pH can have a significant effect on the rheological properties.

Thomas (42) formed a similar type of slurry by fine grinding a small proportion of the coal to form a viscous "vehicle" or "carrier" and this would support the coarse particles enabling transport under laminar flow. This slurry was stable under shutdown conditions. The work of Ansley and Smith (1) and Thomas (42) showed that static stability occurs when the yield stress of the slurry is sufficient to support the coarsest particles. For this purpose some particles must be smaller than about 10 microns and the particles must be flocculated.

Thomas (42) derived a simple criteria to determine the yield stress required to ensure stability of a certain size particle.

$$\tau_{yv} > 0.92\ g\ d\ (\rho_s - \rho)$$

Pertuit et al (34) state that laminar flow is possible if the slurry is statically stable. However, it has been shown by Thomas (43) that

this is not true in some cases, since existing long distance slurry pipelines, whilst statically stable are known to deposit out under turbulent conditions without laminar flow being possible.

Duckworth (13, 14, 15) has reported the transportation of coarse coal having a top size of 20mm in a pipe of 150mm in diameter under laminar flow conditions at a coarse coal fraction ranging from 0 to 0.48 and at total concentration ranging from 53% to 67% providing that the fluid carrier is a non-Newtonian fluid having a yield stress sufficient to support the largest particle.

Another approach for coarse coal slurry transport is to try to achieve "bed slip flow" or a "loose-packed" bed. In this flow regime the slurry travels as a contact load with very little internal movement. The object of the present study is to seek a mechanism that would enable us to predict the energy losses in a moving bed, a moving bed with suspension and in fully heterogeneous suspension flow.

5.3 The Basic Two-Layer Model

During the experiments the existence of two layers was observed, especially for coarse coal transport and so the two-layer model was employed to interpret the experimental measurements.

Although the following theory is identical to that published by Wilson and used by other co-workers (6, 41) a complete description is given since some of the methods of solution are different.

The analysis is based on a force balance on a stationary bed at the point of incipient movement. For steady flow, the driving force must be equal and opposite to the resisting force.

In dense phase flow, the part of the pipe area occupied by the bed of solid is defined by angle β. Figure 5.1 shows the forces and

parameters used in a basic two layer model and from this Figure the geometry of the system can be expressed as follows: (angle of β measured in radians)

$$X = D/2\ (1 - \text{Cos}\ \beta\ ) \qquad 5.1$$

$$A = A_1 + A_2 \qquad 5.2$$

$$A_2 = D^2\ (\beta - \text{Sin}\,\beta\ \text{Cos}\,\beta\ )/4 \qquad 5.3$$

$$S_1 = D(\ \pi - \beta\ ) \qquad 5.4$$

$$S_2 = D\ \beta \qquad 5.5$$

$$S_{12} = D\ \text{Sin}\,\beta \qquad 5.6$$

In the first presentation of the model, the upper layer was assumed particle free and denoted by subscript 1, whilst the lower layer contained a moving bed of particles and is denoted by subscript 2. the interface between these two layers is denoted by subscript 12.

For steady flow, the conservation laws for fluid and particles give:

$$AU_m = A_1U_1 + A_2U_2 \qquad 5.7$$

assuming the velocity profile to be invariant through each layer and assuming that the fluid is incompressible,

$$A_2U_2 = A_2C_2\,U_{s2} + A_2(1-C_2)\ U_{f2} \qquad 5.8$$

C_2 is the volumetric solids concentration and this is slightly larger

than the settled bed concentration, C_b. Solids concentration in a moving bed is assumed invariant with height, although Wilson (47) in recent work demonstrated that there is a particle shear layer, where contact-load particles move relative to each other. He suggests that the variation of concentration with height can be represented by a linear relationship in this layer. However in this work we have used the former assumption and therefore C_b is related to C_2 in the lower layer as follows.

$$C_b U_2 = C_2 U_{s2} \tag{5.9}$$

and in-situ solids concentration, C_s, is related to the actual concentration, C_2, by

$$C_2 A_2 = A C_s \tag{5.10}$$

Also the delivered solids concentration, C_d is related to C_2 by

$$A_2 C_2 \, U_{s2} = A C_d \, U_m \tag{5.11}$$

A momentum balance can be written for the individual layers under conditions of fully developed flow, where the linear frictional pressure drop is i_m.

$$i_m \, g \rho_f - (\tau_1 S_1 + \tau_{12} S_{12})/A_1 = 0 \tag{5.12}$$

$$i_m \, g \rho_f + (\tau_{12} S_{12} - \tau_2 S_2)/A_2 = 0 \tag{5.13}$$

The shear stress signs are shown in Figure 5.1 .

The fluid shear stress at the pipe wall in the upper layer, τ_{f1}, can be defined using the single phase friction factor

$$\tau_{f1} = f_1 U_1^2 \rho_f/2 \qquad 5.14$$

and since the flow is turbulent the Fanning friction factor for a smooth pipe is evaluated using

$$f_1 = 0.046 \left(\frac{\rho_1 D_{e1} U_1}{\mu_f}\right)^{-0.2} \qquad 5.15$$

The characteristic length needed for the evaluation of the Reynolds number is usually one pipe diameter but here the flow is non-circular in each layer and an equivalent diameter, D_e, is used where,

$$D_e = 4 \left(\frac{\text{Surface Area}}{\text{Perimeter}} \right) \qquad 5.16$$

for the upper layer

$$D_{e1} = 4 \left(\frac{A_1}{S_1 + S_{12}} \right) \qquad 5.17$$

and for the lower layer

$$D_{e2} = 4 \left(\frac{A_2}{S_{12} + S_2} \right) \qquad 5.18$$

Televantos (40) made an approximate measurement of velocity in the upper and lower layer and verified that the upper layer travels at higher velocity than the lower layer. The shear stress at the interface can be obtained by considering the velocity relative to the two layers

$$\tau_{12} = f_{12} (U_1 - U_2)^2 \rho_f/2 \qquad 5.19$$

Yalin (50) has suggested that for flow over naturally rough boundaries the value of the friction factor for the interface can be derived from

$$f_{12} = [4 \log_{10} (D/2d) + 3.48]^{-2} \qquad 5.20$$

The average total shear stress at the wall in the lower layer will contain fluid and particles

$$\overline{\tau}_2 = \tau_{f2} + \tau_{s2} \qquad 5.21$$

The fluid boundary shear stress, τ_{f2}, can be calculated from an equation similar to equation 5.14, but using the velocity U_2 and the characteristic length of the lower layer (equation 5.18). However the particular shear stress, τ_{s2}, is the sum of two effects, i.e. the normal force at the pipe wall due to the bed of particles, F_n, multiplied by the coefficient of friction, μ_p, and transmission of stress from the interface through the sliding bed to the pipe wall.

If the upper layer is free of particles, then according to Bagnold (3) the intergranular stress normal to the surface is equal to $\tau_{12}/\tan\phi$ where ϕ is the angle of internal friction. The particulate shear stress will be

$$\tau_{s2} = \frac{F_n}{S_2}\,\mu_p + \frac{\tau_{12}}{\tan\phi}\,S_{12}\,\mu_p \qquad 5.22$$

The total normal stress at the pipe wall, σ_p, according to Wilson (44) is not constant over the area of bed deposit but depends upon the submerged weight of the particles.

$$\frac{d\sigma_p}{dx} = C_2\, g\,(\rho_s - \rho) \qquad 5.23$$

The normal stress at an arbitrary point on the pipe wall can be expressed by integrating the above expression and summing the normal stress over the total area of the pipe occupied by the bed of particles. This will give the total normal force exerted by the bed at the pipe wall, F_n

$$F_n = C_2\, D^2/_2\, g\,(\rho_s - \rho)(\mathrm{Sin}\,\beta - \beta\,\mathrm{Cos}\beta) \qquad 5.24$$

The total shear stress in the lower layer, τ_2, can be obtained from :

$$\tau_2 = \underbrace{f_2 U_2^{\,2}\rho/2}_{\tau_{f2}} + \underbrace{C_2 D^2\, g(\rho_s-\rho)(\sin\beta - \beta\mathrm{Cos}\,\beta)\mu_p/S_2}_{\tau_{s2}}.2 + \underbrace{\mu_p\,\tau_{12}/\tan\phi}_{\tau_{s2}} \qquad 5.25$$

At steady flow in the lower layer, the momentum balance is the sum of two equations, one for the fluid and one for the particles

$$i_m \rho_f g (1 - C_2) + FFP + FFW = 0 \qquad 5.26$$

$$i_m \rho_f g C_2 + FPF + FPW = 0 \qquad 5.27$$

Here FFW and FPW are fluid friction on the fluid and the particle by the wall (or wall drag forces), and FFP, FPF are fluid friction on the fluid by the particles and on the particles by the fluid.

The net interfacial drag must vanish at the particle surface so hydrodynamic drag must be equal in magnitude and of opposite sign

$$FFP + FPF = 0 \qquad 5.28$$

Wall drag forces can be expressed in terms of shear stress as follow

$$FFW = - \tau_{f2} S_2/A_2 \qquad 5.29$$

$$FPW = \tau_{12} S_{12}/A_2 - \tau_{s2} S_2/A_2 \qquad 5.30$$

Ergun (9) has obtained a good semi-empirical correlation for frictional pressure drop for flow through a granular porous mass of particles

$$i_m \rho_f g = 150 \frac{(1-e)^2}{e^3} \frac{\mu_f U_f}{d^2} + 1.75 \frac{(1-e)}{e^3} \frac{\rho_f U_f^2}{d} \qquad 5.31$$

where $e = 1-C_2$

The Ergun equation is used to relate the frictional drag force on the fluid by the particle, FFP, to the relative velocity U_r .

where

$$U_r = U_{f2} - U_{s2} \qquad 5.32$$

By substituting U_r instead of U_f in the equation 5.31 this equation has been used in the iteration to interpret the experimental result. The above set of equations were solved iteratively to predict i_m and other unknown quantities as is explained in Appendix C.

5.4 Two-Layer Model Modification for Dense Phase Flow

For the case of dense phase flow with a wide particle size distribution (fine and mixed coal) the basic model was modified by the use of the mixture density, instead of density of pure water, hence the fluid friction factor in the lower layer f_2 is calculated as a function of mixture density ρ_m where ρ_m can be evaluated from :

$$\rho_m = \rho(1 - C_s) + \rho_s C_s \qquad 5.33$$

The use of mixture density accounts for some suspended fine particles in the carrier fluid.

The procedure to predict the hydraulic gradient is the same as section 5.3 except the fluid shear stress in a lower layer, τ_{f2}, is a function of mixture density.

Televantos (40) modified the basic two-layer model in a very similar way. However, he only applied the simplified version of the two-layer model to his experimental result :

$$i_m = 2\mu_p (S-1) C_s + \frac{\rho_m}{\rho_L} i_f \qquad 5.34$$

and he found this expression very satisfactory for a case of flow where the moving bed occupies the whole of the pipe cross-section.

5.5 Improved Two-Layer Model for Prediction of Suspension Velocity

Although observation was extremely difficult, limited visual observation showed that the majority of the pipe cross-section was full of moving particles especially for fine and mixed size coal. The computational prediction of the results using the two-layer model was in excellent agreement with the experimental results but predicted the existence of two-layer flow for all flow velocities. To understand and analyse this contradiction, the two-layer model was improved to predict the onset of turbulent eddies and also to predict the velocity at which complete suspension occurs and two-layer flow no longer exists.
Figure 5.2 shows the flow parameters and regimes. In this case the upper layer is assumed to have a suspended particle concentration of C_1 and Equation 5.11 and 5.10 will no longer apply.

Assuming no slip between the particles and fluid and existence of complete suspension in the upper layer

At steady state, the continuity equations for each layer are:

for the solid phase

$$AC_d U_m = C_1 U_1 A_1 + C_b A_2 U_2 \qquad 5.35$$

for the liquid phase

$$AC_s = A_1 C_1 + A_2 C_2 \qquad 5.36$$

Also the effect of suspended particles on the fluid shear stress at the pipe wall for each layer can be evaluated by using the mixture density instead of pure fluid density:

$$\rho_{m1} = \rho(1 - C_1) + \rho_s C_1 \qquad 5.37$$

$$\rho_{m_2} = \rho(1 - C_2) + \rho_s C_2 \qquad 5.38$$

So the force balance equations for each layer are:

for the upper layer with complete suspension

$$i_m \rho g - (\tau_{m1} S_1 + \tau_{12} S_{12})/A1 = 0 \qquad 5.39$$

for the lower layer with moving bed

$$i_m \rho g + (\tau_{12} S_{12} - \tau_{m2} S_2)/A2 = 0 \qquad 5.40$$

where the shear stress τ_{m1} in the upper layer is a function of $\bar{\rho}_{m1}$ and lower layer shear stress τ_{m2} is a function of ρ_{m2}.

In contact load transport, the volumetric bed concentration, C_2, is assumed to be equal to the free settled concentration and to remain constant despite the fact that the bed depth or half angle β is changing. Equations 5.35, 5.36, 5.39, 5.40 and 5.31 can be solved iteratively to predict the hydraulic gradient and other unknowns. Provided that the value of A_2 as given in Equation 5.35 is more than or equal to AC_s/C_2 there will not be any suspended particles i.e. $C_1=0$ and when the value of A_2 is less than AC_s/C_2 the value of C_1 can be calculated.

This simple improvement of the two-layer model will enable us to predict the value of threshold velocity and velocity at which complete suspension occurs.

A BBC micro computer was used for the iterative calculations and to predict the value of i_m, β, C_b, and C_1. These computational procedures are given in Appendix C.

Figure 5.1 Two-Layer Model

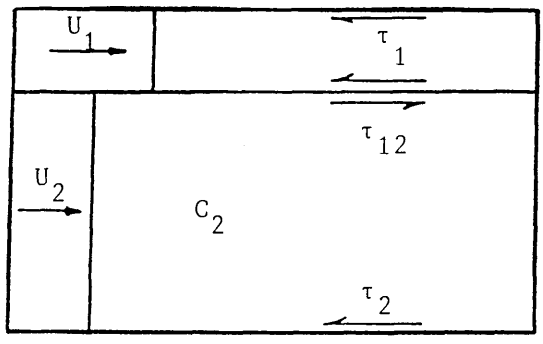

Side View

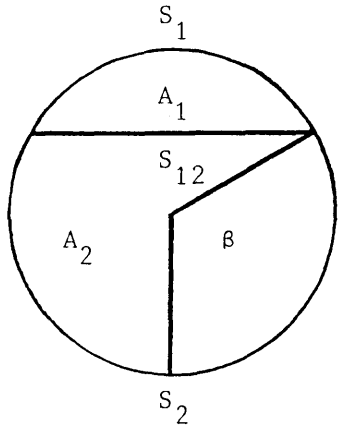

Cross Sectional View

Hypothetical Flow Regime

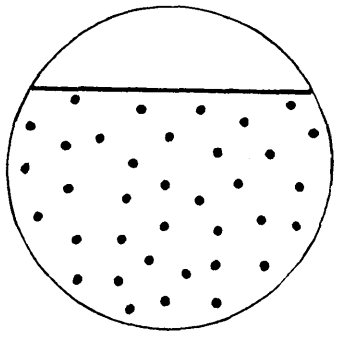

Basic Two-Layer

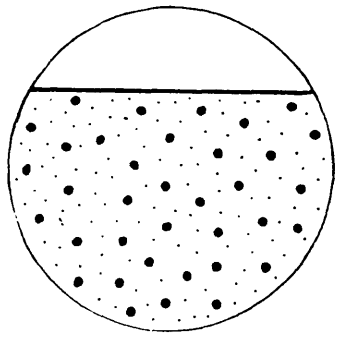

Modified Two-Layer

Figure 5.2 Derived Two-Layer Model

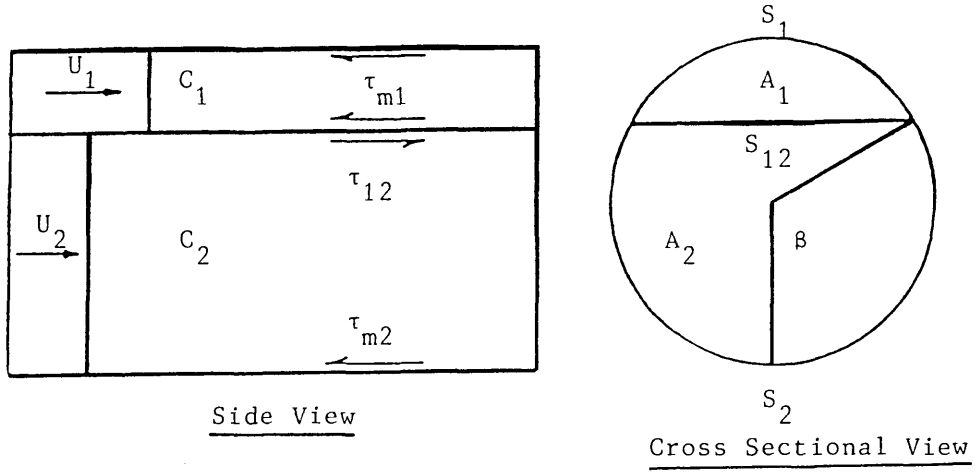

Hypothetical Flow Regime

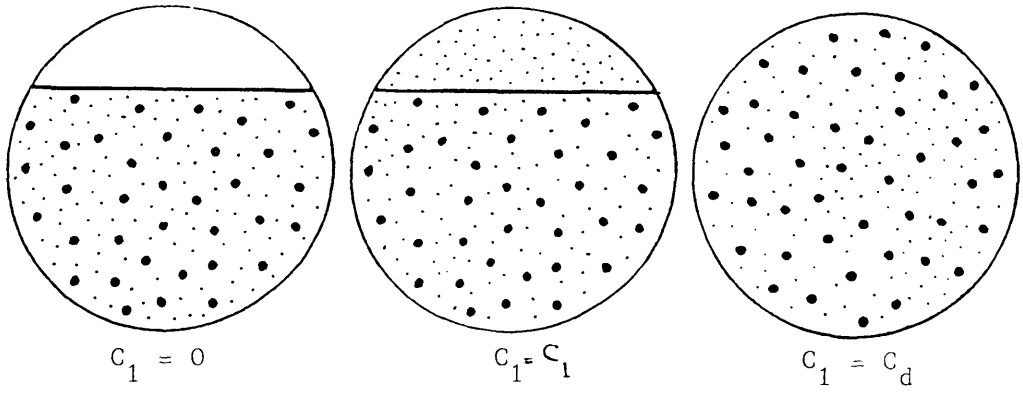

CHAPTER 6

RESULTS AND DISCUSSION

6.1 Experimental Results

6.1.1 Scope of Measurements

Experiments were carried out using a 26mm diameter pipe flow rig. A line diagram of the flow rig is shown in Figure 4.2. The material investigated was Bagworth coal in the size range 0.5-4.0mm. The coal specification is given in Table 3.1.

The aim of the experiments was to provide a complete set of reliable data on coarse coal slurries for different particle sizes in horizontal flow. The coal selected for the work was assumed to be representative of "run-of-the-mine" material and composed of irregular shaped particles of high porosity and of density close to the carrier fluid.

Many successful runs were carried out at different mean slurry velocities. Pressure drop, in-situ solids concentration and delivered solids concentration were independently measured during each run.

The first set of experiments were carried out with pure water in order to establish the pipe roughness and also the acceleration length at a bend. It was found that flow is fully developed at fifty pipe diameters beyond a bend and that the pipeline may be treated as smooth. The water pressure gradient measurements are given in Table 6.1.

Experiments were carried out for several different size ranges of coal i.e. coarse coal in the size range 1-4.0mm with a mean particle diamter (d_{50}) of 3.25mm and fine coal in the size range 0.5-2mm with a mean particle diameter (d_{50}) of 0.975mm.

Experiments were carried out with both these size ranges independently and the results are shown in Figures 6.1 and 6.2 and tabulated in Tables 6.2 and 6.3. Visual observation showed the existence of two-layer flow for coarse coal below 0.7m/s. However, this observation was not possible for fine particles.

A further set of experiments was carried out with a mixture of these two coal samples. This enabled us to perform an investigation of the hydraulic gradient of a well graded sample with a size distribution in the range 0.5-4.0mm and mean particle diameter (d_{50}) of 1.9mm. These results referred to as "mixed coal" are plotted in Figure 6.3 and given in Table 6.4. For comparison the hydraulic gradients of the three coal samples are plotted in Figure 6.4.

The size distribution of all the samples before and after the experimental runs are plotted separately in Figures 6.5 to 6.7 and also given in Tables 6.5 to 6.7.

The variation of in-situ solids concentration and delivered solids concentration against mean slurry velocity are plotted in Figures 6.8 to 6.10 to show the observed fluctuations during the experimental runs. The average value of in-situ and delivered concentration was used for computational purposes.

The aim of this study was to transport coal slurry at the highest possible concentration, preferably near to the freely settled concentration. However, it was not possible to achieve more than 40% by volume even at the highest applied feed hopper pressure and at the highest mean slurry velocity. This could be due to the large particle size, extremely irregular shape of the coal particles and above all the density of coal particles which was very close to that of the carrier fluid.

Table 6.1

PRESSURE GRADIENT DATA FOR WATER ALONE

(In a Horizontal pipeline)

Water Velocity (m/s)	Pressure Gradient (m water/ m pipe)
3.000	0.341
2.530	0.250
2.140	0.186
1.850	0.142
1.670	0.120
1.590	0.108
1.320	0.077
1.160	0.062
1.000	0.047
0.760	0.028

Hydraulic Gradient Correlation

$$i_m = 0.0478\ (U_m)^{1.82}$$

Table 6.2

EXPERIMENTAL DATA FOR COARSE COAL (1-4 mm)

Mean Velocity U_m (m/s)	Hydraulic Gradient i_m (m water/ m pipe)	Volumetric Solid Concentration C_s in-situ	C_d delivered
4.030	0.670	0.297	0.252
3.951	0.657	0.300	0.261
3.830	0.601	0.260	0.260
3.441	0.507	0.247	0.272
3.382	0.467	0.300	0.285
3.348	0.454	0.281	0.210
2.793	0.336	0.292	0.285
2.790	0.343	0.299	0.265
2.590	0.336	0.281	0.248
2.220	0.239	0.275	0.255
2.072	0.254	0.319	0.272
2.034	0.206	0.265	0.260
1.949	0.221	0.268	0.232
1.880	0.214	0.283	0.218
1.840	0.183	0.305	0.270
1.811	0.181	0.280	0.280
1.810	0.212	0.284	0.286
1.740	0.196	0.240	0.238
1.699	0.173	0.250	0.240
1.600	0.178	0.288	0.247
1.575	0.172	0.280	0.278
1.547	0.149	0.256	0.255
1.478	0.160	0.280	0.252
1.374	0.136	0.299	0.245
1.342	0.130	0.266	0.255
1.331	0.128	0.288	0.205
1.290	0.137	0.238	0.262
1.238	0.134	0.292	0.229
1.180	0.117	0.283	0.220
1.129	0.125	0.270	0.265
1.113	0.113	0.257	0.200
1.070	0.120	0.263	0.266
1.040	0.110	0.252	0.255
1.009	0.112	0.322	0.255
0.997	0.118	0.280	0.210
0.887	0.101	0.293	0.230
0.860	0.103	0.312	0.255
0.850	0.101	0.275	0.270
0.810	0.091	0.265	0.238
0.751	0.093	0.260	0.240
0.706	0.085	0.281	0.252
0.605	0.081	0.279	0.252
0.520	0.085	0.281	0.260
0.461	0.077	0.256	0.230
0.439	0.083	0.279	0.260
0.380	0.075	0.281	0.264
0.290	0.077	0.260	0.244

Table 6.3

EXPERIMENTAL DATA FOR FINE COAL (0.5-2mm)

Mean Velocity U_m (m/s)	Hydraulic Gradient i_m (m water/ m pipe)	Volumetric Solid Concentration C_s in-situ	Volumetric Solid Concentration C_d delivered
3.220	0.593	0.359	0.350
2.870	0.412	0.357	0.350
2.420	0.354	0.365	0.374
2.360	0.354	0.383	0.350
2.180	0.324	0.366	0.374
1.900	0.264	0.367	0.320
1.830	0.264	0.367	0.350
1.540	0.217	0.335	0.318
1.410	0.183	0.394	0.370
1.380	0.196	0.335	0.320
1.230	0.174	0.369	0.350
1.150	0.160	0.353	0.318
1.050	0.159	0.405	0.350
1.040	0.151	0.348	0.320
0.970	0.135	0.372	0.333
0.960	0.143	0.377	0.374
0.952	0.138	0.394	0.330
0.943	0.138	0.337	0.318
0.910	0.139	0.408	0.325
0.870	0.134	0.329	0.318
0.810	0.128	0.338	0.318
0.780	0.127	0.354	0.340
0.770	0.117	0.330	0.330
0.720	0.120	0.329	0.350
0.720	0.118	0.357	0.318
0.690	0.119	0.349	0.320
0.620	0.114	0.365	0.320
0.570	0.110	0.325	0.320
0.480	0.114	0.357	0.350
0.460	0.112	0.342	0.318
0.430	0.117	0.363	0.318
0.415	0.112	0.335	0.318
0.380	0.112	0.355	0.318
0.330	0.108	0.352	0.325
0.310	0.110	0.390	0.318
0.230	0.112	0.345	0.340
0.220	0.110	0.351	0.318
0.210	0.104	0.362	0.333
0.150	0.103	0.333	0.321

Table 6.4

EXPERIMENTAL DATA FOR MIXED COAL (0.5-4mm)

Mean Velocity U_m (m/s)	Hydraulic Gradient i_m (m water/ m pipe)	Volumetric Solid Concentration C_s in-situ	Volumetric Solid Concentration C_d delivered
3.400	0.713	0.370	0.326
3.120	0.518	0.322	0.314
2.820	0.493	0.356	0.326
2.694	0.455	0.437	0.350
2.330	0.374	0.319	0.323
2.311	0.358	0.393	0.332
2.300	0.384	0.467	0.384
2.106	0.306	0.390	0.335
1.965	0.290	0.363	0.365
1.950	0.283	0.388	0.347
1.900	0.280	0.468	0.375
1.827	0.259	0.341	0.304
1.810	0.248	0.384	0.359
1.650	0.205	0.399	0.344
1.611	0.215	0.366	0.329
1.600	0.200	0.373	0.360
1.591	0.214	0.434	0.332
1.587	0.201	0.434	0.367
1.521	0.192	0.406	0.323
1.460	0.188	0.346	0.319
1.410	0.172	0.384	0.364
1.370	0.184	0.385	0.341
1.344	0.162	0.362	0.310
1.323	0.169	0.393	0.365
1.305	0.174	0.370	0.332
1.226	0.159	0.380	0.353
1.220	0.153	0.350	0.317
1.155	0.138	0.384	0.372
1.078	0.142	0.401	0.332
1.034	0.122	0.392	0.346
0.986	0.119	0.346	0.301
0.983	0.132	0.370	0.352
0.976	0.134	0.406	0.319
0.929	0.123	0.363	0.341
0.817	0.112	0.378	0.352
0.810	0.107	0.351	0.299
0.723	0.112	0.385	0.344
0.650	0.100	0.358	0.352
0.645	0.100	0.350	0.366
0.552	0.096	0.397	0.362
0.499	0.104	0.391	0.342
0.492	0.095	0.369	0.310
0.490	0.101	0.347	0.314
0.483	0.099	0.369	0.361
0.426	0.103	0.402	0.370
0.386	0.097	0.382	0.280
0.352	0.104	0.443	0.339
0.325	0.099	0.443	0.359
0.322	0.108	0.437	0.341
0.311	0.094	0.372	0.344
0.292	0.096	0.375	0.323
0.260	0.100	0.354	0.249
0.230	0.107	0.391	0.365
0.190	0.102	0.385	0.342

6.1.2 Effect of Volumetric Slurry Concentration and Particle Size Distribution on the Experimental Results

The effect of solids concentration on the hydraulic gradient is shown in Figure 6.4. Previous workers have shown an increased pressure gradient with increasing solid concentration. This is also observed in the high velocity range in this work, i.e. above the velocity where heterogeneous suspension is predicted. However, an interesting result has been found below the suspension velocity. The hydraulic gradient for the transport of mixed coal (C_s = 0.39) is less than the value for fine coal (C_s = 0.36) even though the solids concentration and mean particle diameter of the former is larger. This is a very significant finding since it suggests the possibility of transporting a high concentration slurry at a low pressure gradient with consequent reduction in the specific energy consumption. The mechanistic behaviour of mixed slurries probably depends upon many other parameters, though the only important difference between the mixed slurry and the fine and coarse coal slurries was the well graded wide size distribution.

The effect of wide size distribution was also observed when the free and pack settled concentrations of mixed size slurry were measured and found to be higher than for fine size slurry (see Appendix B Table B.II).

It appears that particle size distribution has a pronounced effect on the hydraulic gradient of coarse coal slurry transportation.

Kazanskij et al (28) have also found that the addition of fine particles to a sand-water mixture can reduce the pressure drop by 30% at low velocity.

6.2 Comparison of the Experimental Results with Two-Layer Model Predicton

6.2.1 Introduction

In order to obtain a mechanistic understanding of the experimental results, four different theoretical approaches to the two-layer model were studied.

1. The basic two-layer model attributed to Wilson (49) (designated the BASIC model) assumes that the upper layer is free of particles and a moving bed of solids exists in the lower layer.

2. The modified two-layer model similar to Televantos (40) (designated the MODIFIED model) is similar to the basic model except that the fluid shear stress in the lower layer is determined by using the mixture density to account for the existence of the particles in the carrier fluid.

3. The two-layer model derived in this work (designated the DERIVED model) assumes the existence of suspended particles in the upper layer and moving bed flow in the lower layer and allows prediction of the threshold and suspension velocity of the slurry.

4. Doron et al (12) have recently published another modified two-layer model (designated the DORON model) which assumes heterogeneous suspension in the upper layer and bed flow in the lower layer.

The differences between these four approaches are shown schematically in Figures 5.1, 5.2 and 6.33.

6.2.2 Results of the Basic & Modified Two-Layer Model Analysis

The solid lines shown on Figures 6.11 to 6.13 give the pressure gradient as predicted by the basic Wilson two-layer model as described in 5.3. The computational procedure described in Appendix C was used to predict the pressure gradient and the fit of the experimental points is excellent especially at low velocity (below 1m/s) for all the coal samples. However, the fit is less satisfactory at higher velocity especially for the coal samples containing fine particles in suspension (see Figures 6.12 and 6.13).

The modified two-layer analysis for dense phase flow (described in Section 5.4) gives a very satisfactory prediction of the pressure gradient for the entire velocity range for both fine and mixed coal. These predictions are shown as a solid curve in Figures 6.14 and 6.15.

To obtain a mechanistic understanding of these models, it is crucial to perform a sensitivitiy analysis to assess the significance of the parameters used. The analysis is based on the application of the basic model for coarse coal and modified model for fine and mixed coal.

6.2.3 Sensitivitiy Analysis on the Parameters Used in the Model

6.2.3.1 Frictional Forces

There are two distinct frictional forces to be considered in the pipe flow analysis of a moving bed of solids. Firstly, there is frictional drag by the particles on the fluid and the wall and, secondly the effect of fluid frictional forces on the wall and on the particles.

As relative motion occurs between the particles, then a frictional resistance is set up within the moving bed of solids. The internal resistance of the particles to shear and stress at the wall are related to the intergranular shear stress normal to the surface and equal to

$\tau_{12}/\tan\phi$ where ϕ is the internal angle of friction.

The internal angle of friction used in all calculations was 59^{o} (52), however a variation of ϕ from 20^{o} to 65^{o} did not have a significant effect on the prediction of the pressure gradient. This is shown in Figure 6.16 typically for fine coal particles at a velocity of 1.2m/s.

The particulate shear stress at the wall is given by $F_n . \mu_p$ where F_n is the normal force at the pipe wall due to the bed of solids and μ_p is the coefficient of sliding friction (i.e. $\frac{\text{Force}}{\text{Load}}$). The value of μ_p is rarely constant in these systems. In general, it has been suggested (6) that the value of μ_p is independent of velocity and does not change as the mean slurry velocity changes. Motamedi (32) has found that the coefficient of friction is rarely constant but depends on the mechanical and interfacial rheology of the specific material making up the bed deposit. The most important factor governing the value of μ_p is the bed load concentration, i.e. the number of grains in contact per unit area. Motamedi (32) experimentally measured the coefficient of sliding friction for Bagworth coal and found a value of 0.4 ± 0.1 in most cases, though the value of static friction was 20% higher.

The value of the coefficient of sliding friction between the particles and the wall has a pronounced effect on the prediction of the two layer model. The effect of increasing the value of μ_p is to increase the pressure gradient. For design purposes the value assigned to the friction coefficient is therefore of great importance. The μ_p values used were predicted by trial and error using the two-layer model and they are within the range measured by Motamedi. A value of 0.42 was used for coarse coal, and values of 0.48 and 0.39 were taken for fine and mixed coal respectively. These values are greatly dependent on the interfacial rheology and the concentration of these suspensions.

In the model the value of the particulate shear stress, τ_{s2} is very dependent on μ_p and bed concentration though less dependent on mean slurry velocity. Thus τ_{s2} does not change significantly even though this is an important parameter in the model. The interfacial shear stress, τ_{12}, is very small and therefore does not have a significant effect on the model prediction. The frictional force of the particles on the fluid, FFP, is a function of fluid wall shear stress, τ_2, interfacial shear stress (τ_{12}) and particulate shear stress, τ_{s2}. Neither τ_2 nor τ_{12} change significantly with velocity, so that the fluid wall shear stress is the important variable factor. The model shows that the wall shear stress is very small at low velocity compared to the particulate shear stress indicating that the flow behaviour is dominated by particulate friction. The fluid wall shear stress becomes more significant as the velocity increases. This explains the significance of the effect of μ_p at low velocity and particle density at higher velocity and why the theoretical prediction of the pressure gradient agrees very well with experimental data at low velocity. As the velocity is increased it was found that the pressure gradient could be better correlated by taking into account the effect of the density of the slurry on the fluid wall shear stress. The effect was pronounced in the case of slurries having fine particles in suspension. This correction was not needed for the coarse coal sample since the slurry was almost free of suspended fine particles.

6.2.3.2 Effect of Other Parameters

The model was also used for the prediction of the interface between the two layers, i.e. the half angle β . The model shows that the value of the half angle β decreases as the velocity increases. At low

velocity the value of β approaches the full pipe and the bed concentration approaches the in-situ solids concentration. As the velocity increases the value of β decreases initially and then reaches a constant value and bed concentration approaches the packed concentration. This was predicted by Televantos et al (41). The location of the interface is not constant and changes with velocity. The variation of the predicted β value with velocity for three coals is plotted on Figure 6.17. A possible explanation for the decrease of values with velocity is that turbulent eddies occur as the velocity increases and the high differential velocity between the two layers decreases the bed depth. Unfortunately it was not possible to make independent measurement of the bed depth.

The variation of mean particle diameter, d_{50}, did not effect the prediction significantly either.

The basis two-layer model has satisfactorily predicted the pressure gradient for coarse coal and the modified two-layer model for fine and mixed coal. However, the prediction of the existence of two distinct layers in the entire flow range is rather unrealistic especially at high velocity. It is more likely that the bed depth will get smaller and eventually all the particles will be suspended as velocity increases.

The reason that this model continues to predict a decreasing value of β is due to problems in the mathematical convergence of the computations and the basic assumptions used. Therefore, the model does not rigorously validate the mechanistic behaviour of the particles at high velocity.

6.2.4 Analysis of the Velocity Effect

At low velocity the value of the fluid wall shear stress is very small so that the frictional drag force, FFP, is dominated by the magnitude of the particle shear stress. If one assumes that there is no fluid turbulence affecting the transport and the pipe is almost full of settled solids with bed concentration equal to the in-situ solid concentration, then the value of the pressure gradient is dominated by the term $2\ \mu_p(S-1)C_s$. This term is deduced by simplification of the two-layer model at low velocity.

The value of β approaches π and therefore $\tau_{12} = 0$ and $S_2/A_2 = 4/D$.

Also, the particle shear stress becomes

$$\tau_{s2} = (\rho_s - \rho)\ C_s\ D/2\ \ g\mu_p$$

and the fluid shear stress can be obtained from

$$\tau_{f2} = 0.046 \left(\frac{\rho U_m D}{\mu} \right)^{-0.2} (\rho_m/2) U_m^2 \qquad 6.2$$

The pressure gradient $i_m = \left(\frac{\tau_{f2} + \tau_{s2}}{g\rho}\right) S/A$ can be simplified as follows:-

$$i_m = \frac{\tau_{f2}}{\rho g}\ S/A + 2(S-1)\ \mu_p\ C_s \qquad 6.3$$

At low velocity, the value of τ_{f2} in equation 6.3 approaches zero as $U_m \rightarrow o$

. Therefore

$$i_m = 2(S-1) \mu_p C_s \qquad 6.4$$

This value has been predicted and used by many workers and agrees well with the present experimental results (see Table 6.8).

As the velocity increases, turbulent eddies suspend some fine particles and therefore the bed height decreases. This decrease in the bed height is shown in Figure 6.17. The slurry is now transported in two layers; an upper layer with fine particles in suspension at much higher velocity as observed by Televantos (40), and a lower layer with a moving bed of particles at higher concentration. This is the transition domain between the full pipe condition with a bed of particles moving wholly in contact load with no intergranular movement and a moving bed with some shear movement on the top layer of the bed section and the rest of the bed moving with no intergranular movement.

As the velocity increases further, the fluid shear stress increases and turbulent eddies will suspend more particles until all the particles are suspended and there is no relative velocity, U_r, between the solids and liquid, i.e. $U_{f2} = U_{s2}$ or hold-up velocity is equal to one. At this velocity we have a heterogeneous suspension with all the particles fully suspended. The mean slurry velocity at which U_r is zero is obtained by analysing the two-layer model and the values are given in Table 6.9 for each coal sample.

Above this velocity, the two-layer model assumption is not strictly valid, nevertheless the model still predicts values of the pressure gradient similar to the experimental points.

Table 6.8 Tabulated Hydraulic Gradient at the Point of Slip

Coal Size d_{50} (mm)	Mean in-situ Solid Concentration C_s	Coefficient of Friction μ_p	i_m calculated from Equation 6.4	i_m from experimental result at low throughput velocity
0.975	0.358	0.48	0.113	0.11 $\pm$ 0.001
1.9	0.39	0.38	0.097	0.099 $\pm$ 0.001
3.25	0.269	0.42	0.074	0.074 $\pm$ 0.001

Table 6.9 Predicted Suspension Velocity using Modified Two-Layer Model

Coal Size	d_{50} (mm)	Threshold Velocity predicted by Derived Model	Suspension Velocity predicted by Derived Model	Suspension Velocity predicted by analysis of Basic & Modified Model results
Coarse	3.25	1.26	1.72	1.4 - 1.6
Mixed	1.9	0.95	1.18	1.1 - 1.2
Fine	0.975	0.96	1.12	1.0 - 1.1

It is extremely unrealistic to have two layers at high velocity especially for coal slurry (solids density near to the fluid density). Because of this contradiction, the model has been used to predict the velocity at which the first particle is suspended, i.e. the threshold velocity, and also the velocity at which all the particles are suspended, i.e. suspension velocity, U_H.

6.2.5 Result of the Derived Model for Prediction of Suspension Mechanism

The derived model is explained in detail in Section 5.5. The predicted pressure gradient using this model has been fitted to the experimental points and is shown in Figures 6.18 to 6.20.

It is obvious that the model is only valid as long as the two layer flow regime exists. The fundamental assumption of the model is that at low velocity the coal slurry is transported in two layer flow with the upper layer having a concentration of $C_1 = 0$ and lower layer having a concentration equal to the settled concentration of the coal sample. As the velocity increases the upper layer is no longer free of particles and the velocity at which the first particle is suspended i.e. the threshold velocity, can be predicted. As the velocity increases further the value of C_1 approaches C_d and the bed depth decreases asymptotically. The prediction of the bed depth or half angle β by this model is plotted against the mean slurry velocity U_m and is shown on Figure 6.21. The value of β gradually decreases with U_m but as particles start to suspend there is a sudden almost asymptotic decrease to zero as predicted. The behaviour of the model is shown in Figure 6.21 very clearly. The first sudden decrease correlates with the threshold velocity U_T and the second decrease of β approaches the suspension velocity U_H asymptotically. These predicted velocity values are also

tabulated in Table 6.9.

These results are extremely interesting since they predict, as expected, that the fine and mixed coal samples start to suspend at a lower velocity than coarse coal.

The value of the suspension velocity predicted by this derived model and the result of U_H obtained by analysing the basic and modified two-layer model (given in Table 6.9) are in excellent agreement.

The improved model readily predicts the threshold and suspension velocities for the design of slurry transportation and identifies the limit of validity of the two-layer approach.

When slurry is transported as a heterogeneous suspension the pressure gradient can be predicted by treating the suspension as a single phase fluid and using the Blasius equation. The viscosity of the slurry is calculated using the Thomas empirical equation (21).

$$\mu_m = [1 + 2.5C_s + 10.05C_s^2 + 0.00273\, e^{16.6C_s}] \qquad 6.5$$

The threshold and suspension velocities have been compared using the empirical correlations presented by Spells, Durand, Newitt, Zandi and Govatos.

The threshold velocity was calculated using Equation 2.12 for three coal sizes; the hindered settling velocity was obtained by using the Richardson and Zaki (35) expression (details are given in Appendix B) and the drag coefficient was calculated using the Massey graph (29).

Equations 2.16, 2.17 and 2.18 were used to calculate the suspension velocities for the three coal slurries. These calculated results are given in Table 6.10.

Table 6.10 Calculated Threshold and Suspension Velocities using Empirical Correlation

Coal Particle		Hindered Settling Velocity U_t	Drag Coefficient C_D	Velocity (m/s)			
				Threshold U_T	Suspension U_H		
	d_{50} (mm)	(m/s)		Spells Equ. 2.12	Zandi Equ. 2.16	Durand Equ. 2.17	Newitt Equ. 2.18
Coarse	3.25	0.083	1.1	0.102	0.74	2.32	1.15
Mixed	1.9	0.026	1.2	0.017	1.41	1.48	0.78
Fine	0.975	0.014	2.0	0.009	0.72	1.29	0.64

Comparison of Tables 6.9 and 6.10 shows that the threshold velocity predicted by Spells is rather low and there is a large variation in calculated values of U_H. However, the average value obtained from the Newitt and Durand expressions agrees well with the predicted value of U_H calculated from either of the two-layer models.

6.2.6 Comparison of the Results with Other Work

It is important to apply the model used in the present work to results obtained in other laboratories and to check the validity of the model for different particle sizes, solids concentration and especially for larger pipe diameter and for different solids density.

The validity of the model for different particle density and higher solids concentration is achieved by applying the modified two-layer model to the results obtained by two previous researchers using the same pipeline.

Televantos (40) used the same pipeline and measured the hydraulic conveying of sand-water mixtures, with particle density 2650kg/m^3, mean particle diamter (d_{50}) of 0.295mm, in-situ solids concentration (C_d) of 0.538 and delivered solids concentration of (C_d) of 0.481. He obtained rather high in-situ volumetric solids concentrations, invariably higher than the free settled concentration (0.504). He used a simplified form of the two-layer model to analyse his results.

$$i_m = 2\mu_p (S-1) C_s + \frac{\rho_m}{\rho} i \qquad 6.6$$

He assumed that all the solid particles were transported in the sliding bed regime and occupied the entire pipe cross section. The value

of the coefficient of sliding friction for sand particles was 0.51.

The modified two-layer approach has been applied to his results and the predicted pressure gradient agrees very well with the experimental points as is shown by the solid curve in Figure 6.22.

Brown (6) also used the same pipeline and observed the hydraulic behaviour of sand particles having a mean particle diameter (d_{50}) of 0.32mm, average in-situ solids concentrations (C_s) of 0.481 and average delivered solids concentration (C_d) of 0.466. He analysed his results in much the same way as Televantos.

Figure 6.23 shows the result of applying the present modified model to Brown's results and the predicted pressure gradient line agrees very well with the experimental points. The derived two-layer model was also used to predict the threshold velocity and suspension velocity.

Figure 6.24 shows the variation of β with mean slurry velocity and gives the threshold velocity U_T as about 1.1m/s and the suspension velocity U_H as about 1.8m/s. Brown reported the existence of a distinct two-layer flow regime (clear water and bed load) below a mean velocity of 0.9m/s.

The validity of the model for larger pipe diameter was also determined by applying the model to the results of Gaskell (19). He transported polyester chips of size 4 x 4 x 2mm of density 1340kgm^{-3} in a 50.8mm diameter pipe. Figure 6.25 shows the result of applying the modified model to his experimental results. Unfortunately his results were obtained at variable solids concentration; therefore an average concentration of 0.31 $\pm$ 3% was used for model prediction. the coefficient of sliding friction for polyester ships was 0.27. The predicted pressure gradient agrees reasonably well with the experimental results as seen in Figure 6.25. This figure also shows a comparison of

a similar particle density, mean particle diameter and solid concentration but was transported in a 26mm diameter pipeline.

The comparison shows that at low velocity the pressure gradient essentially depends on the characteristics of the solids, i.e. particle density, size distribution and solids concentration rather than on pipe diameter. However at high velocity the value of the pressure gradient is much reduced in a larger diameter pipeline.

The modified two-layer model can be applied satisfactorily to predict pressure gradient at high concentrations, increased solids density and in larger diameter pipe flow.

6.2.7 Comparison of the Results with Doron Improved Two-Layer Model

Doron et al (12) have adapted the two-layer model in order to predict the mean concentration and concentration profile of suspended particles in the upper layer. They have assumed the existence of a heterogeneous suspension in the upper layer and a freely settled bed of particles in the lower layer. Particle interchange between the upper and lower layer at high velocity is attributed to turbulent eddies.

In addition to the usual conservation equations they used the diffusion equation to drive the dispersion mechanism of the solid particles in the upper layer. They represented the flow mechanism by a set of five equations as follows.

At steady state, the continuity equations for each layer are:

for the solid phase

$$U_1 C_1 A_1 + U_2 C_2 A_2 = U_m C_s A \qquad 6.7$$

for the liquid phase

for the liquid phase

$$U_1(1-C_1)A_1 + U_2(1-C_2)A_2 = U_m(1-C_s)A \qquad 6.8$$

The force balance equations for each layer are:

for the upper dispersed layer

$$A_1 \frac{dP}{dx} = -\tau_1 S_1 - \tau_{12} S_{12} \qquad 6.9$$

for the lower bed layer

$$A_2 \frac{dP}{dx} = - F FP - \tau_2 S_2 + \tau_{12} S_{12} \qquad 6.10$$

The following diffusion equation is used to account for turbulent dispersion:

$$\varepsilon' \frac{\partial C^2(y)}{\partial y^2} + U_t \frac{\partial C(y)}{\partial y} = 0 \qquad 6.11$$

where C(y) is the local volumetric concentration in the upper layer, ε' is the local diffusion coefficient and U_t is the particle local terminal settling velocity. The above equation is integrated twice to obtain the solids concentration profile in the upper layer in terms of the mean diffusion coefficient (ε) and hindered terminal velocity (U_t'):

$$C(y) = C_2 \exp\left[- \frac{U_t'}{\varepsilon} (y - y_2)\right] \qquad 6.12$$

where ε' is defined in terms of the shear velocity and the hydraulic radius of the upper layer. Thus

$$\varepsilon' = 0.052\ U^*\ D_{e1}/2$$

where

$$U^* = U_1(f_{12}/2)^{\frac{1}{2}}$$

Integration of equation 6.12 gives the mean solid concentration in the upper dispersed layer in terms of Θ_2 (where $\Theta_2 = \beta - \pi/2$) and γ where the angle γ defines a point in the upper dispersed layer.

$$C_1 = \frac{C_2 D^2}{A_1} \int_{\Theta 2}^{\pi/2} \exp\left[-\frac{U_t' D}{2\varepsilon}\ (\sin\gamma - \sin\Theta_2)\right] \cos^2\gamma\ d\gamma \qquad 6.13$$

where Θ_2, A_1, A_2, S_1, S_{12} and S_2 can all be expressed in terms of the bed height y_2 (see Figure 6.33).

Equations 6.7, 6.8, 6.9, 6.10, and 6.13 can be solved for the five unknown variables: U_1, U_2, C_1, y_2 and i_m given any set of operational parameters for the two phases.

The set of equations can be simplified for different flow regimes, i.e. stationary bed, moving bed and fully suspended flow. However, the value of this work lies in the prediction of the mean dispersed concentration and concentration distribution in the upper layer.

The Doron model has been applied to the present work. The hydraulic gradient predicted by the Doron improved two-layer model for coarse coal

is presented in Figure 6.26. It is shown that the agreement of the model prediction with the experimental results is very good at high velocity but the model overpredicts the pressure gradient at lower velocity. This could be due to the fact that the model predicts the existence of a suspension in the upper layer at low velocity which contradicts our visual observation of the behaviour of a coarse coal suspension. A distinct two-layer bed flow with clear water in the upper layer was visually observed below 0.7m/s.

The model was also employed to predict the hydraulic gradient, mean solid concentration in the dispersed upper layer and the bed interface for fine and mixed size coal. These predictions are presented in Figures 6.27 and 6.28.

The agreement of the hydraulic gradient prediction was reasonably good but the model over-predicts the pressure gradient for fine coal below 0.4m/s. The model failed to predict the pressure gradient above 1.5m/s. After analysing the model parameters individually it was found that the ratio of the upper layer velocity to the lower layer velocity approaches unity at this mean velocity. The continuity equations (Equations 6.7 and 6.8) no longer apply and the model will not converge to calculate the value of the pressure gradient. This is rather interesting, since Doron et al did not predict this discontinuity since they did not examine the validity of their model at solid concentrations greater than 25% (11).

This model is able to predict the mean solid concentration in the upper dispersed layer, C_1, and thus the variation of C_1 in terms of mean slurry velocity is given in Figure 6.29 for the three sizes used in this work. The predicted results show that the value of C_1 is at its highest at low velocity and decreases with increase in velocity until a constant

value is attained. For the case of fine and mixed coal C_1 decreases by about 1.5%. It appears that the model predicts two-layer flow at low mean velocity with the bottom layer moving as a bed of particles with solid concentration C_2 and a suspension of maximum and almost constant mean concentration in the upper layer. This is rather unrealistic since it is expected that more particles suspend in the upper layer as velocity increases until a velocity is reached where all the particles are suspended and the mean solid concentration C_1 approaches the input solid concentration. However, more experimental measurements of the concentration in the upper layer are needed to verify the behaviour of the suspended particles.

Finally, the result of an analysis of all four versions of the two-layer models is presented in one graph for comparison. Figures 6.30, 6.31 and 6.32 show the experimental pressure gradient results for each coal size and the separate theoretical predictions.

It is concluded that the modified two-layer model predicts the pressure gradient extremely well for a dense phase slurry with fine particles in suspension (fine and mixed coal) and the basic two-layer model predicts the pressure gradient well for a coarse particle slurry with no suspension of the fine particles (coarse coal).

The improved model derived here satisfactorily predicts the pressure gradient up to the predicted point of total heterogeneous suspension of particles. Beyond this point the two-layer model does not rigorously apply. The slurry must now be treated as a single phase fluid with the appropriate mixture density and viscosity. Pressure gradient can be predicted using the Blasius equation or other suitable non-Newtonion equation.

The Doron equations predicted the pressure gradient rather well for a mixed coal slurry with a fine suspension in the upper layer. However, the Doron equation fits the pressure gradient data less well at high velocity.

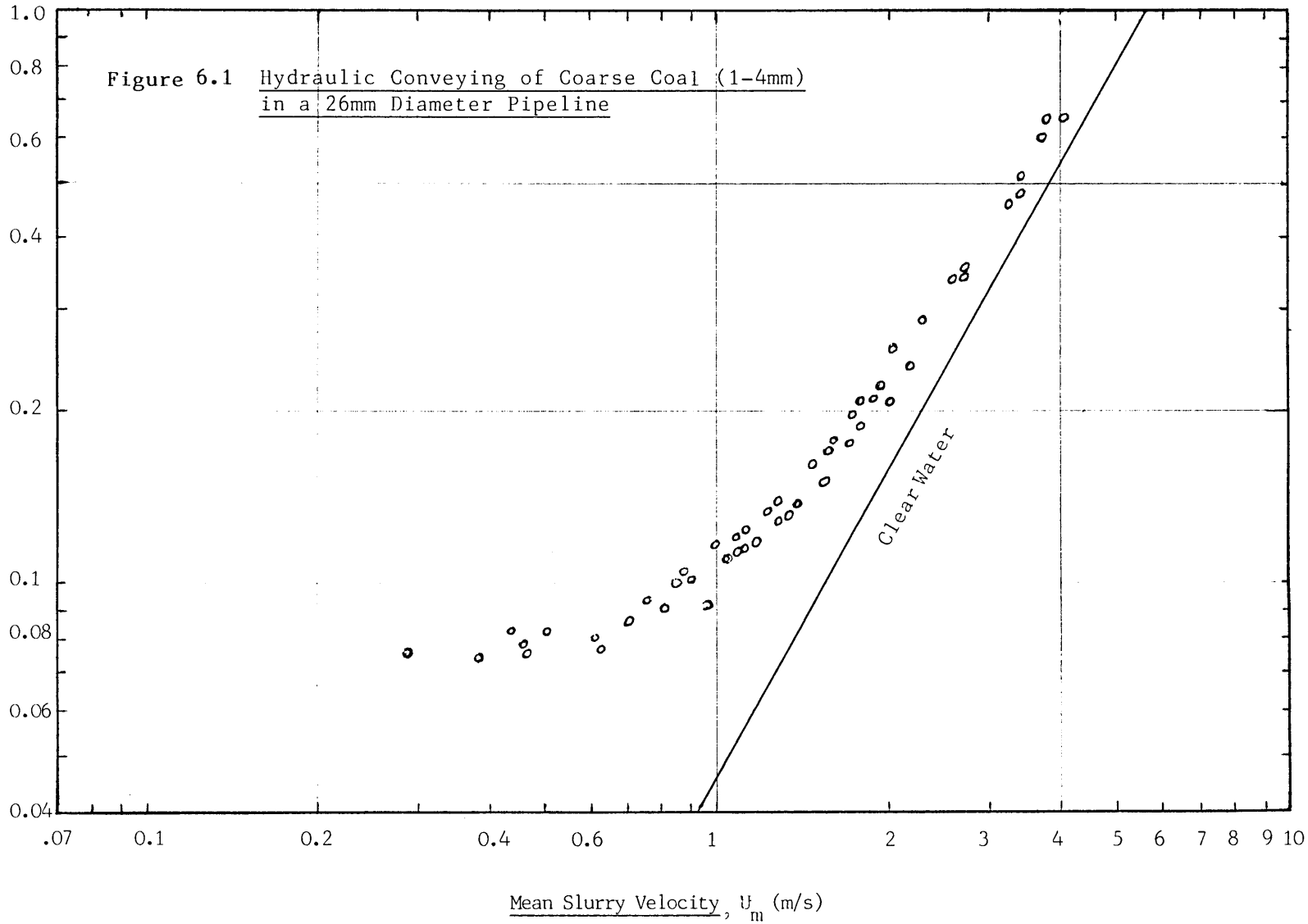

Figure 6.1 Hydraulic Conveying of Coarse Coal (1-4mm) in a 26mm Diameter Pipeline

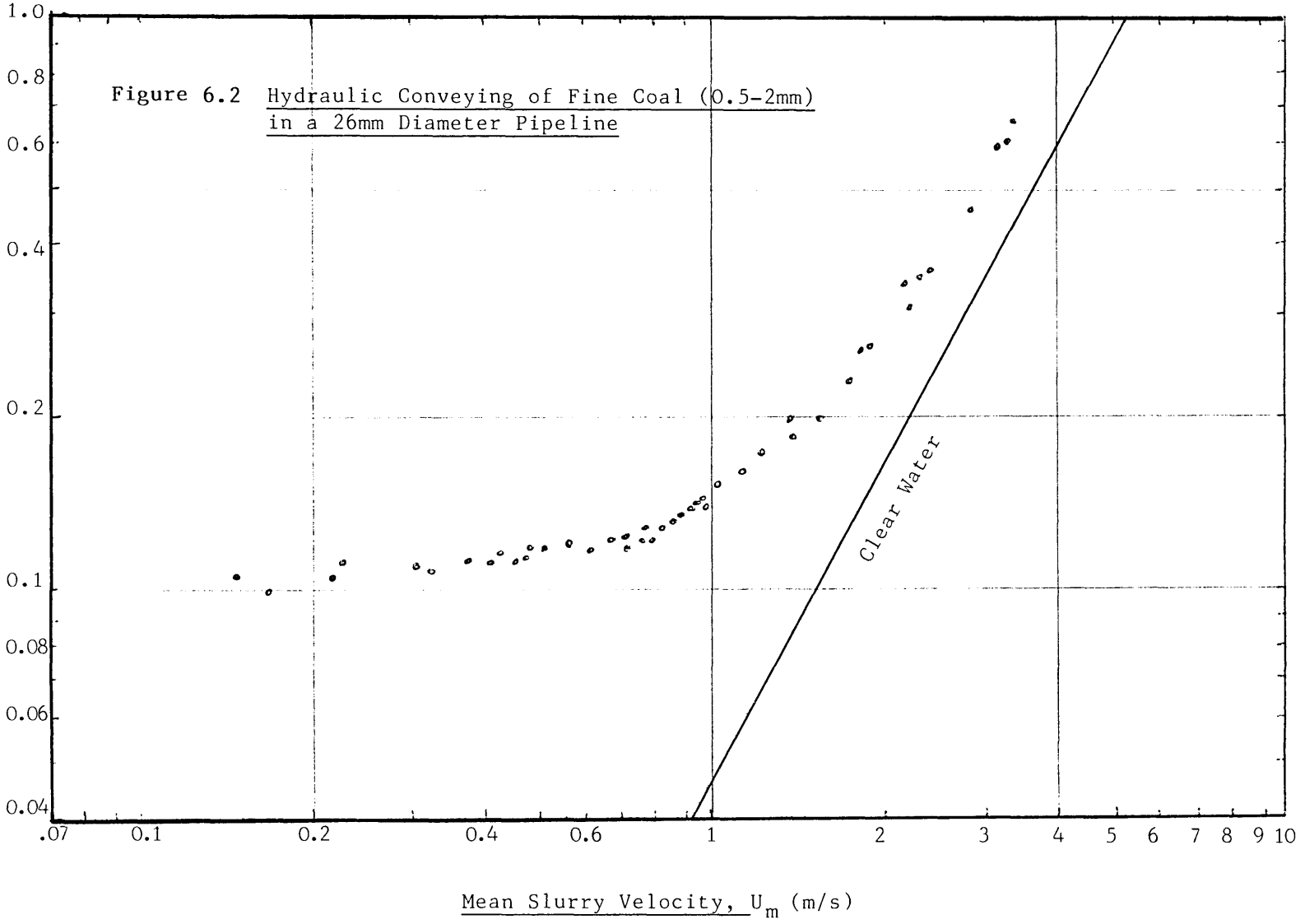

Figure 6.2 Hydraulic Conveying of Fine Coal (0.5-2mm) in a 26mm Diameter Pipeline

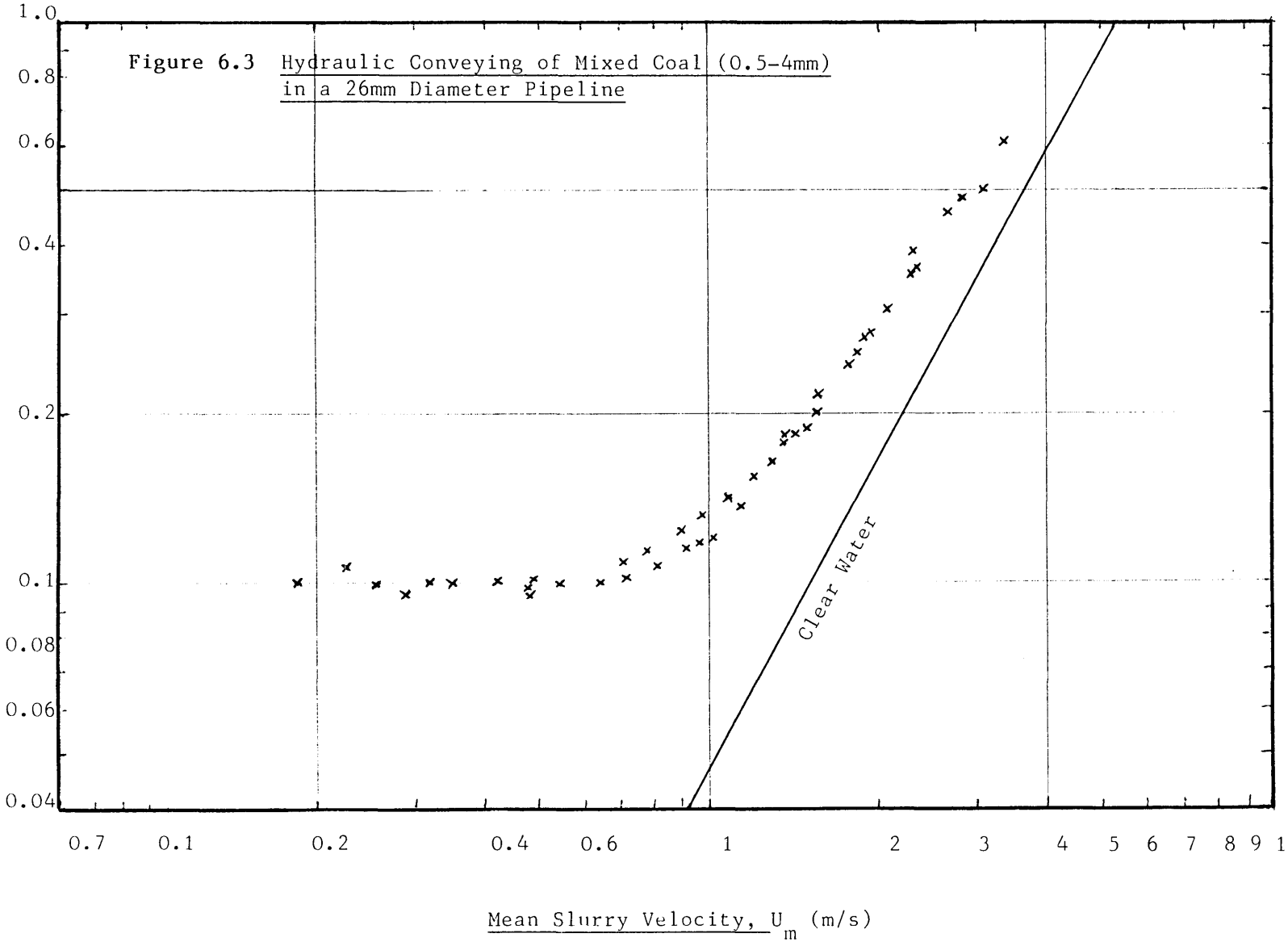

Figure 6.3 Hydraulic Conveying of Mixed Coal (0.5-4mm) in a 26mm Diameter Pipeline

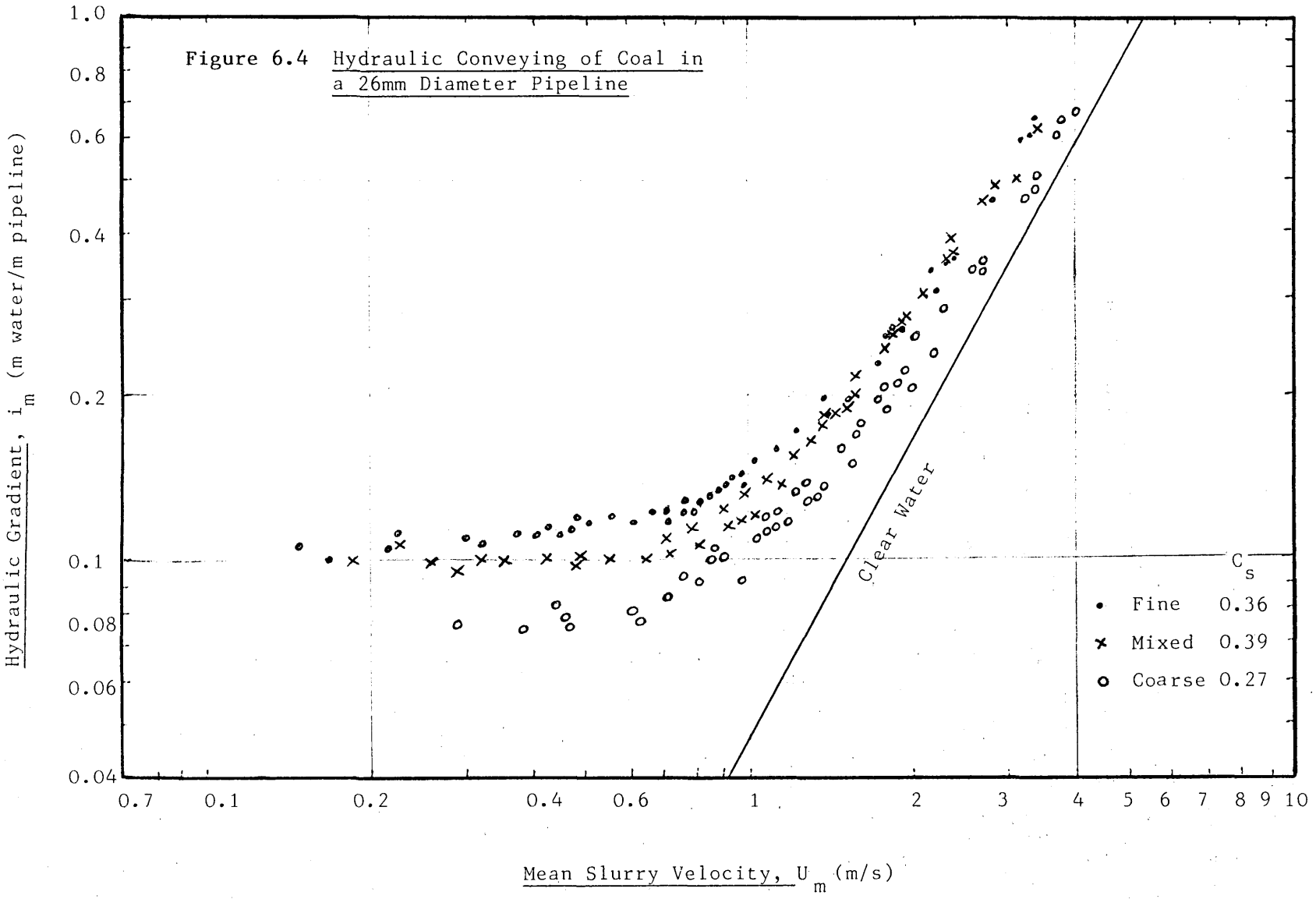

Figure 6.4 Hydraulic Conveying of Coal in a 26mm Diameter Pipeline

Figure 6.5 Sieve Analysis for Coarse Coal

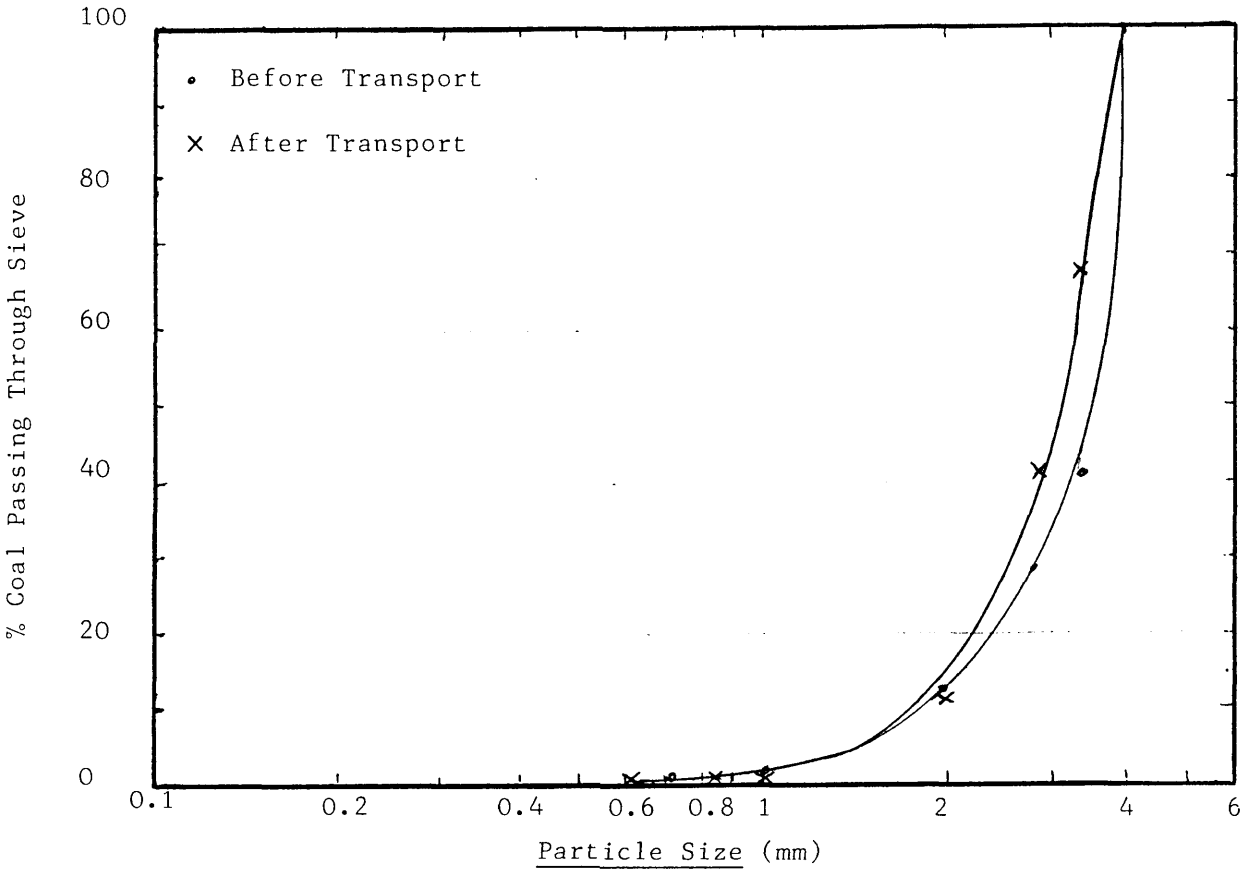

Aperture Size (mm)	% Passing Through Sieve	
	Before Transport	After Transport
4.00	100	100
3.35	41.49	67.43
2.80	28.88	42.21
2.00	12.39	11.03
1.00	1.42	1.27
0.85	-	0.097
0.710	0.11	-
0.60	-	0.062

Table 6.5 Size Distribution for Coarse Coal

Figure 6.6 Sieve Analysis for Fine coal

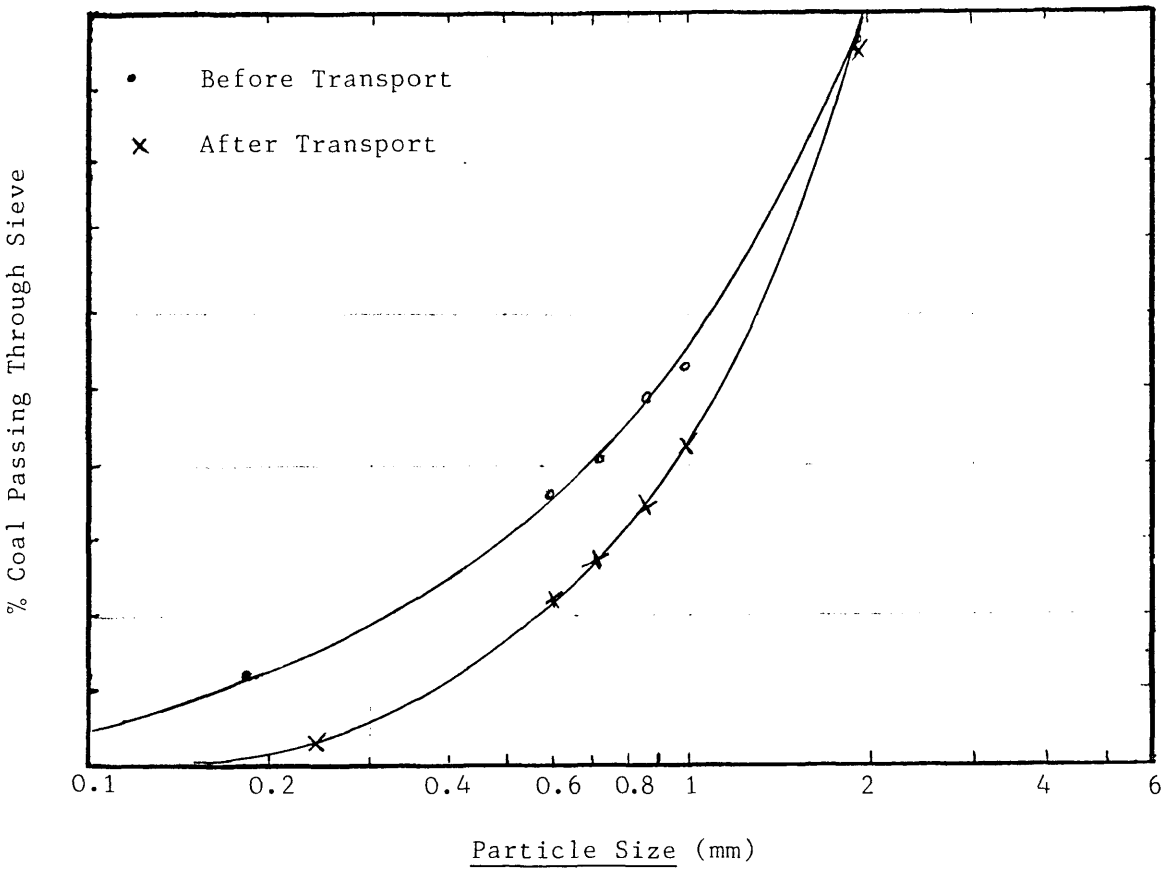

Aperture Size (mm)	% Passing Through Sieve	
	Before Transport	After Transport
2.0	98.05	97.3
1.0	55.20	44
0.85	49.08	35.7
0.91	41.0	27.5
0.60	37.94	24.2
0.25	-	4.4
0.18	12.81	-

Table 6.6 Size Distribution of Fine Coal

Figure 6.7 Sieve Analysis For Mixed Coal

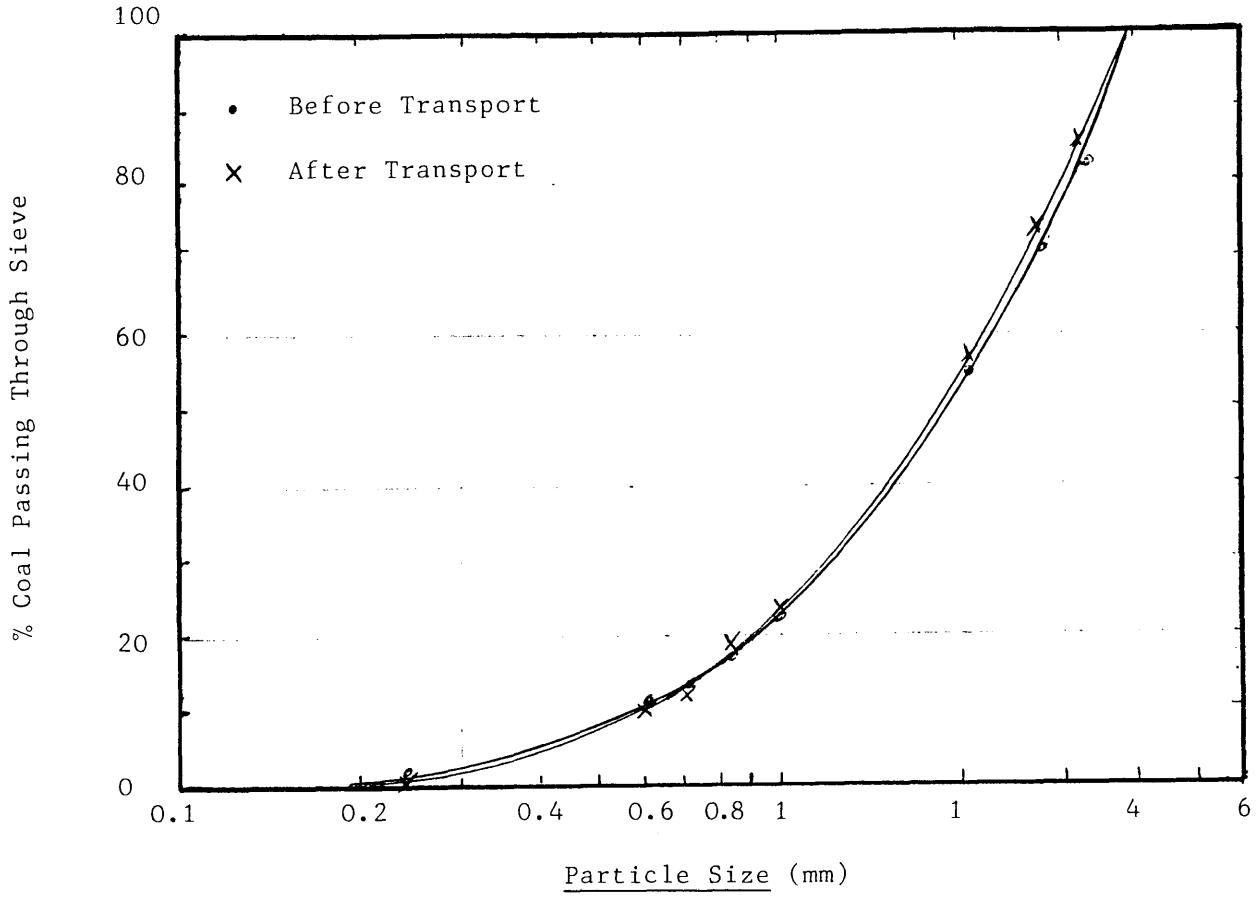

Aperture Size (mm)	% Passing Through Sieve	
	Before Transport	After Transport
3.35	83.4	86.3
2.8	71.5	74.2
2.1	54.4	56.8
1.0	23.7	23.9
0.85	18	17.9
0.91	14	13.5
0.60	12	11.0
0.25	2.2	1.6

Table 6.7 Size Distribution of Mixed Coal

Figure 6.8 Variation of Solid Concentration with Slurry Velocity for Coarse Coal

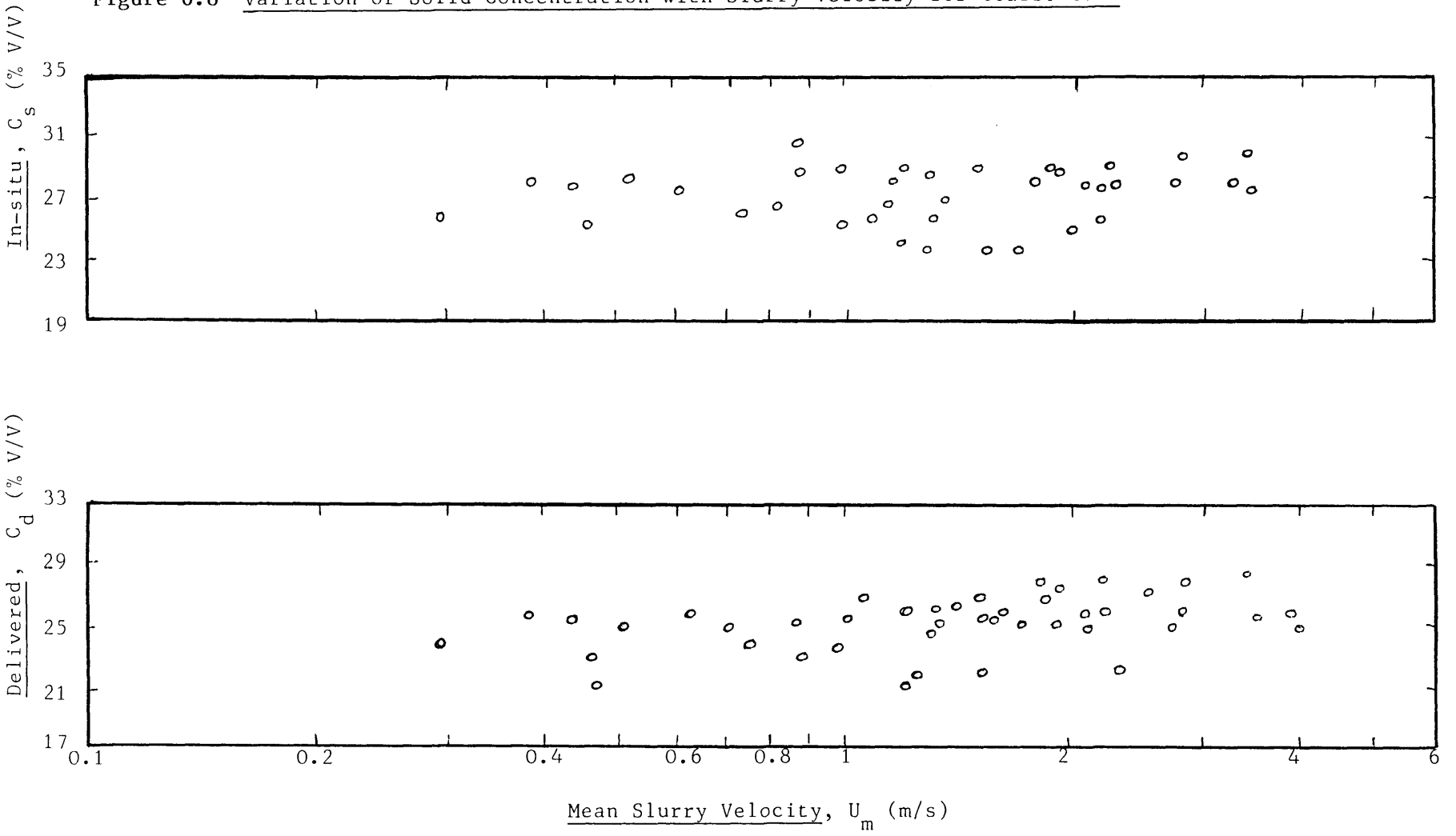

Figure 6.9 Variation of Solid Concentration with Mean Velocity for Fine Coal

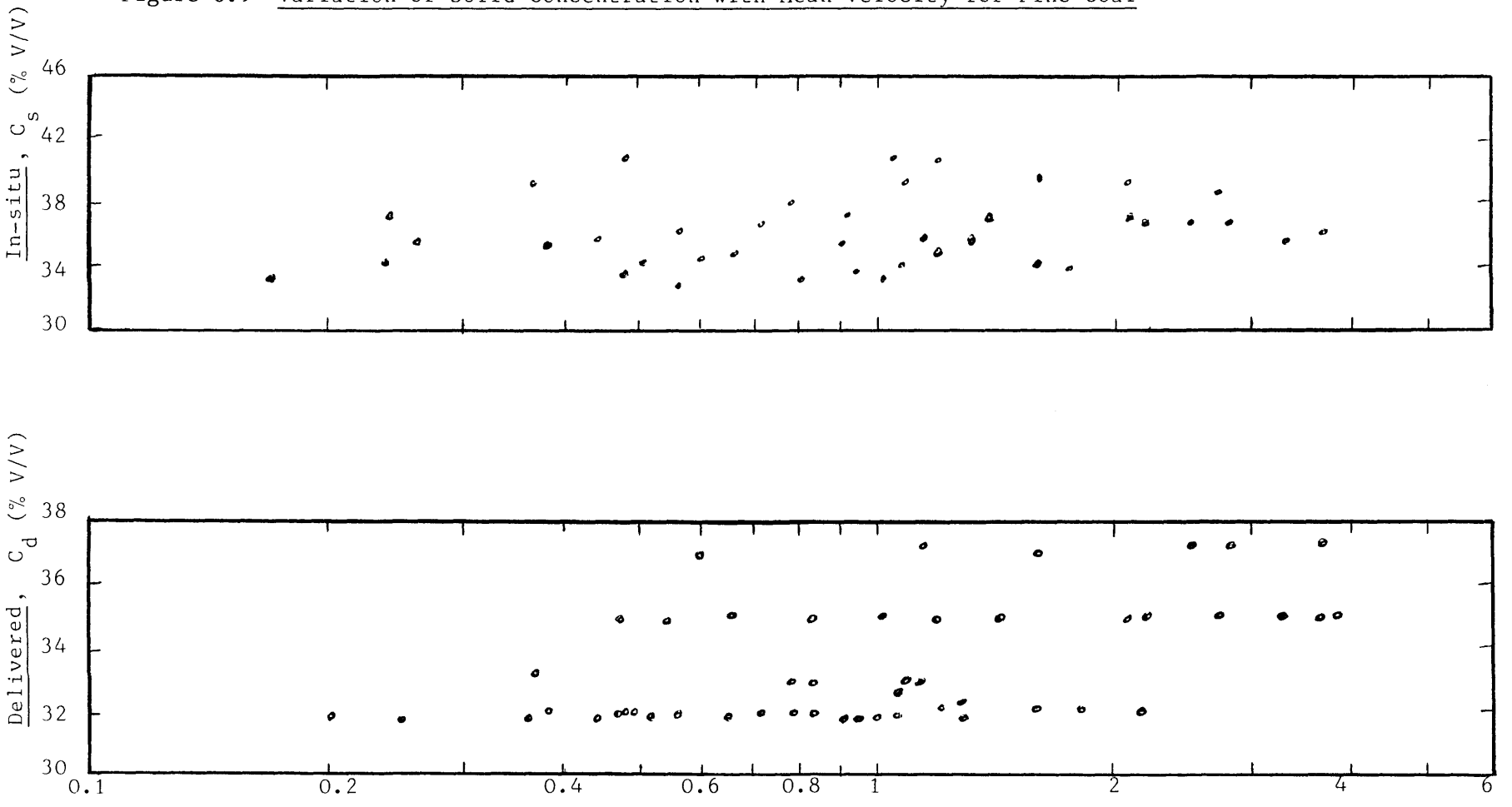

Figure 6.10 Variation of Solid Concentration with Slurry Velocity for Mixed Coal

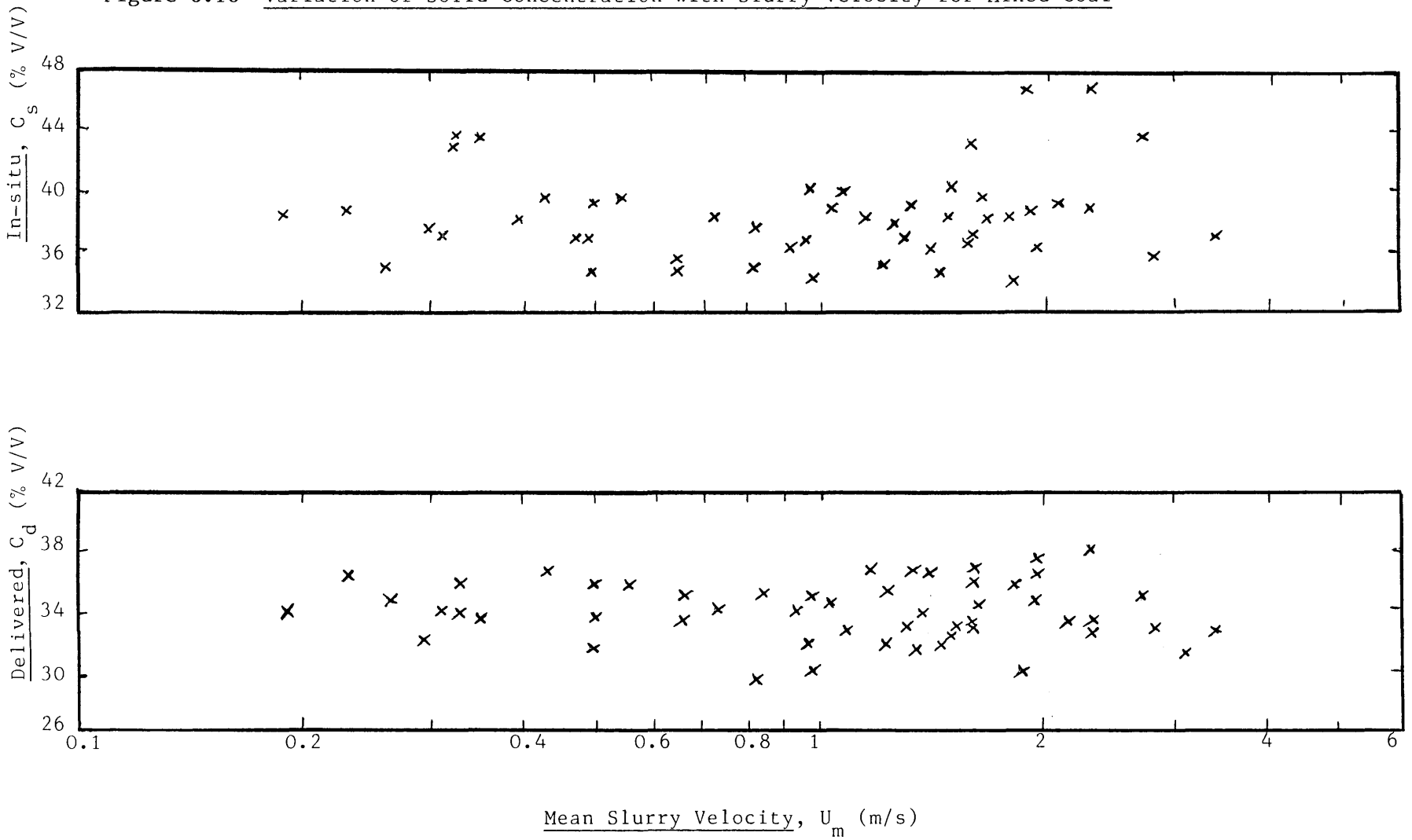

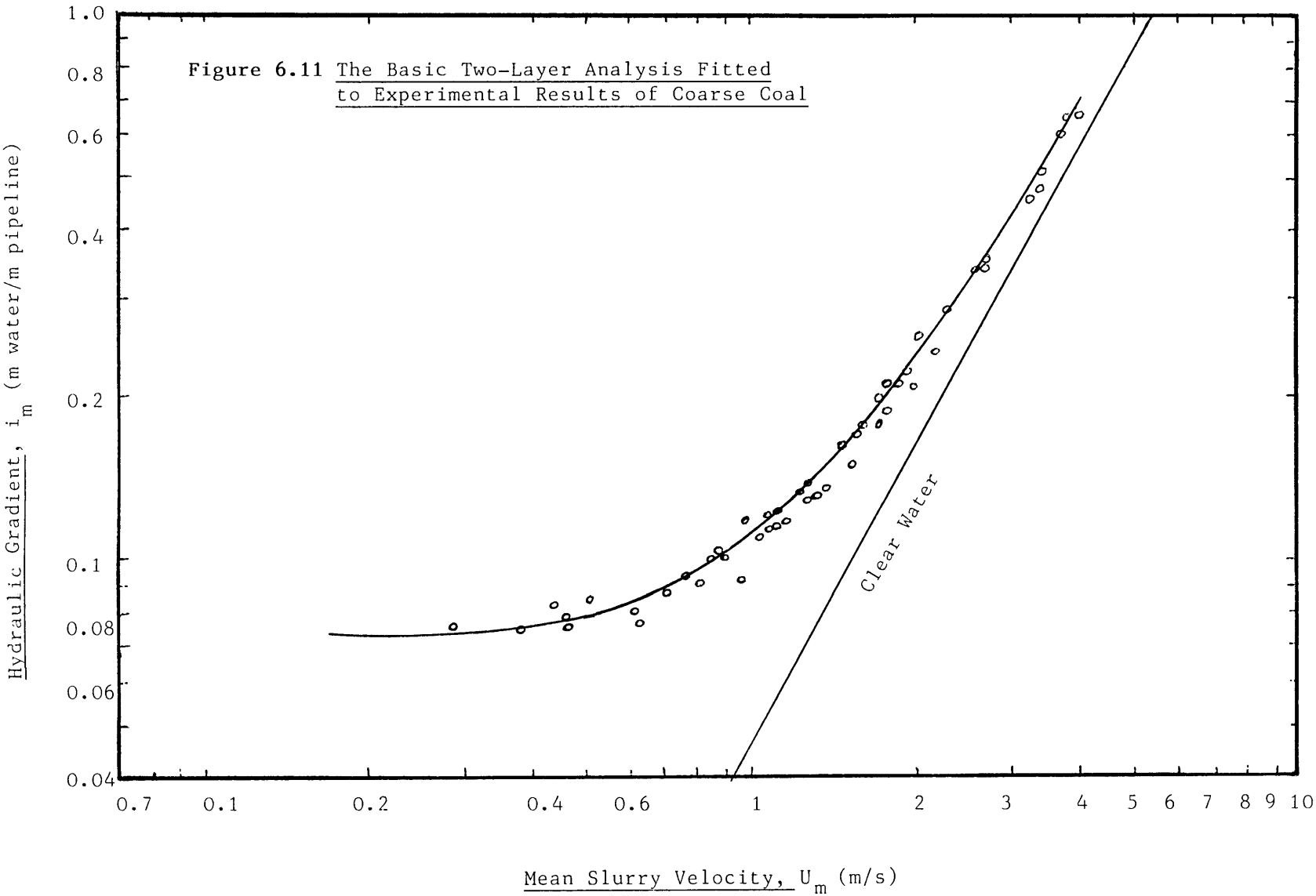

Figure 6.11 The Basic Two-Layer Analysis Fitted to Experimental Results of Coarse Coal

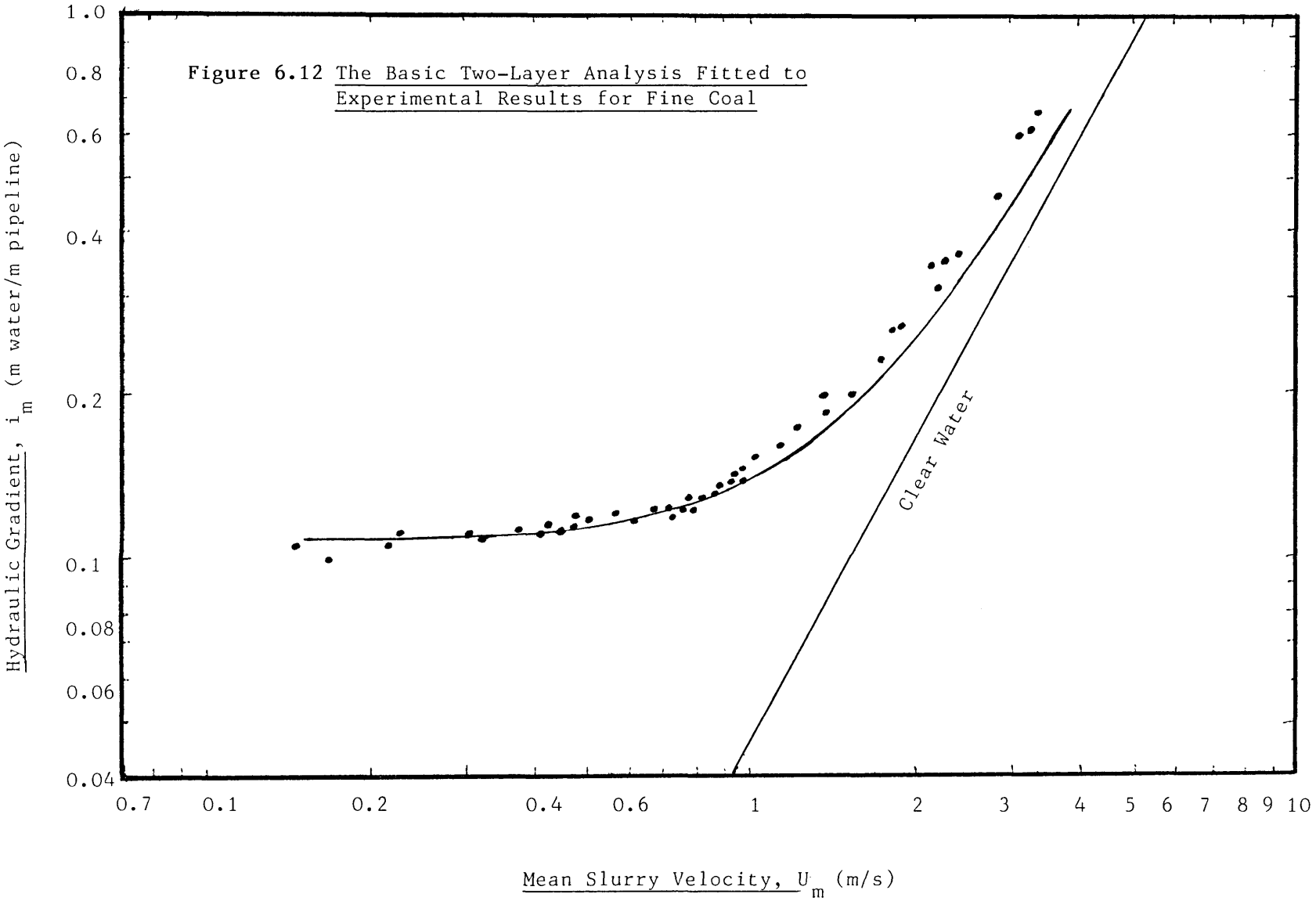

Figure 6.12 The Basic Two-Layer Analysis Fitted to Experimental Results for Fine Coal

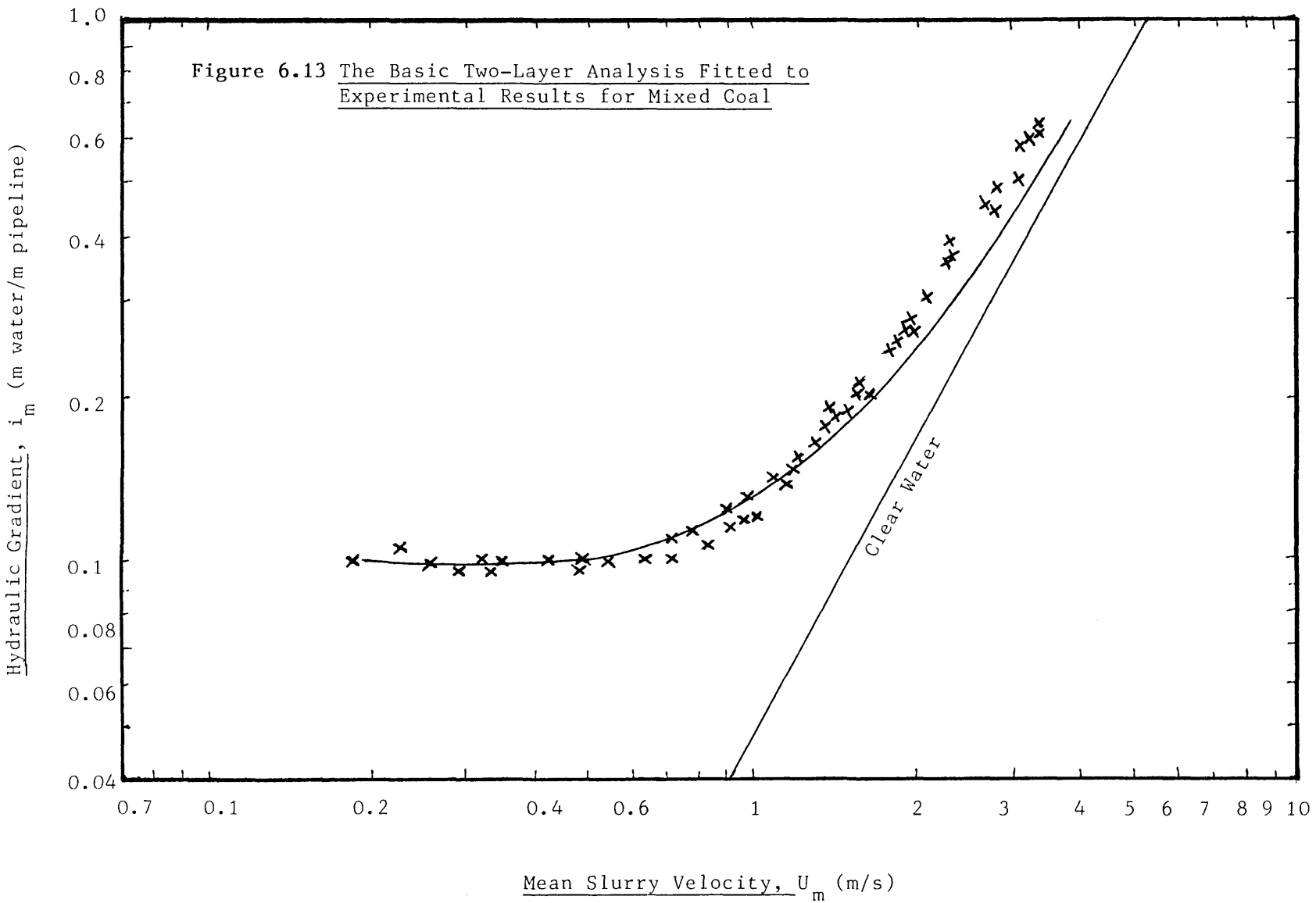

Figure 6.13 The Basic Two-Layer Analysis Fitted to Experimental Results for Mixed Coal

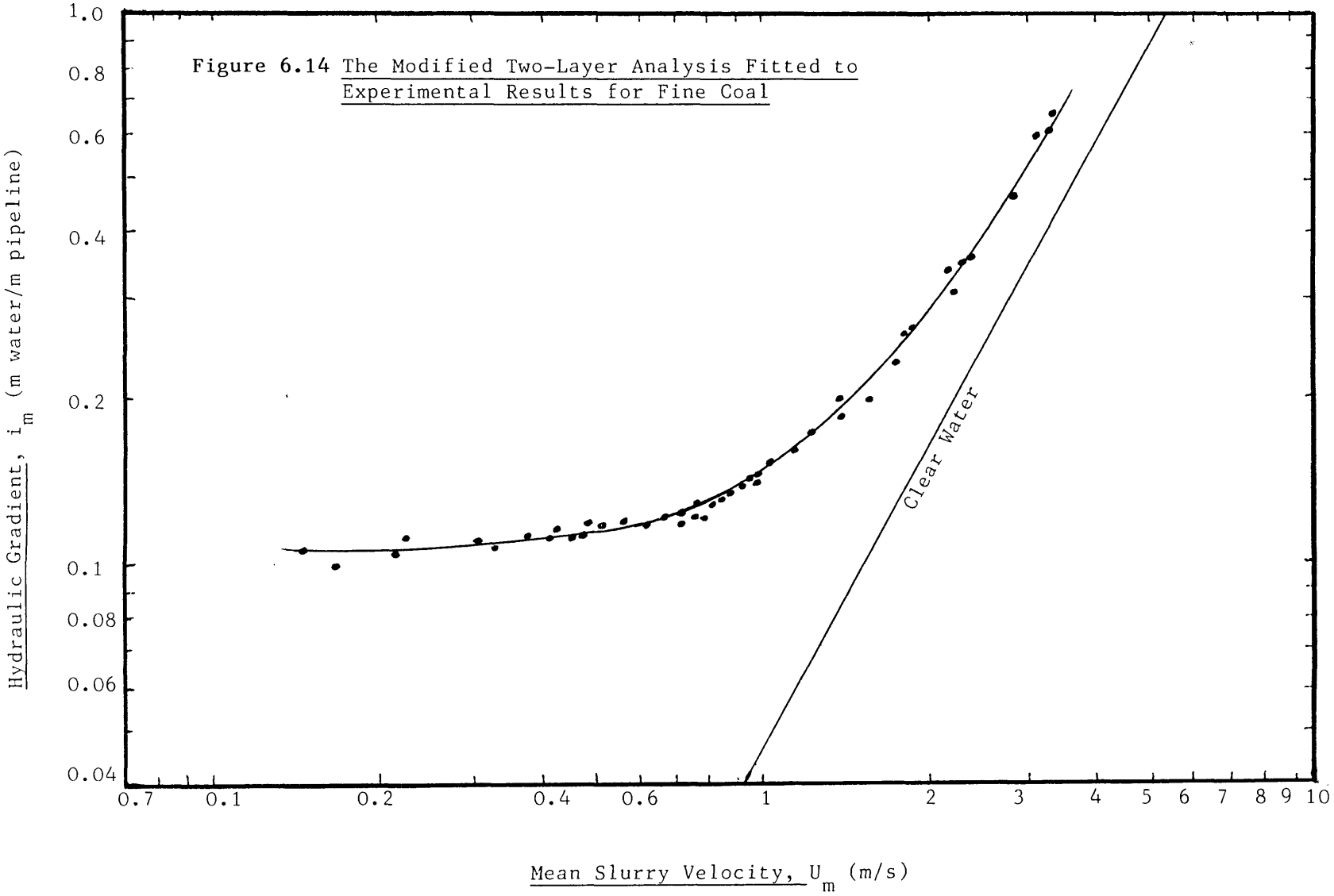

Figure 6.14 The Modified Two-Layer Analysis Fitted to Experimental Results for Fine Coal

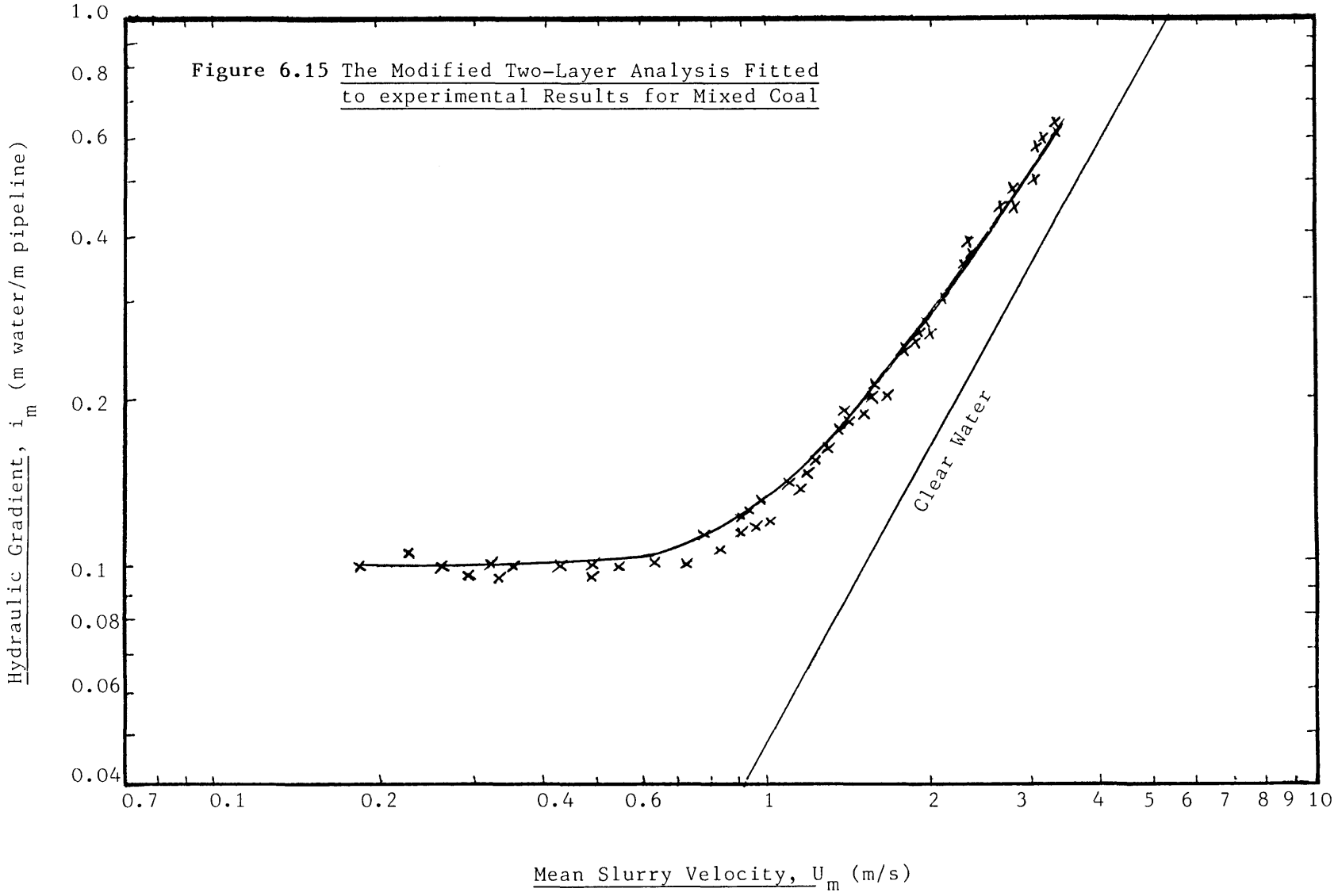

Figure 6.15 The Modified Two-Layer Analysis Fitted to experimental Results for Mixed Coal

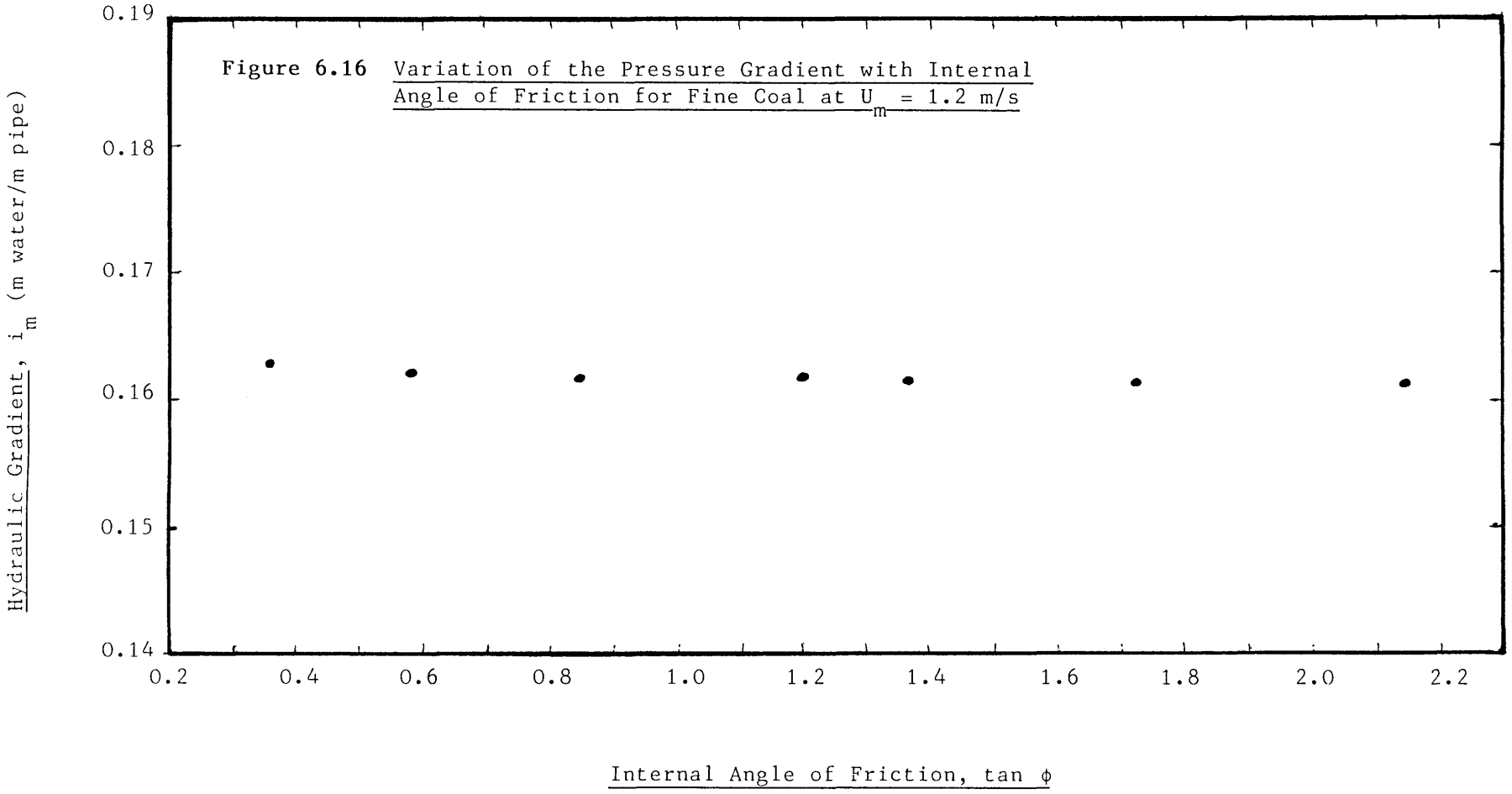

Figure 6.16 Variation of the Pressure Gradient with Internal Angle of Friction for Fine Coal at U_m = 1.2 m/s

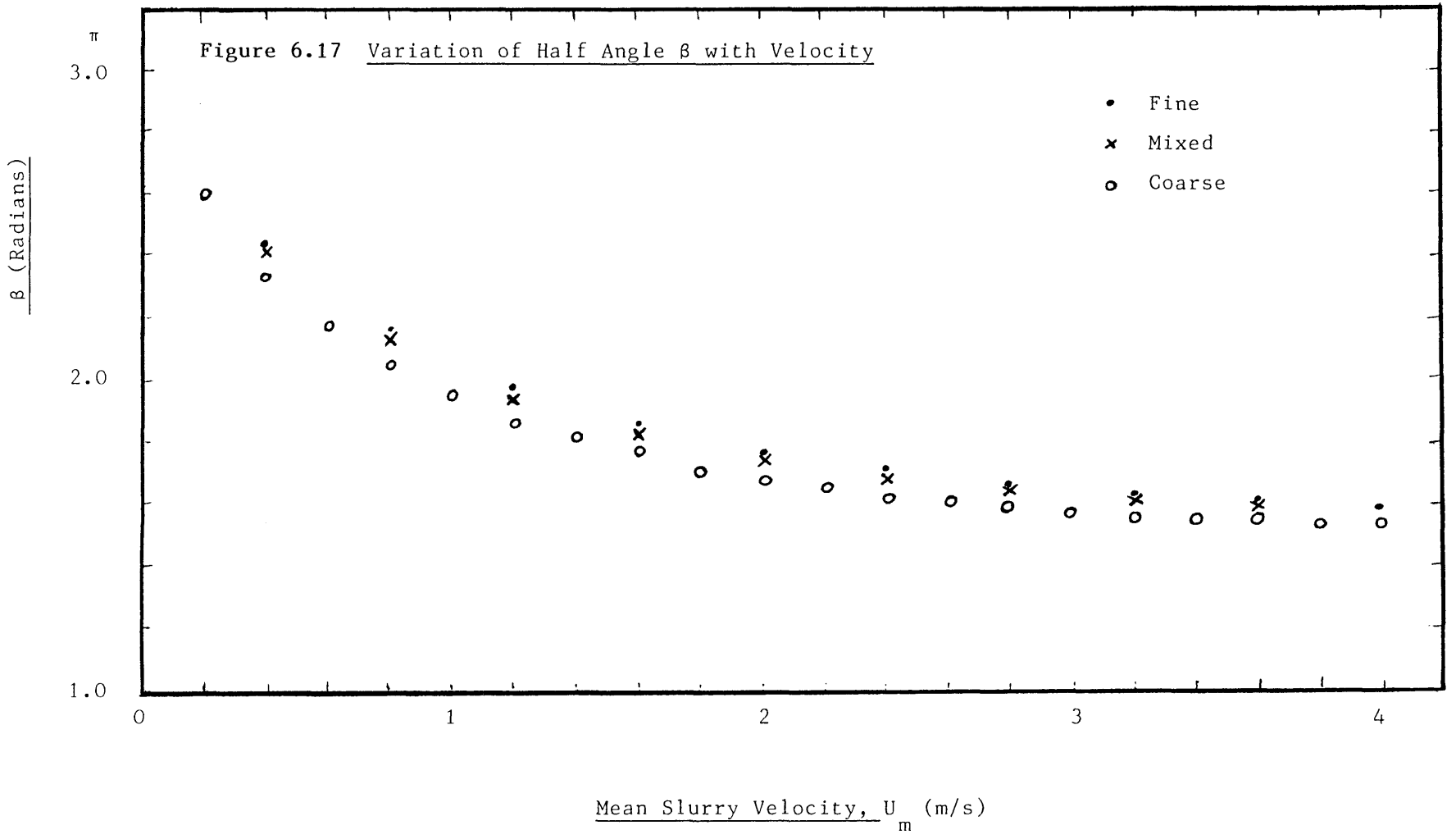

Figure 6.17 Variation of Half Angle β with Velocity

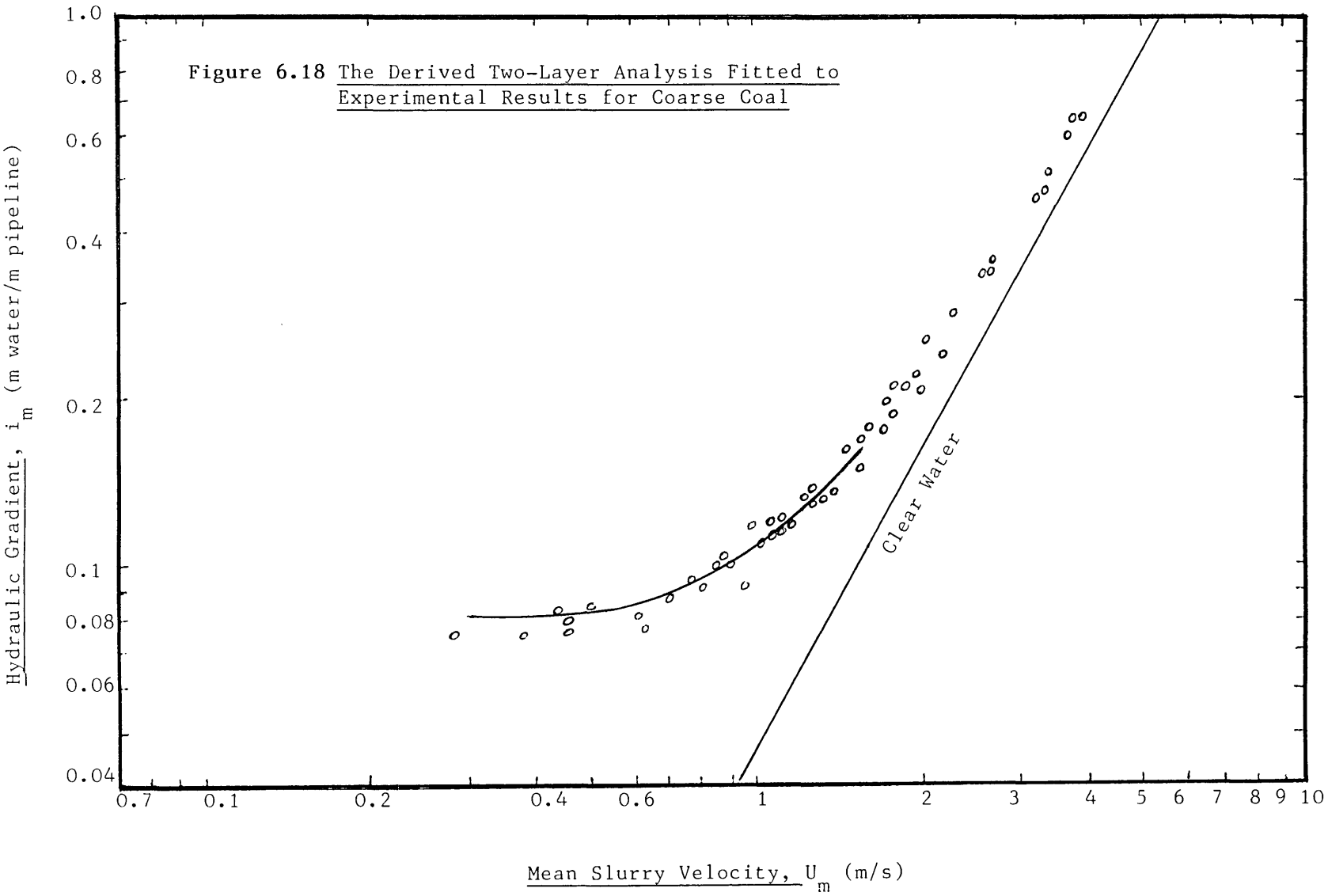

Figure 6.18 The Derived Two-Layer Analysis Fitted to Experimental Results for Coarse Coal

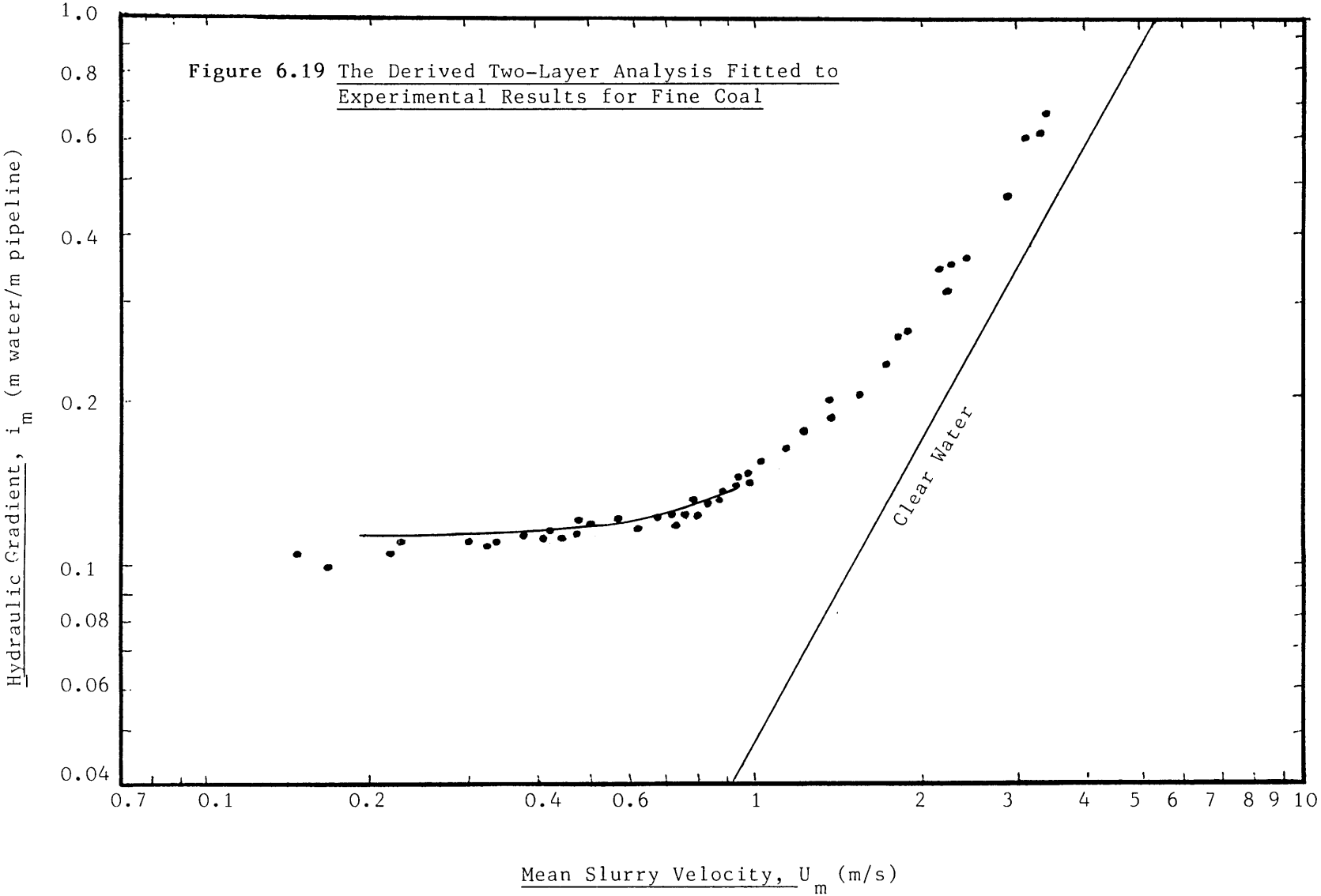

Figure 6.19 The Derived Two-Layer Analysis Fitted to Experimental Results for Fine Coal

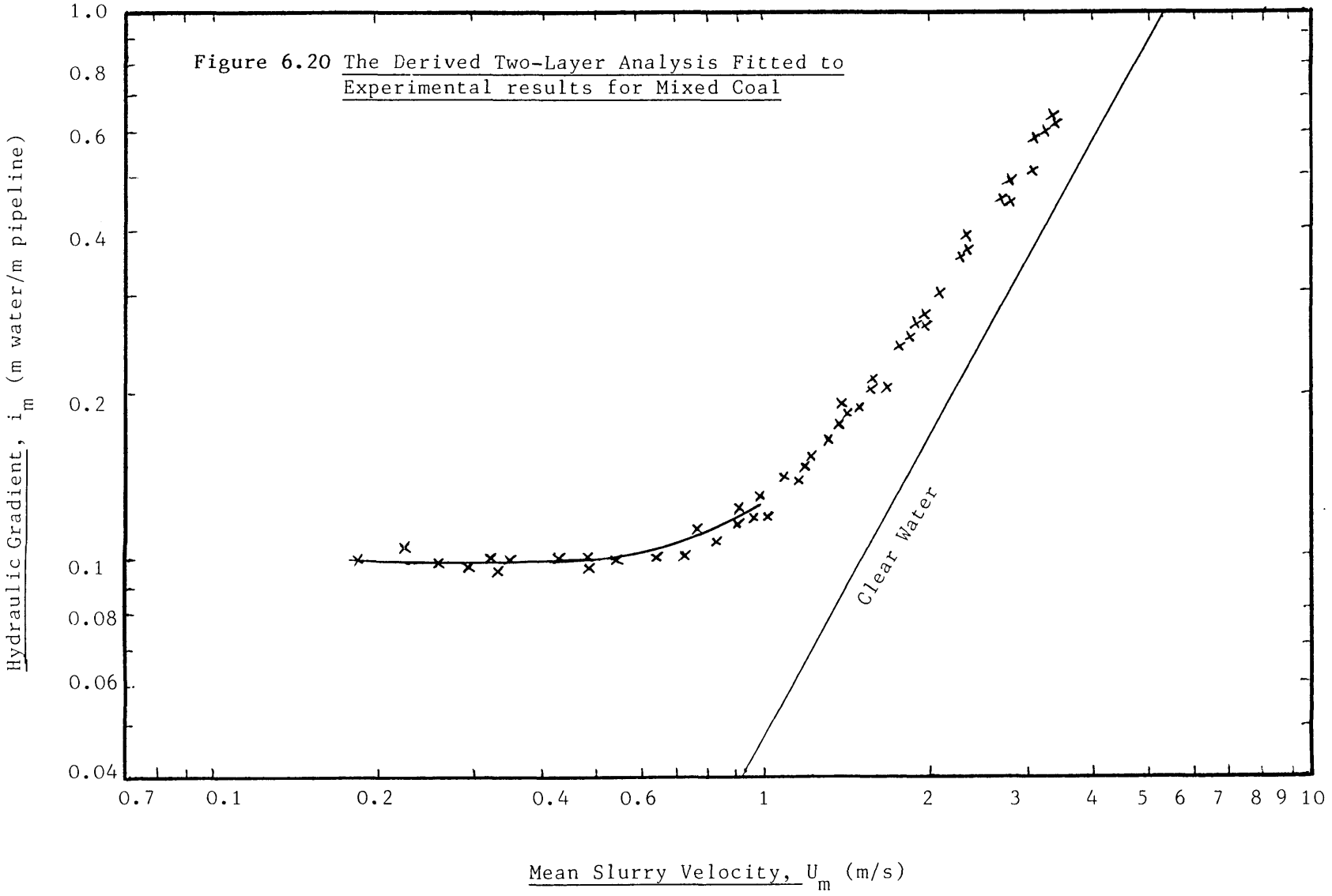

Figure 6.20 The Derived Two-Layer Analysis Fitted to Experimental results for Mixed Coal

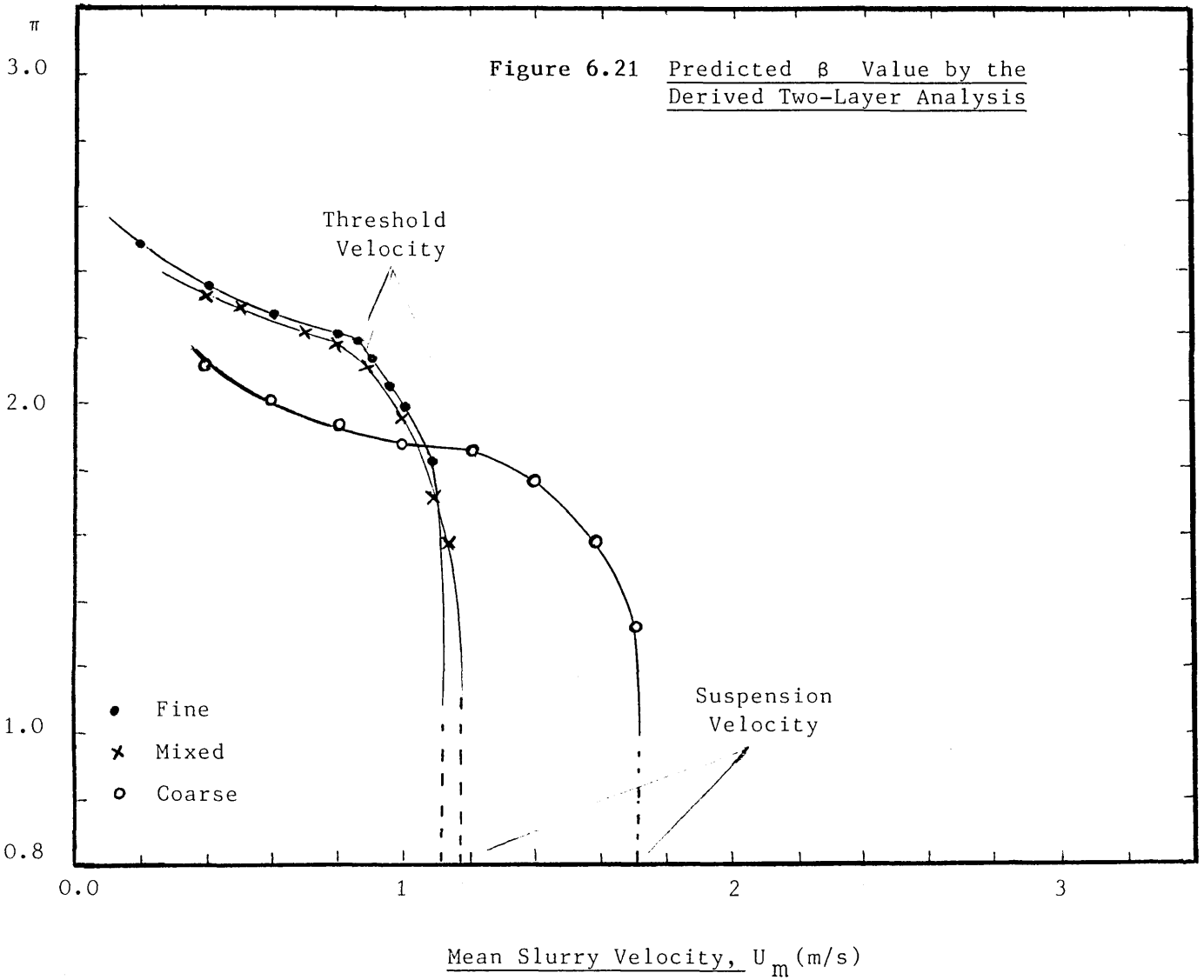

Figure 6.21 Predicted β Value by the Derived Two-Layer Analysis

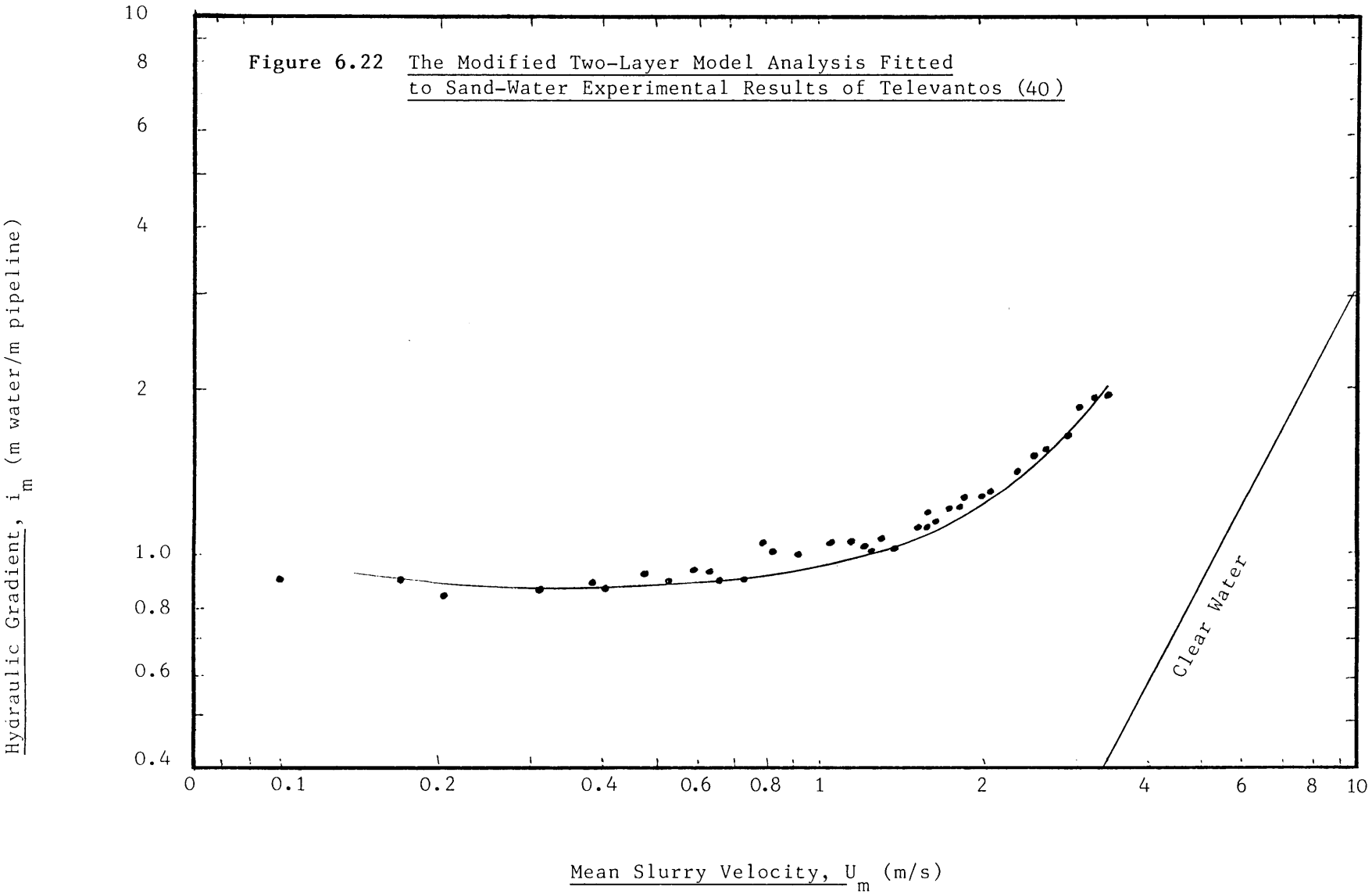

Figure 6.22 The Modified Two-Layer Model Analysis Fitted to Sand-Water Experimental Results of Televantos (40)

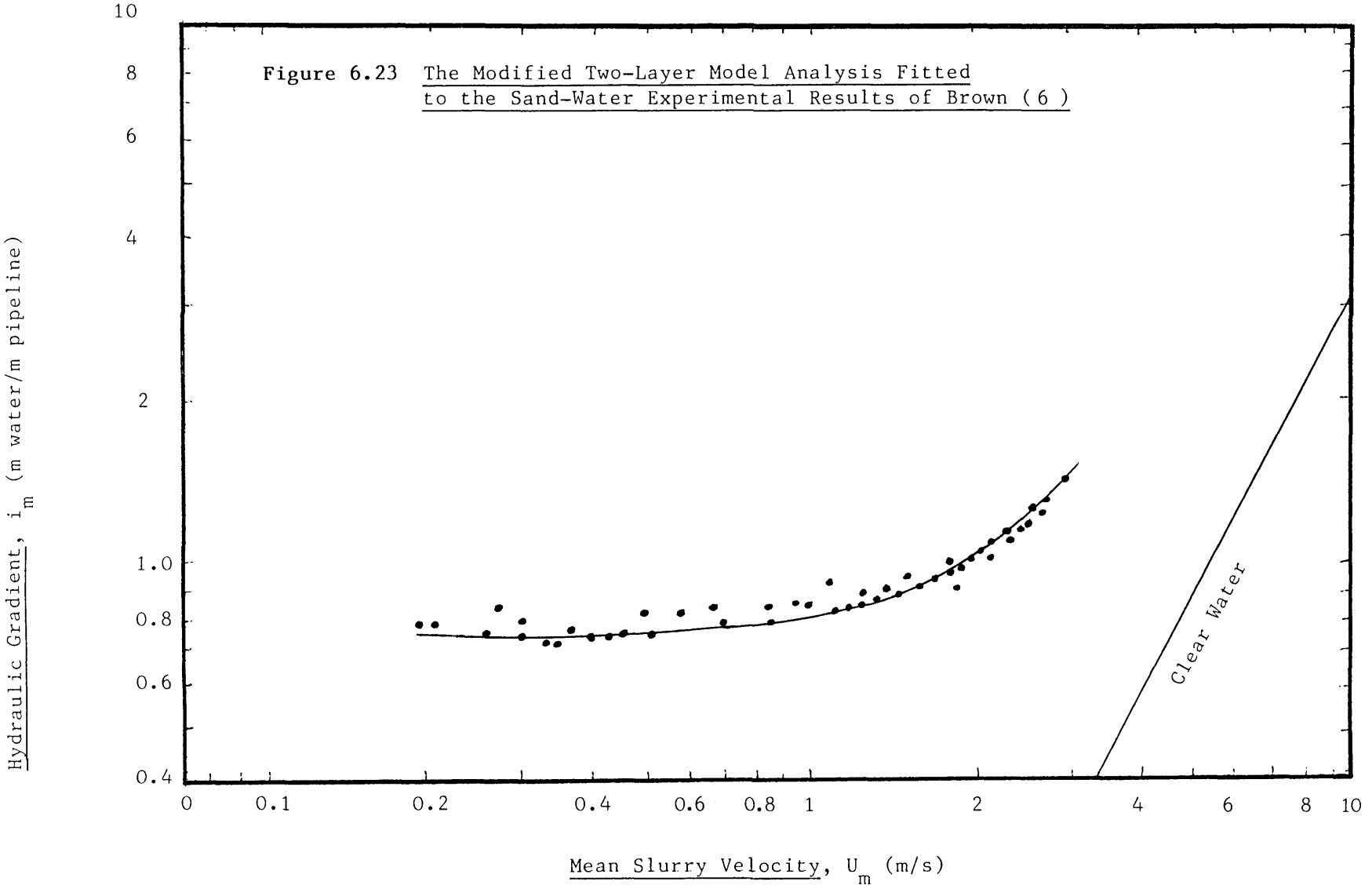

Figure 6.23 The Modified Two-Layer Model Analysis Fitted to the Sand-Water Experimental Results of Brown (6)

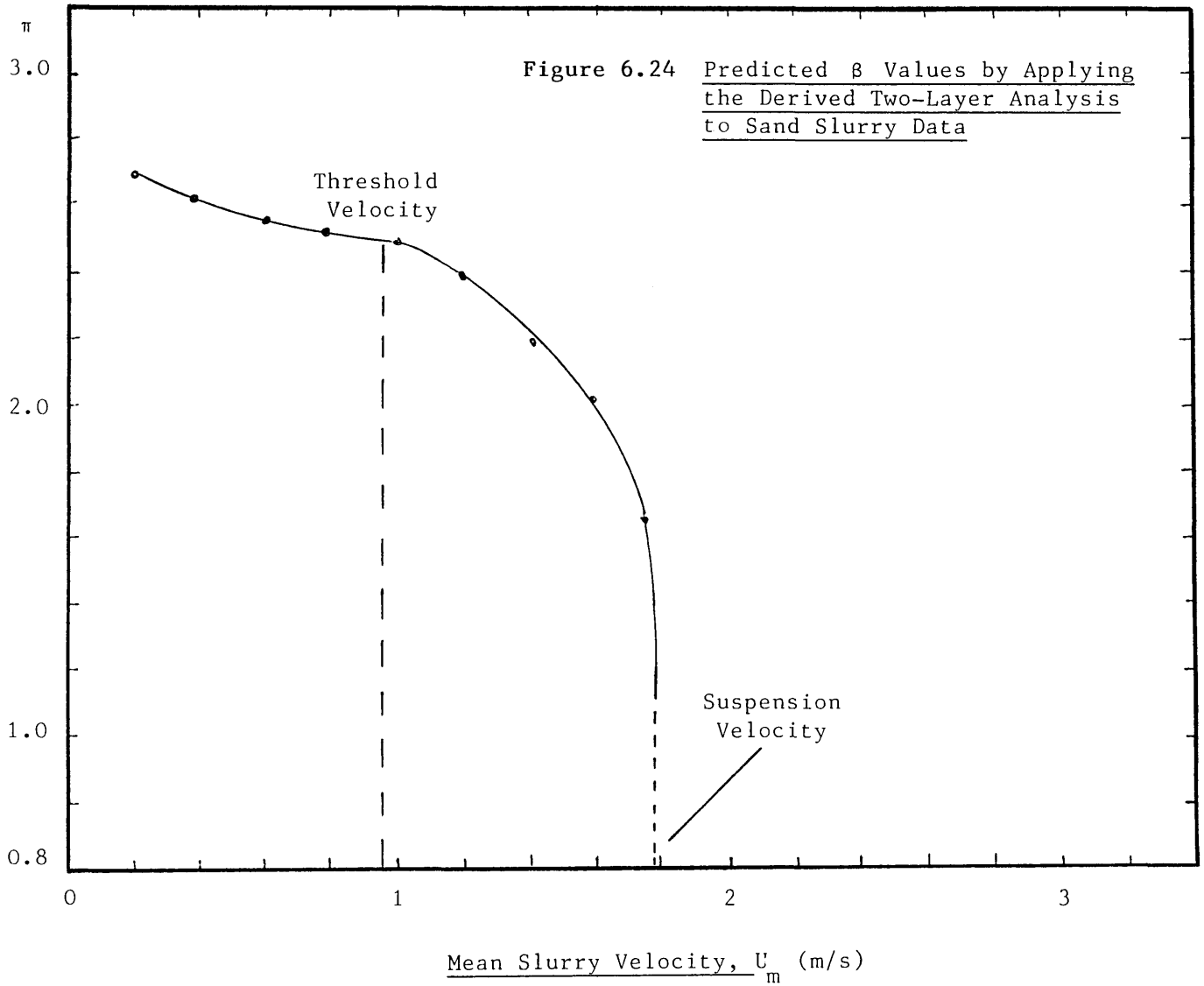

Figure 6.24 Predicted β Values by Applying the Derived Two-Layer Analysis to Sand Slurry Data

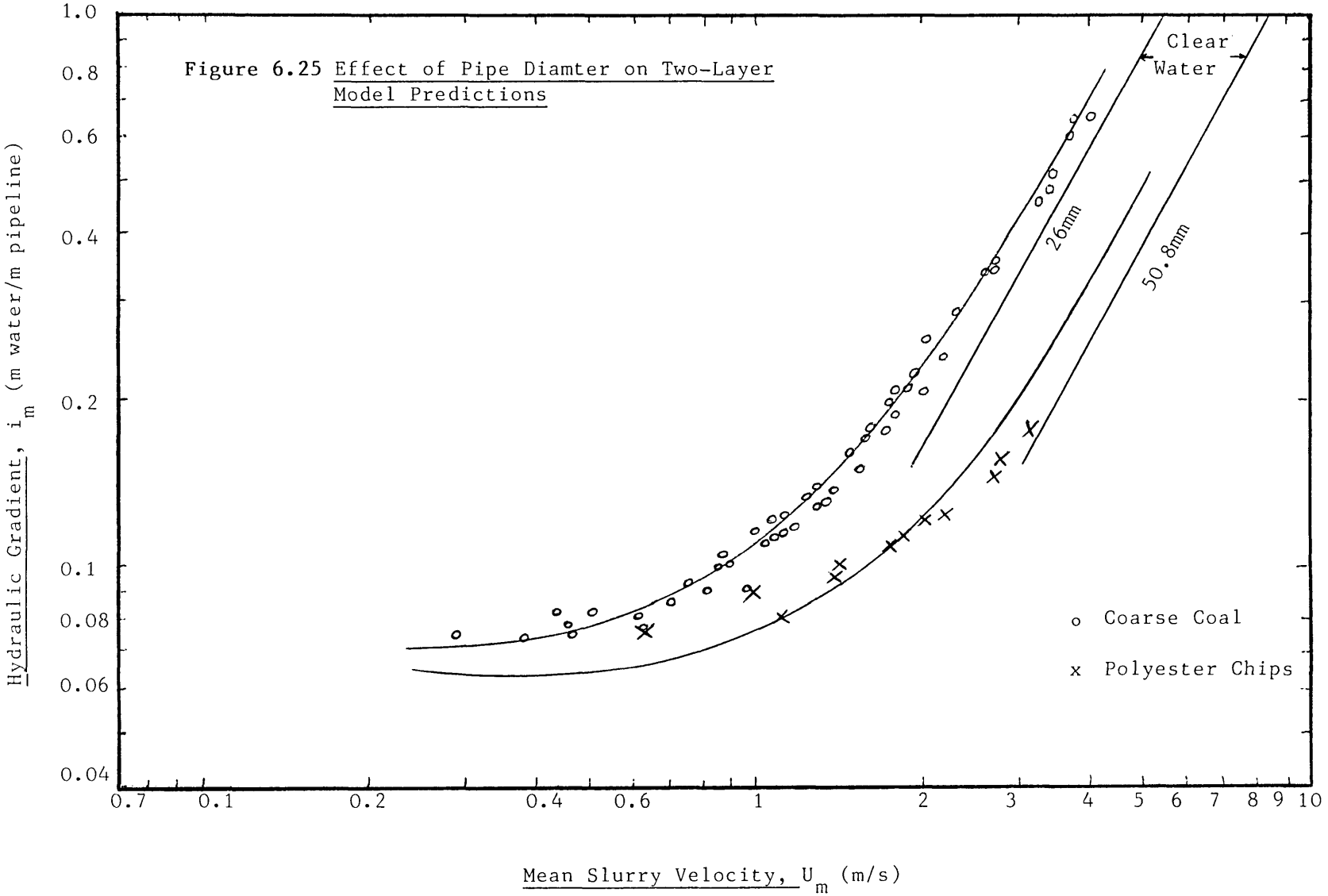

Figure 6.25 Effect of Pipe Diamter on Two-Layer Model Predictions

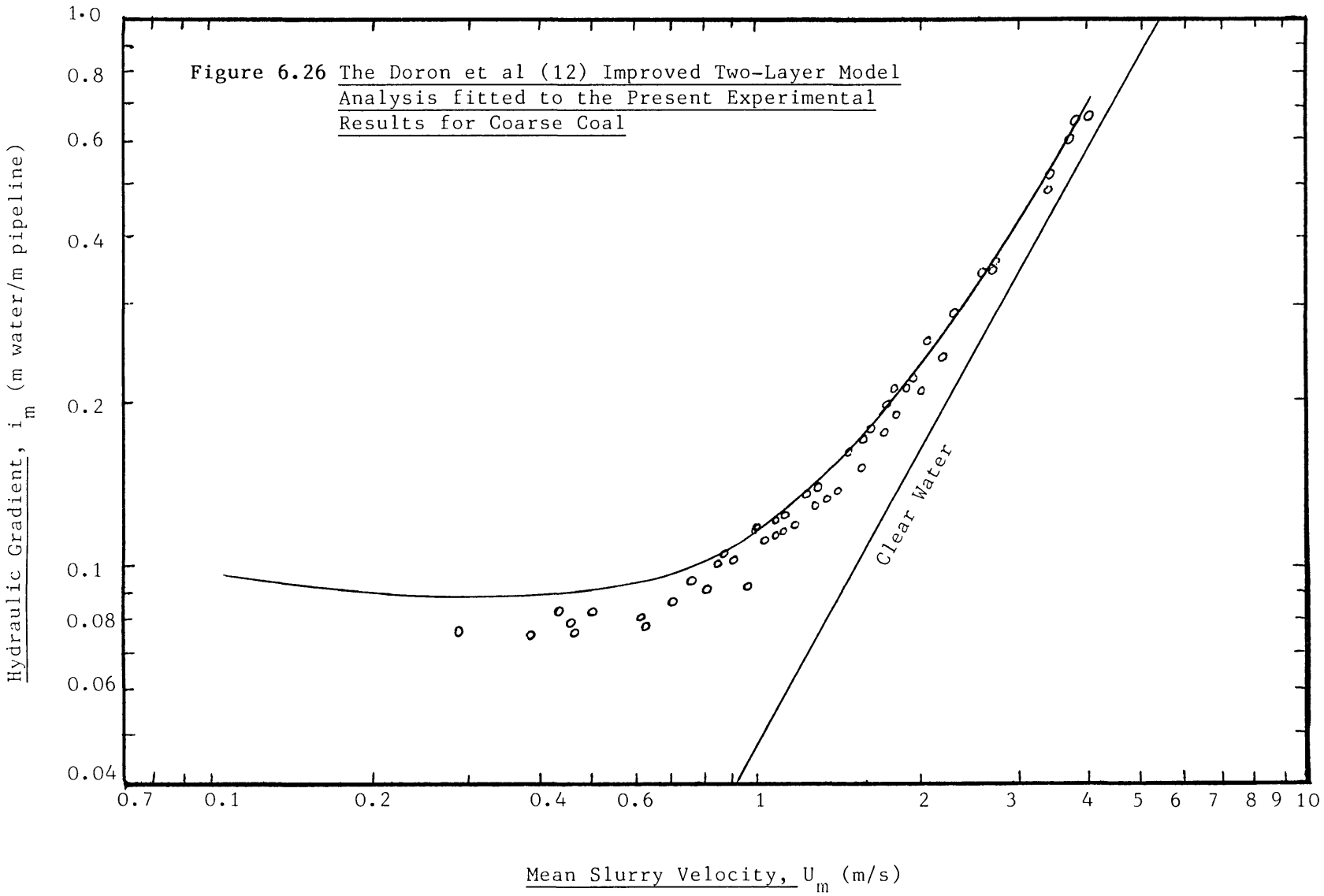

Figure 6.26 The Doron et al (12) Improved Two-Layer Model Analysis fitted to the Present Experimental Results for Coarse Coal

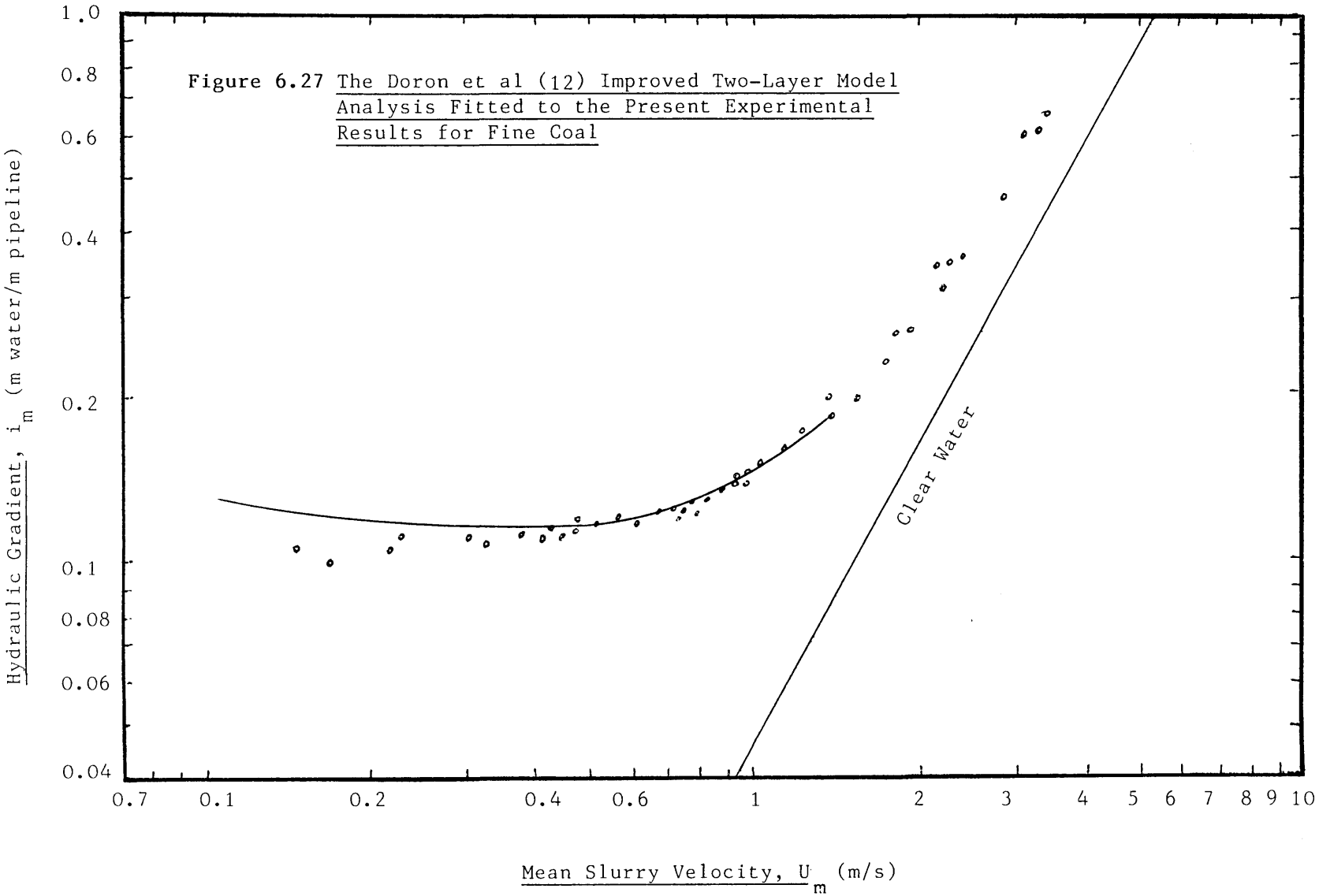

Figure 6.27 The Doron et al (12) Improved Two-Layer Model Analysis Fitted to the Present Experimental Results for Fine Coal

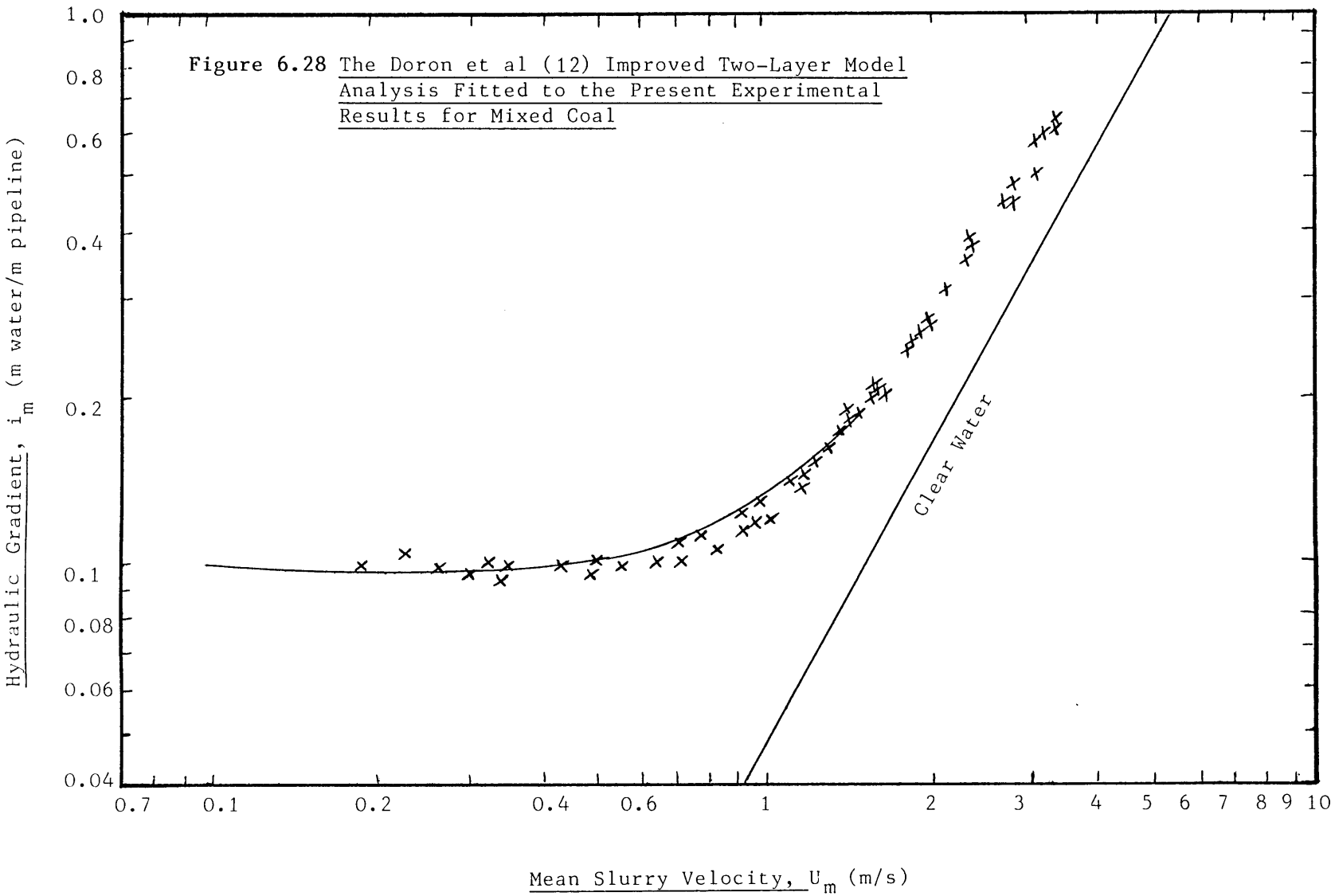

Figure 6.28 The Doron et al (12) Improved Two-Layer Model Analysis Fitted to the Present Experimental Results for Mixed Coal

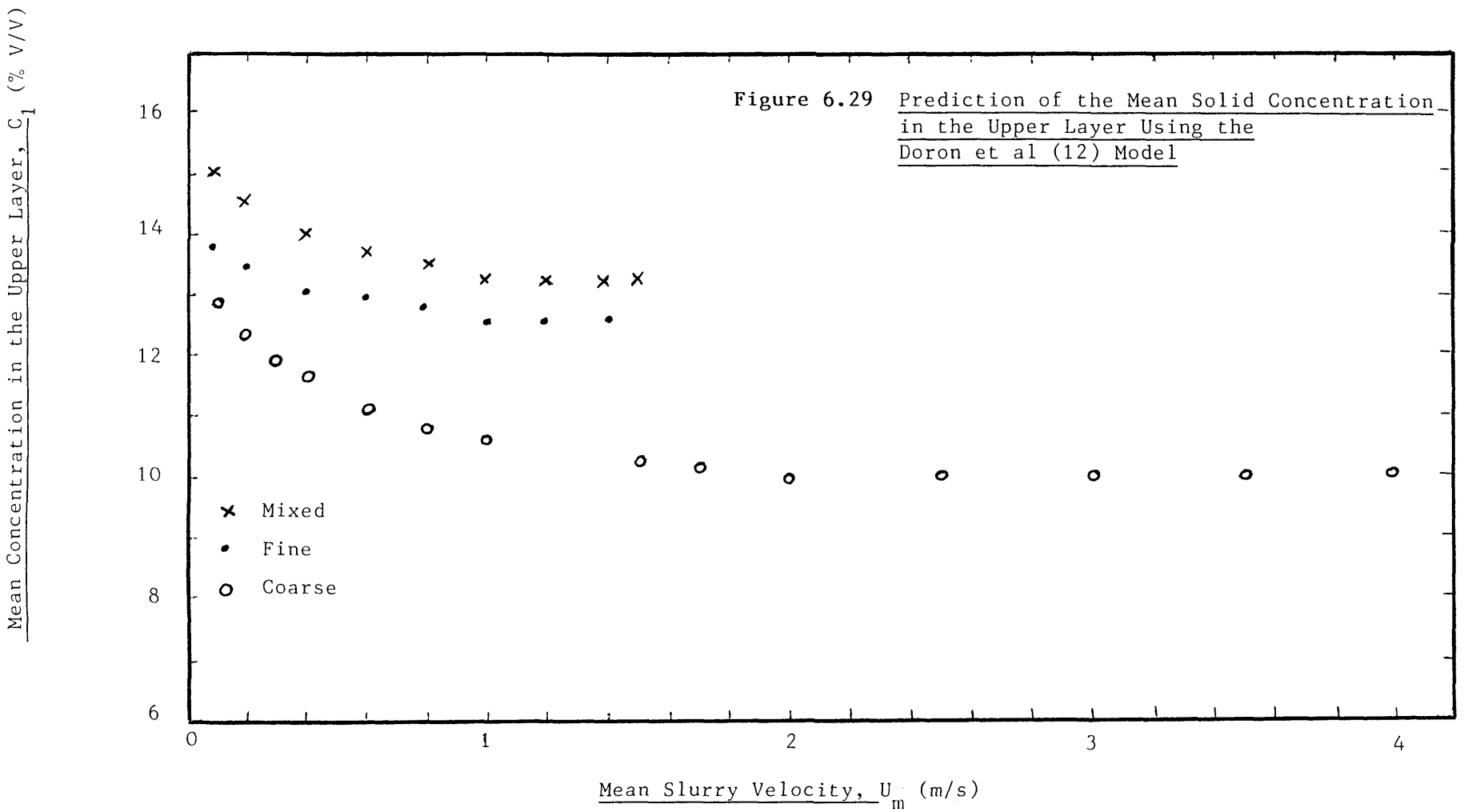

Figure 6.29 Prediction of the Mean Solid Concentration in the Upper Layer Using the Doron et al (12) Model

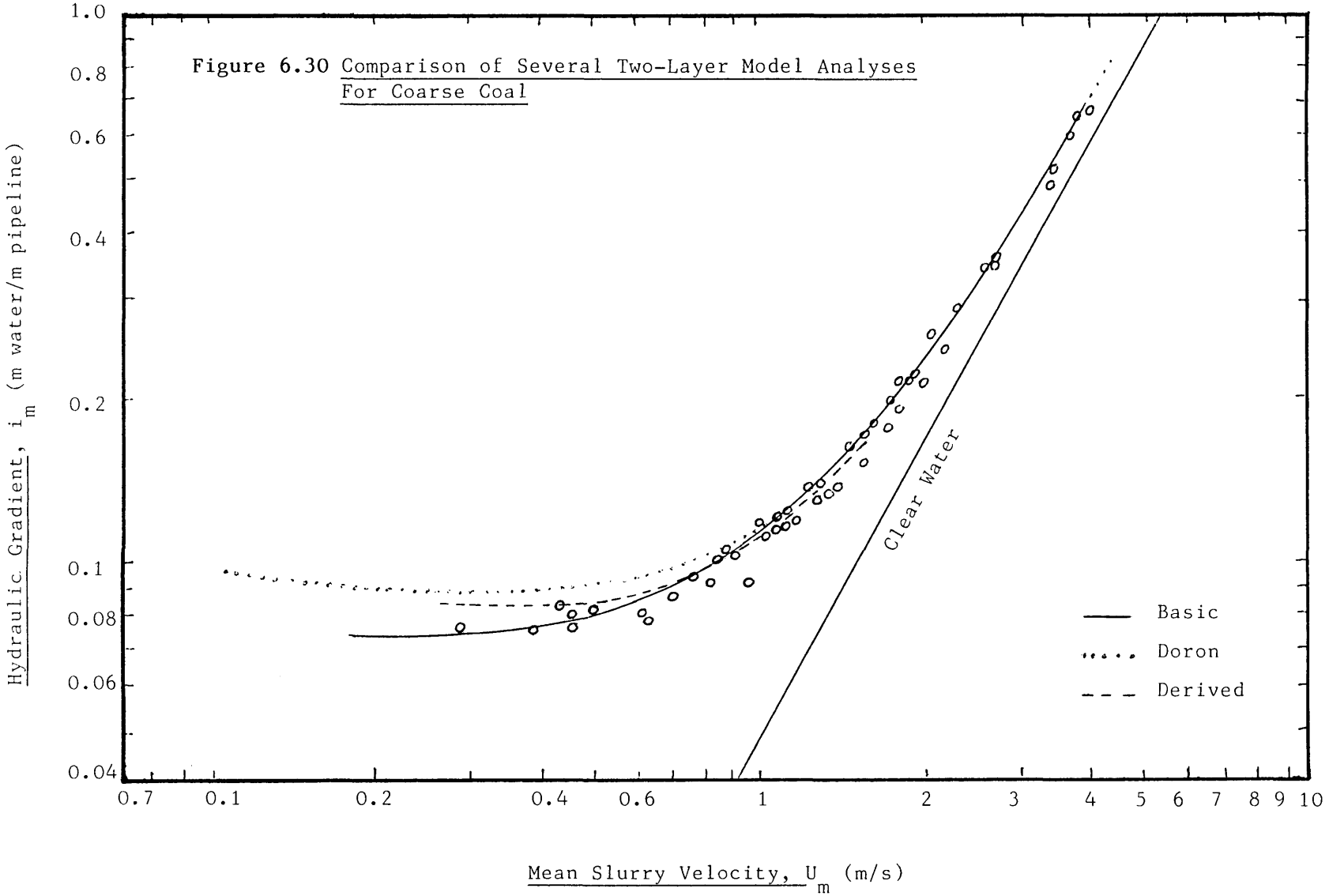

Figure 6.30 Comparison of Several Two-Layer Model Analyses For Coarse Coal

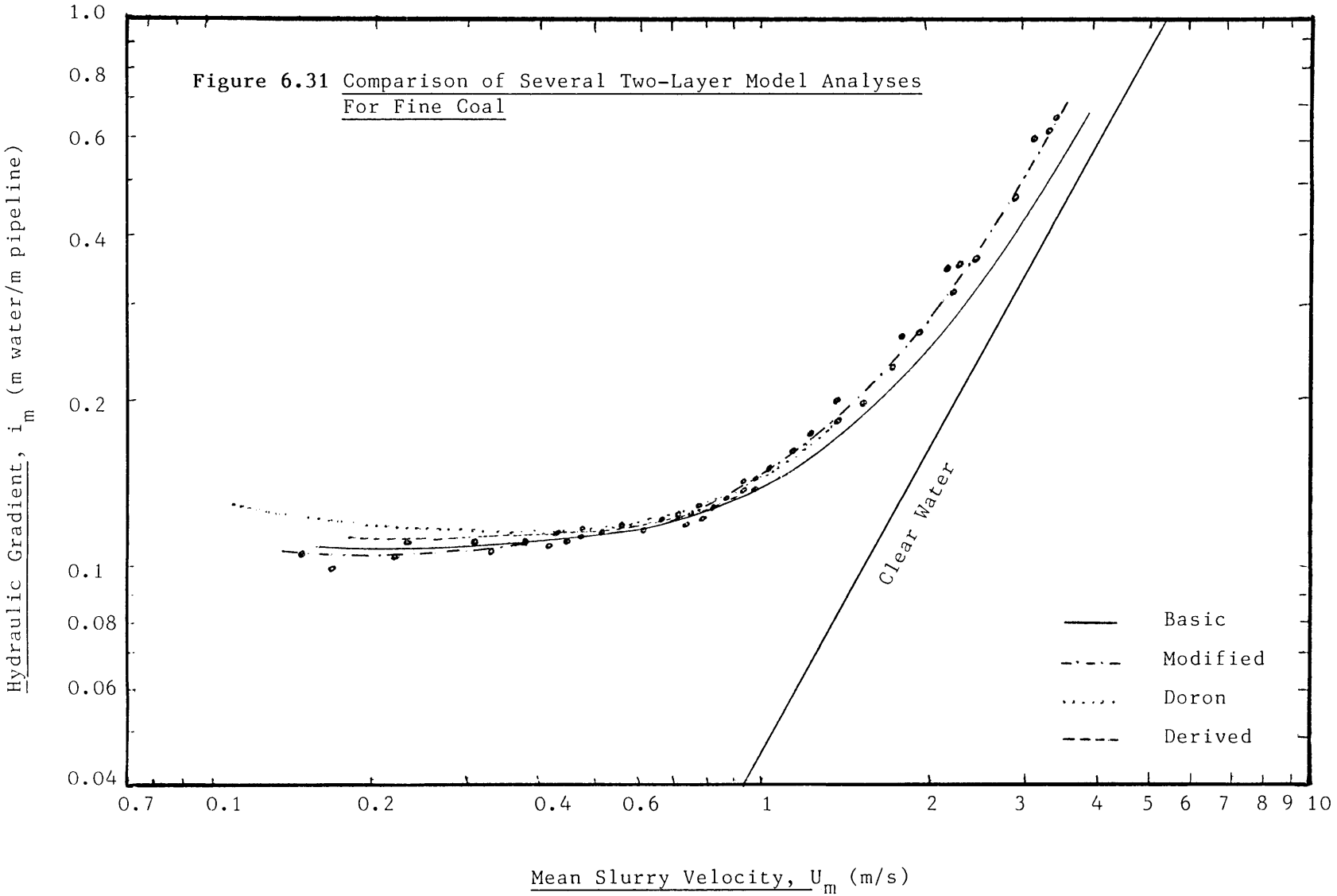

Figure 6.31 Comparison of Several Two-Layer Model Analyses For Fine Coal

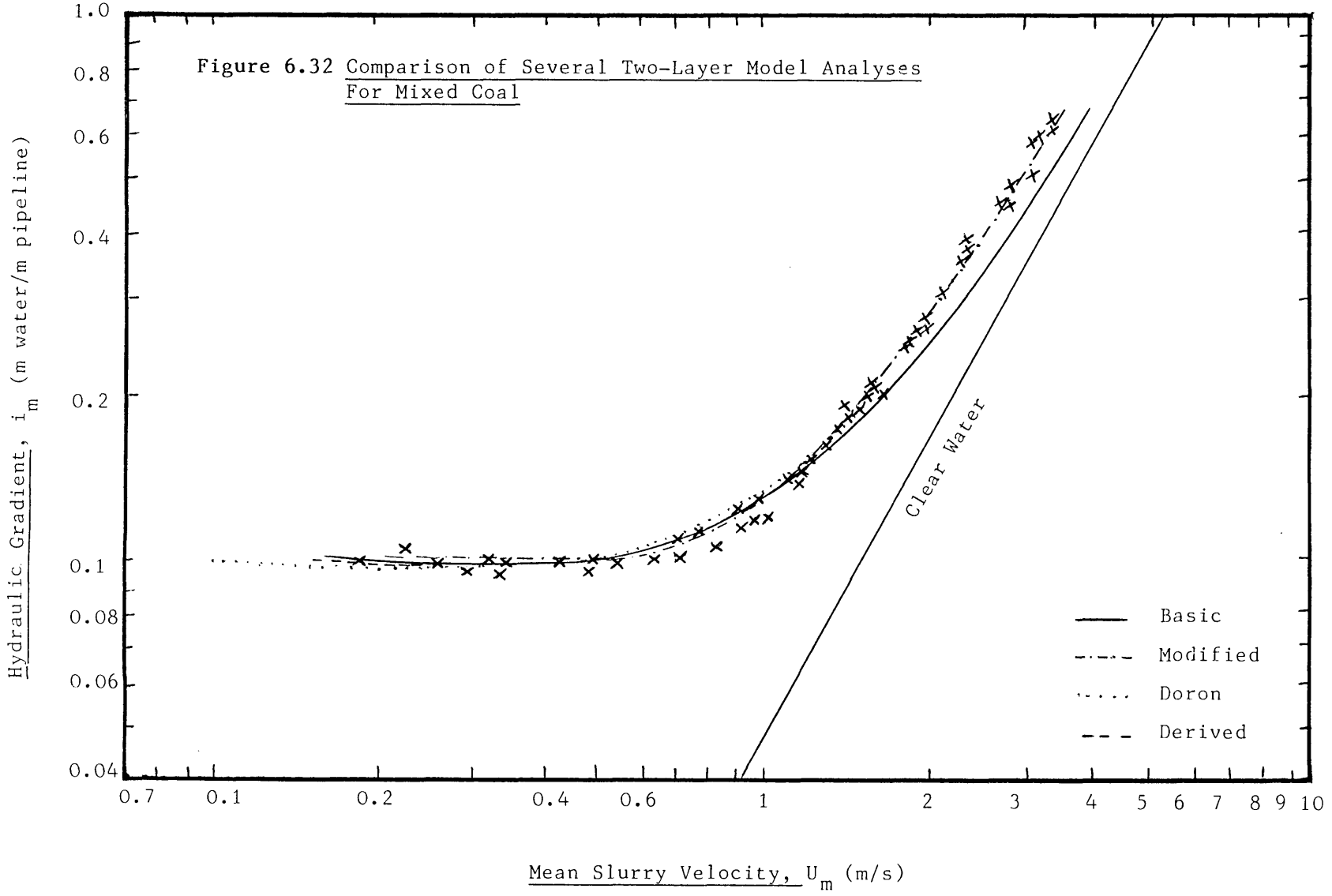

Figure 6.32 Comparison of Several Two-Layer Model Analyses For Mixed Coal

Figure 6.33 Doron et al (12) Model

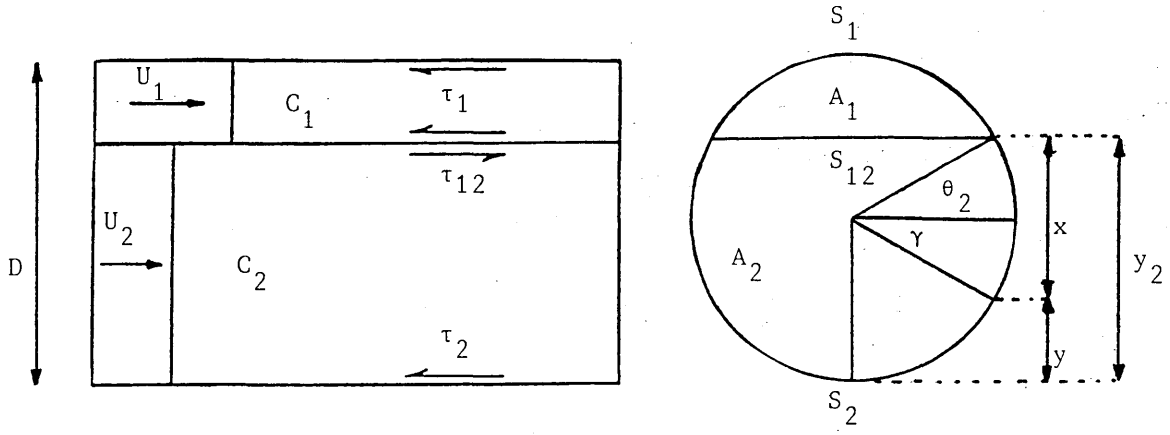

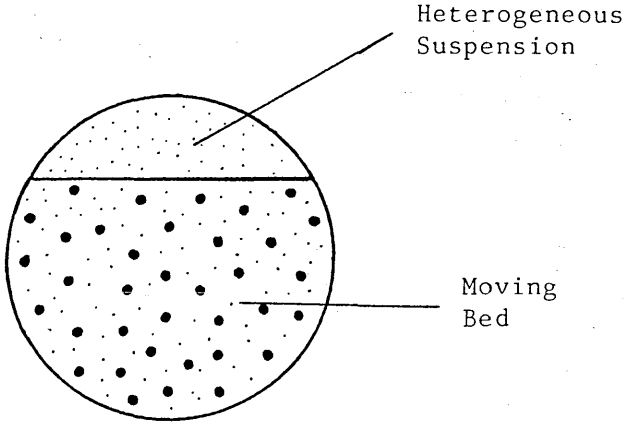

Hypothetical Flow Regime

CHAPTER 7

CONCLUSIONS

7.1 Summary

Experiments have been performed to analyse the flow mechanism of coarse particle suspensions. The experiments were carried out in a 26mm horizontal pipeline with three different sizes of coal, coarse coal of size range 1-4mm and d_{50} = 3.25mm, mixed coal of size range 0.5-4mm and d_{50} = 1.9mm, and fine coal of size range 0.5-2mm and d_{50} = 0.975mm. The hydraulic gradient, in-situ volumetric solids concentration and delivered solids concentration were measured for mean slurry velocities of 0.2-4m/s.

The experimental results were analysed using four different versions of the two-layer model.

(a) the basic model treats pipeline flow by considering a distinct upper layer free of particles and a moving bed of solids in the lower layer.

(b) the modified model for a case of dense phase flow involves fine particles, by using the mean mixture density rather than the clear fluid density in the calculation of fluid shear stress at the pipe wall.

(c) the present improved model accounts for the existence of suspended particles in the upper layer. At low velocity there are two distinct layers with an upper layer free of particles

As the velocity increases to the threshold velocity, there is some suspension of particles in the upper layer. As the velocity increases further to reach the suspension velocity, two layer flow disappears and heterogeneous suspension flow exists. The velocity of suspension of the first particle, the threshold velocity, and also the velocity for complete heterogeneous suspension, i.e. the suspension velocity, can be predicted.

(d) a modified approach to the two-layer model recently published by Doron et al (12) was also applied to the present experimental results for a further comparison. They based the modified approach on the existence of heterogeneous suspension in the upper layer and bed flow in the lower layer.

7.2 Horizontal Flow

1. Coarse coal having a ratio of maximum particle size to pipeline diameter of 1:6.5 was successfully transported using an indirect pumping system in order to reduce attrition and abrasion of the pump and also to minimise particle degradation.

2. Coal slurries with a wide size range distribution can be transported at a higher concentration than with a narrow size range distribution despite the fact that the mean particle size is larger in the former.

3. The size range distribution of particles comprising a slurry has a significant effect on the characteristic hydraulic gradient/mean

velocity curve.

4. A wide size distribution, i.e. large packing density, reduces the pressure drop in the hydraulic transportation of coal slurries. Fine particles tend to occupy the voidage between coarse particles and this stabilises the flow, i.e. the presence of fine particles forms a carrier fluid of similar density to the coal, and effectively supports the coarse particles.

5. The horizontal flow of high concentration coarse coal-water slurries with no fine particles suspended in the carrier fluid can be interpreted using the basic two-layer model.

6. The horizontal flow of high concentration dense phase flow, i.e. fine and mixed coal, with fine particles in suspension is best interpreted using a modified form of the two-layer model.

7. The modified model was applied to the results of other investigators, for material of different density, higher solid concentration, and larger pipe diameter and the predictions agreed well with their experimental measurements of hydraulic gradient.

8. The analysis of the two-layer model was interrogated to establish the behaviour of the individual parameters and their effect on predictions. The result of these analyses are summarised:-

a) the variation of internal angle of friction did not have a significant effect on the prediction of the pressure gradient.

b) the value of the coefficient of sliding friction has a pronounced effect on the prediction of the two-layer model.

c) at low velocity, the model prediction is dominated by particulate shear stress and at higher velocity the fluid wall shear stress becomes more significant. This explains the significance of the effect of coefficient of sliding friction at low velocity and particle or slurry density at higher velocity.

d) The variation of mean particle diameter, d_{50}, did not affect the prediction significantly.

e) It was found that the relative velocity, $U_r = U_{f2} - U_{s2}$ in the lower layer approaches zero at high mean slurry velocity for the present coal-water suspension (i.e. a heterogeneous flow regime exists) though the model continues to predict the existence of two-layer flow and the correct value of the hydraulic gradient.

9. The derived two-layer model has been used to predict the threshold velocity (the transition velocity between the bed flow regime and the bed flow with particle suspension in the upper layer), and also the suspension velocity (the transition velocity between the bed flow with particle suspension and heterogeneous suspension).

10. The improved two-layer model was applied to the experimental results and predicted a transition velocity very close to the value visually observed. This model satisfactorily predicts the hydraulic

gradient/mean velocity relationship up to the point of complete heterogeneous suspension, where two-layer flow no longer exists.

11. The Doron version of the two-layer model was applied to the present experimental results. The correlation of hydraulic gradient was different for each size and was not particularly consistent. The model also failed to predict the pressure gradient at higher velocity since the ratio of the upper layer velocity and the lower layer velocity approached unity and the computation failed to converge.

12. It was found that the relative velocity approaches zero at approximately the same mixture velocity using any version of the two-layer model. This phenomenon has not been observed before.

7.3 Suggestions for Future Work

In the present work, effort has been made to understand and comprehend the mechanism of different flow regimes in the hydraulic transportation of coal-water slurries. Interesting experimental results were obtained for coal-water slurries; in a 26mm diameter horizontal pipe. The application of the two-layer model analysis has been studied and an attempt has been made to improve the application of the model using several detailed modifications in order to predict the velocities at which different flow regimes exist.

The prediction of threshold and suspension velocities are very important and useful for the design of a hydraulic conveying system. The hydraulic gradient predicted using the derived model agrees well with the present experimental results and the prediction of threshold and

suspension velocities agrees with the visual observation of the flow regime. However, the application of the derived model for the prediction of these velocities can only really be generalised and used globally for design purposes, when the predictions are compared with direct experimental measurements. It would be beneficial to the understanding of hydraulic conveying mechanisms if the local velocity and local in-situ concentration of the slurry could be measured experimentally over the whole cross section of the pipe.

By directly measuring the value of the slurry velocity in both layers and also the local in-situ concentration in each layer, the depth of the two-layer interface can be measured and directly compared with a theoretical prediction. Then, the true application of any version of the two-layer model could be validated.

These further studies will give a complete understanding of the mechanism of the different flow regimes in the hydraulic conveying of coal-water slurries.

NOMENCLATURE

Description

Figure		Units
A	Cross-sectional area of pipe	L^2
A_1	Area of Upper Layer in Two-Layer Analysis	L^2
A_2	Area of Lower Layer in Two-Layer Analysis	L^2
C_D	Drag Coefficient of single particle at infinite dilution	-
C_d	Delivered Volumetric Solid Concentration (%V/V)	-
C_s	In-situ Volumetric Solid Concentration (%V/V)	-
C_b	Settled Bed Solid Concentration	-
C_1	Solid Concentration in the Upper Layer Suspension	-
C_2	Actual Solid Concentration in the Bed	-
C(y)	Local Volumetric Concentration	-
D	Pipe Diameter	L
d	Particle Diameter	L
d_{50}	Average Particle Diameter as determined by screen size analysis	L
D_e	Equivalent Diameter	L
D_{e1}	Equivalent Diameter in the Upper Layer	L
D_{e2}	Equivalent Diameter in the Lower Layer	L
F_n	Normal force at the Pipe Wall due to bed of solid	MLT^{-2}
FFP	Fluid Friction on the Fluid by the Particle	$ML^{-2}T^{-2}$
FPF	Fluid Friction on the Particle by the Fluid	$ML^{-2}T^{-2}$
FFW	Fluid Friction on the Fluid by the Wall	$ML^{-2}T^{-2}$
FPW	Fluid Friction on the Particle by the Wall	$ML^{-2}T^{-2}$
f_m	Friction Factor for Suspension	-
f_f, f	Friction Factor for Fluid	-

		Units
f_1	Friction Factor for the Upper Layer defined by Equation 5.15	-
f_{12}	Friction Factor for the Interface defined by Equation 5.20	-
f_2	Friction Factor in the Lower Layer	-
g	Acceleration due to Gravity	LT^{-2}
H_R	Hold-Up Ratio U_{f2}/U_{s2}	-
I_o	γ-ray Intensity (Absolute)	T^{-1}
I_E	Intensity with Empty Pipe	T^{-1}
I_s	Intensity with Pipe full of Slurry	T^{-1}
I_w	Intensity with Pipe full of Water	T^{-1}
i, i_w	Head Loss due to Water alone	-
i_s	Head Loss due to Presence of Solids	-
i_m	Total or Slurry Hydraulic Gradient	-
K, k	Constant	-
L	Length of Pipe	L
L_n	Natural Logarithm to the base e	-
N_I	Dimensionless Parameter defined by Equation 2.20	-
S_I	Density Ratio (ρ_s/ρ_L)	-
S_1	Perimeter Associated with Upper Layer	L
S_2	Perimeter Associated with Lower Layer	L
S_{12}	Length of Interface in Two-Layer Model	L
U_D	Deposition Velocity	LT^{-1}
U_f	Fluid Velocity	LT^{-1}
U_H	Suspension Velocity	LT^{-1}
U_m	Mean Slurry Velocity	LT^{-1}
U_T	Threshold Velocity	LT^{-1}
U_t	Terminal Falling Velocity	LT^{-1}

		Units
U'_t	Hindered Settling Velocity	LT^{-1}
U_1	Velocity of the Upper Layer	LT^{-1}
U_2	Velocity of the Lower Layer	LT^{-1}
U_{f2}	Local Fluid Velocity at Lower Layer	LT^{-1}
U_{s2}	Local Solid Velocity at Lower Layer	LT^{-1}
U_r	Relative Velocity ($U_{f2} - U_{s2}$)	-
U^*	Shear Velocity	LT^{-1}
du/dr	Shear Rate	T^{-1}
V_s	Volume	L3
W_s	Total Mass of Solid	M
X	Depth of the Pipe Occupied by the Bed of Solid	L
X_p	Pipe Thickness	L
X_L	Path Length	L
y, y_2	Bed Geometry defined by Figure 6.33	L

GREEK LETTERS

α	Richardson and Zaki Number	-
β	Half Angle Subtended by Bed Deposit defined by Figure 5.1	radian
Ψ	Shear Intensity Parameter defined by Equation 2.9	-
Φ	Transport Parameters defined by Equation 2.10	-
μ, μ_f	Viscosity of Pure Water	L^2T^{-1}
μ_m	Apparent Viscosity of Slurry	
μ_P	Coefficient of Sliding Friction between a granular mass and solid boundary	L^2T^{-1}
μ_i	Mass Absorption Coefficient	L^2M^{-1}
μ_s	Mass Absorption Coefficient of Solid Particles	L^2M^{-1}
μ_p	Mass Absorption Coefficient of Pipe Wall material in Equation 4.4	L^2M^{-1}

		Units
μ_w	Mass Absorption Coefficient of Fluid in Equation 4.4	L^2M^{-1}
ρ, ρ_L	Fluid Density	ML^{-3}
ρ_s	Solid Density	ML^{-3}
ρ_p	Pipe Wall Density	ML^{-3}
ρ_m	Mixture Density	ML^{-3}
ρ_{m1}	Mixture Density in the Upper Layer	ML^{-3}
ρ_{m2}	Mixture Density in the Lower Layer	ML^{-3}
γ	Angular Co-ordinate defined by Figure 6.33	radian
θ_2	Bed Angle ($= \beta - \pi/2$) defined in Figure 6.33	radian
τ	Shear Stress	$ML^{-1}T^{-2}$
τ_{yv}	Yield Stress of Carrier Fluid	-
τ_1	Shear Stress in the Upper Layer	$ML^{-1}T^{-2}$
τ_2	Shear Stress in the Lower Layer	$ML^{-1}T^{-2}$
τ_{12}	Interfacial Shear Stress	$ML^{-1}T^{-2}$
τ_{f1}	Fluid Shear Stress	$ML^{-1}T^{-2}$
τ_2	Average Total Shear Stress in the Lower Layer	$ML^{-1}T^{-2}$
τ_{f2}	Fluid Shear Stress in the Lower Layer	$ML^{-1}T^{-2}$
τ_{s2}	Particulate Shear Stress	$ML^{-1}T^{-2}$
ϕ	Angle of Internal Friction	degree
ε'	Local Diffusion Coefficient	-
ε	Mean Diffusion Coefficient	-
σ	Normal Stress	$ML^{-1}T^{-2}$
σ_p	Normal Stress due to Solids	$ML^{-1}T^{-2}$
l	Tangent of Angle of Repose	degree
l'	Tangent of Angle of Wall Friction	degree

SUBSCRIPTS

Figure

b	Bed
d	Delivered or Input
E	Empty Pipe
f	Fluid, Frictional
m	Mixture
n	Normal
p	Pipe
r	Relative
s	Solids
t	Total
w	Water
1	Upper Layer of Two-Layer Model
2	Lower Layer of Two-Layer Model
12	Interface of Two-Layer Model

REFERENCES

1. Ansley, R.W. and Smith, T.N.
"Motion of Spherical Particles in a Bingham Plastic"
A.I.Ch.E. Jnl, Vol.13, No.16, pp.1193-1196 (1967)

2. Babcock, H.A.
"Heterogeneous Flow of Heterogenous Solids"
Symp. of Solid-Liquid Flow in Pipes, Univ. Pennsylvania,
Ed. Zandi, I., pp.125-48 (1968)

3. Bagnold, R.A.
"The Flow of Cohensionless Grains in Fluids"
Philos. Trans. R. Soc. A 249, p.235, (1956)

4. Bantin, R.A.
"Hydraulic Transport of Solids-Water Mixtures at High Concentrations"
Ph.D. Thesis, Univ. London, (1972)

5. Blatch, N.S.
"Trans. A.S.C.E., 57, 400 (1906)

6. Brown, N.P.
"Friction Mechanisms in Hydraulic Conveying at High Solids Concentration"
Ph.D. Thesis Univ. London, (1980)

7. Chhabra, R.P. and Richardson, J.F.
"Hydraulic Transport of Coarse Gravel Particles in a Smooth Horizontal Pipe"
Chem. Eng. Res. Des, Vol.61, (Sept 1983) 313

8. Chhabra, R.P. and Richardson, J.F.
"Hydraulic Transport of Coarse Particles in Viscous Newtonian and Non-Newtonian Media in a Horizontal Pipe"
Chem. Eng. Res. Des,, Vol.63, (Nov 1985), 390

9. Coulson, J.M. and Richardson, J.F.
Chemical Engineering II, Second Ed. Pergaman Press (1968)

10. Durand, R. and Condolios, E.
"The Hydraulic Transport of Coal and Solid Materials in Pipes"
Proc. Colloq. Hydraulic Transportation, London (Nov 1952)

11. Doron, P. and Banea, D.
"Effect of Operational and Physical Variables on the Pressure Drop in Solid-Liquid Flow Through Horizontal Pipes".
Multphase 3 B.H.R.A. Hague, 1987

12. Doron, P., Granica, D. and Barnea, D.
"Slurry Flow in Horizontal Pipes - Experimental and Modelling"
Int. J. Multiphase Flow Vol.13, No.4, pp.535-547, 1987.

13. Duckworth, R.A., Pullman, L. and Lockyear, C.F.
"The Hydraulic Transport of Coarse Coal at High Concentration"
Journal of Pipelines, 3 (1983) 251-265

14. Duckworth, R.A., Pullman, L. Lockyear, C.F., and Lenard, J.A.
"The Long Distance Transport of Coarse Coal by Pipeline"
Chemeca Sep 1983

15. Duckworth, R.A., Lockyear, C.F., Pullman, L., Littlejohn, M.H., and Lenard, J.A.
"Prediction of Pressure Gradients for the Transport of Coarse Coal in a Fine Coal Carrier"
Transportation Conf., Perth, 30 Oct-1 Nov (1984). The Inst. of Engrs. Aust.

16. Elsibai, N.G., Snoek, P.E., and Pitts, J.D.
"The Effect of Particle Size Distribution on the Economics of Short Distance Coal Slurry Pipelines"
Proc. 7th Int. Tech. Conf. on Slurry Transportaion, (Lake Tahoe, U.S.A., 23-26 March 1982), B.A. Sakkested(ed, Washington, D.C., U.S.A. Slurry Transportation Association, 1982, pp.371-395.

17. Elliot, D.E. and Gliddon, G.J.
"Hydraulic Transport of Coal at High Concentrations"
Proc. 1st Int. Conf. on the Hydrotransport of Solids in Pipes B.H.R.A. Cranfield, paper G2 (1970).

18. Gaessler, H.
Doctoral Dissertation, Technische Hochschule,
Karsruhe, W.Germany (1967)

19. Geskell, R.
"Horizontal Hydraulic Transport of coarse Mineral Solids"
Ph.D. Thesis Univ. Leeds, July 1979.

20. Govier, G.W. and Charles, M.E.
"The Hydraulics of the Pipeline Flow of Solid-Liquid Mixtures"
Engineering Journal, 44, 50, August (1961).

21. Govier, G.W. and Aziz, K.
"The Flow of Complex Mixtures in Pipes"
Van Nostrand Reinhold (1972)

22. Gilies, R.G., Hass, D.B., Small, M.H., Husband, W.H.W.
S.R.C. No. E.725-7.C-81 Sep. (1981)

23. Gandhi, R.L.
"An Overview of Slurry Pipelines"
J. of Pipelines 3, 1-11 (1982)

24. Hass, D.B., Husband, W.H.W. and Shook, C.A.
"The Development of Hydraulic Transport of Large Sized Coal in Canada - Phase I"
Hydrotransport 5, 5th International Conf. on the Hydraulic Transport of Solids in Pipes, May 1978.

25. Hubbell, J.H.
Photon Cross-Section Attenuation Coefficients and Energy Absoprtion Coefficients from 10 kev to 100 Gev.
Nat. Stand Ref. Data Syst. Nat. Bur. Stand. 29, Washington (1969).

26. Hayden, J.W. and Stelson, T.E,
"Hydraulic Conveyance of Solids by Pipes"
Symp. of Solid-Liquid Flow in Pipes, Univ. Pennsylvania Ed. I.Zandi, pp.148-63 (1968).

27. Justin, T. Long,
"Engineering for Nuclear Fluid Reprocessing"
Gordon and Breach, 1967.

28. Kazanskij, I., Brahl, H. and Hinsch, J.
"Influence of Added Fine Particles on the Flow Structure and the Pressure Losses in Sand-Water Mixtures"
Hydrotransport 3, 3rd Int. Conf. on the Hydraulic Transport of Solids in Pipes, May 1974.

29. Massey, B.S.,
"Mechanics of Fluids"
D. Van Nostrand Company Limited, London, p.295 (1968)

30. Newitt, D.M., Richardson, J.F., Abbot, M. and Turtle, R.B.
"Hydraulic Conveying of Solids in Horizontal Pipes"
Trans. Instn. Chem. Engrs., Vol. 33, 93 (1955)

31. Newitt, D.M., Richardson, J.F., Shook, C.A.
"Hydraulic Conveying of Solids in Horizontal Pipes, Part II: Distribution of the Particles and Slip Velocity"
Proc. of the Symp. on the Interaction Between Fluids and Particles Instn. Chem Eng. London P.87, 1962.

32. Motamedi, F.
"Interface Traction of Coal Particles"
M.Sc. Thesis Univ. London, 1985

33. Parzonka, W., Kenchington, J.M., and Charles, M.E.
"Hydrotransport of Solids in Horizontal Pipes: Effects of Solids Concentration and Particle Size on the Deposit Velocity"
Can. J. of Chem. Eng. Vol. 59, June 1981.

34. Pertuit, P., Tennant, J.D., Lawler, H.L. and Cowper, N.T.
"Application of Stabilised Slurry Concepts of Pipeline Transportation of Large Pa;rticles of Coal"
Prec. 3rd Int. Tech. Copnf. on Slurry Transportation 29-31, Las Vegas, ppl64-176, March 1978.

35. Richardson, J.F., and Zaki, W.N.
"The Sedimentation of a Suspension of Uniform Spheres under Conditions of Viscous Flow".
Chem. Eng. Sci., V.3, p.65 (1954)

36. Rose, H.E., and Duckworth, R.A.
"The Transport of Solid Pa;rticles in Liquids and Gasses"
The Engineer, 227, 392 (1969)

37. Shook, C.A. and Daniel, S.M.
"Flow of Suspensions of Solids in Pipelines, Part I, Flow with a Stable Stationary Deposit"
Can. J. Chem. Eng., 43, 56 (1965)

38. Shook, C.A. and Daniel, S.M.
"A Variable Density Model on the Pipeline Flow of Suspension"
Can. J. Chem. Eng., 47, 196 (1969)

39. Spells, K.E.
"Correlations for Use in Transport of Aqueous Suspensions of Fine Solids Through Pipes"
Trans. Inst. Chem. Engrs, London, Vol.33, P.79 (1955)

40. Televantos, Y.
"The Flow Mechanism of Hydraulic Conveying at High Solids Concentrations"
Ph.D. Thesis Univ. London, 1977

41. Televantos, Y., Shook, C.A., Carleton, A., Streat, M.
"Flow of Slurries of Coarse Particles at High Solids Concentration."
Can. J. Chem. Eng., 57 255-262, June 1979.

42. Thomas, A.D.
"A Rational Design Philosophy for Long Distance Slurry Pipeline"
The Trans. of the Instn. of Engineers, Aust p.22-23 (1977)

43. Thomas, A.D.
"Coarse Particles in a Heavy Medium Turbulent Pressure Drop Reduction and Deposition under Laminar Flow"
Proc. 5th Int. Conf. on the Hydraulic Transport of Solids in Pipes, May 8-11 (1978), Hannover, Paper D5.

44. Wilson, K.C., Streat, M., and Bantin, R.A.
"Slip-Model Correlation of Dense Two-Phase Flow"
Proc. Hydratransport 2, B.H.R.A., Paper B1 (1972)

45. Wilson, K.C., and Watt, W.E.
"Influence of Particle Diameter on the Turbulent Support of Solids in Pipeline Flow"
Proc. Hydrotransport 3, B.H.R.A., Paper D1 (1974)

46. Wilson, K.C.
"A Unified Physically-Based Analysis of Solid-Liquid Pipeline Flow"
Proc. Hydrotransport 4, B.H.R.A., Paper A1 ;(1976)

47. Wilson, K.C.
"Analysis of Contact-Load Distribution and Application to Deposition Limit in Horizontal Pipes"
J. of Pipeline, 4 (1984) 171-176.

48. Wilson, K.C., Clift, R., Addie, G.R. and Carstens, M.R.
"A Mechanistically-Based Method for Scaling Pipeline Tests for Settling Slurries"
Proc. Hydrotransport 8, B.H.R.A., Paper B1, p.91-101 (1982)

49. Wilson, K.C.
"A Formula for the Velocity Required to Initiate Particle Suspension in Pipeline Flow"
Proc. Hydrotransport 2, Paper E2, B.H.R.A., (1972)

50. Yalin, M.S.
"Mechanics of Sediment Transport"
Pergaman Press (1972)

51. Zandi, I., and Govates, G.
"Heterogeneous Flow of Solids in Pipelilnes"
Proc. A.S.C.E. J. of the Hydraulic, 93, 145 (1967)

52. Zenz, F.A., Othmer, D.F.
Fluidization and Fluid-Particle Systems"
Reinhold Pub. Corp., New York (1960)

A P P E N D I X A

APPENDIX A

A.I Calibration of Gamma Ray Density Gauge

A gamma ray density gauge was used to measure in-line solid concentration in the pipeline.

The theory and procedure is explained in detail in section 4.2.3. the calibration is a relationship between volumetric in-line concentration and Ln (I_s/I_E) / Ln (I_w/I_E). The calibration reading for coal using the horizontal gauge are plotted in Figure 4.4.

The output value of the count-rate in 100 second integration time for an empty pipe (I_E) and a pipe full of water (I_w) were:-

I_E = 767070

I_w = 499215

The long integration time reduces an error due to the fluctuation of the computer Analogue Digital Convertor (ADC).

A.II Pressure Transducers

The calibration procedure is explained in section 4.2.2. and the calibration apparatus is given in Figure 4.4.

The output from each transducer is converted into a digital value via an ADC and BBC computer. This value is then multiplied by 1.8 volts and divided by 65536 to give an output in volts. The final value is an average of ten readings taken over each 10 mseconds and the one having a standard deviation less than 0.002 is accepted for experimental analysis. The calibration is a relationship between this value and the pressure

drop (in mm Hg) for each transducer.

The reading and result for the horizontal transducer is plotted in Figure A.I.

Hydraulic gradient (m water/m pipeline) for each section is calculated by multiplying the pressure drop value by 13.602 E-3 and dividing by the length of the pipe section, in this case length of the horizontal section = 4.253m.

The computer ADC gives a fluctuation of 128 digit equivalent to error of 128 x 1.8/65536 = $\pm$0.003 in every analogue reading.

The horizontal transducer was found to give a linear voltage output with differential pressure. A linear regression line was fitted to the data as follows:

for horizontal line

$$P = 148.933\ AV + 3.253$$

where,

P = differential pressure in mm Hg

AV = average of 10 readings taken over each second times 1.8/65536.

A.III Calibration of the Magnetic Flowmeter

The flow meter was used to measure the mean slurry velocity during a run. The calibration procedure is explained in section 4.2.1.

The calibration is given by a relationship between the volumetric flow rate (m/s) and the average of 10 readings taken over one sec. The

final calibration equation is:

Flow Rate (m/s) = 3.3133E-6 x (Average number of pulses)

The mean velocity was calculated from:

Velocity U_m = Flow Rate/Cross section area of pipe.

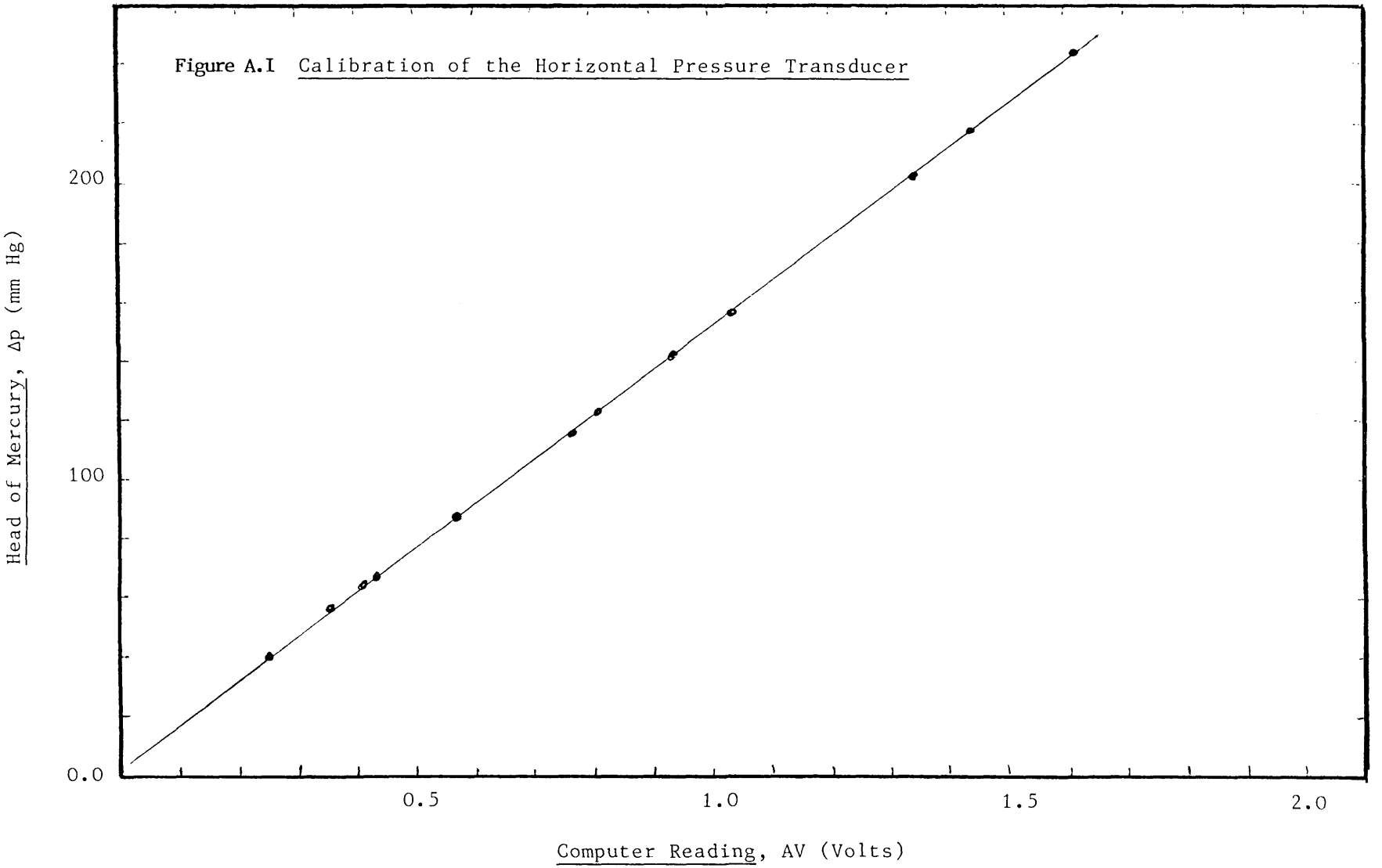

Figure A.I Calibration of the Horizontal Pressure Transducer

A P P E N D I X B

APPENDIX B

B.I Terminal Settling Velocity

The hindered terminal velocity of each coal size is determined experimentally. Settling tests were performed by allowing a spray of particles to fall a distance of 2m in a vertical 80mm diameter QVF glass column containing distilled water. The time taken for the front and tail ends of the sample of particles to settle was measured. This procedure was carried out several times. The average hindered terminal velocity of each coal size is given on Table B.I.

It was felt that these tests were unsatisfactory. The hindered settling velocity was therefore also determined from theory using the Galileo number:

$$Ga = d^3 \rho(\rho_s - \rho)g/\mu^2$$

The free settling velocity, U_t of a spherical particle is given by:

$$Ga = 18Reo \qquad Ga<3.6$$

$$GA = 18Reo + 2.7Reo^{1.887} \qquad 3.6<Ga<10^5$$

$$Ga = 1/3(Reo)^2 \qquad 10^5<Ga$$

where Reo is the Reynolds number based on the particle diameter.

$$Reo = \frac{U_t \rho d}{\mu}$$

Therefore U_t can be determined using the equivalent diameter of the particles.

Hindered settling velocity, U'_t, can be obtained by the Richardson and Zaki (35) method. They showed that

$$U'_t = U_t \ (1 - C_s)^{\alpha}$$

where for

Reo<0.2	$\alpha = 4.6$
0.2<Reo<1	$\alpha = 4.4Reo^{-0.03}$
1<Reo<500	$\alpha = 4.4Reo^{-0.1}$
500<Reo	$\alpha = 2.4$

The hindered settling velocities calculated using the Richardson and Zaki (35) method are shown in Table B.I.

The values of U'_t calculated by the Richardson and Zaki (35) method were used throughout the calculations.

B.II Free and Packed Settled Concentration

The loosest packing arrangement of particles under static conditions is known as the free settled concentration and the maximum packing arrangement of the particles is known as a packed settled concentration.

The free settled concentration was measured by placing a known weight of coal particles in a 25mm diameter measuring cylinder filled with water and closed at one end. The cylinder containing coal-water was turned up-side down and then the coal slurry was allowed to settle. The packed settled concentration was determined by vibrating this loose column of solids until no further packing could be achieved. This

procedure was carried out several times for each coal size and the averaged values are given in Table B.II.

B.III Frictional Properties of Coal Particles

The angle of repose, angle of wall friction and angle of internal friction were determined for coal particles.

Motamedi (32) has measured the angle of repose and angle of wall friction for coal particles of size 1-3.0mm. Values of 37^{o}-38^{o} and 30^{o} were reported respectively.

The value of angle of internal friction ϕ has been calculated using the correlation given by Airey (52).

$$\tan \phi = l + \sqrt{l \left(\frac{1 + l^2}{l + l'} \right)}$$

where l = tangent of the angle of repose

l' = tangent of the angle of wall friction.

This ϕ value is calculated to be 59.4^{o}.

Table B.I Calculated and Experimental Hindered Settling Velocity

Coal Sample	C_s	d_{50} mm	U_t Using Ga Number m/s	U'_t Using Richardson and Zaki m/s	U'_t Experimentally Determined m/s
Coarse	0.27	3.25	0.177	0.083	0.123
Mixed	0.39	1.9	0.095	0.026	0.117
Fine	0.36	0.975	0.053	0.014	0.058

TABLE B. II

Physical Properties of the Coal

Coal Sample	Mean Particle Diameter d_{50}	Particle Density	Solid Concentration		Hindered Settling Velocity (ms^{-1})	Coefficient of Sliding Friction
			Free Settled	Pack Settled		
Fine	0.975	1.325	43	52	0.014	0.48
Mixed	1.9	1.325	47	54	0.026	0.39
Coarse	3.25	1.325	42	48.5	0.083	0.42

(Density and Viscosity of Water at 20°C; $\rho_f = 998.2\ kg/m^3$, $\mu_f = 1.002 \times 10^{-3}\ Nsm^{-2}$)

APPENDIX C

APPENDIX C

C.I Computational Procedure used to Predict i_m for the Basic Two-Layer Model

The following iterative procedure was used in order to predict the pressure gradient, i_m, lower layer concentration, C_2, and the two-layer interface, β.

1. The physical properties of the carrier fluid and the coal are given in Appendix B.

2. The mean slurry velocity, mean particle diameter (d_{50}), mean delivered and mean in-situ solid concentration were taken as a mean input variable.

3. Using an assumed value of β the areas, A, A_1, and A_2 and wetted perimeters, S_1, S_{12} and S_2 were computed by using equations 5.1 through 5.6.

4. Knowing the value of in-situ solid concentration, C_s, the actual bed concentration, C_2, could be calculated from $C_2 = AC_s/A_2$.

5. Giving the first estimate of C_b as C_2, with a knowledge of the mean slurry velocity U_m, the mean velocity of each layer, U_1, U_2 could be calculated. This enables the shear stresses for the fluid and the particles for each layer to be calculated.

6. Between equation 5.26 and 5.27 pressure gradient term can be eliminated. Using equation 5.29 and 5.30 the value of the drag

force on the fluid by the particle, FFP, can be obtained from

$$FFP = \tau_{f2}\ S_2\ C_2/A_2 + \tau_{12}\ .\ C_2\ .\ S_{12}/A_2 - \tau_{s2}\ (1-C_2)\ S_2/A_2$$

on the other hand FFP can also be calculated from Ergun Equation.

Using relative velocity in the Ergun equation and rearrange it, it will give the following quadratic equation

$$Y\ U_r^2 + X\ U_r + FFP = 0$$

where

$$Y = \frac{1.75\ C_2\ \rho}{d\ (1-C_2)^3}$$

$$X = \frac{150\ C_2^2\ \mu}{d^2\ (1-C_2)^3}$$

Knowing the value of FFP the relative velocity can be calculated from the answer to the quadratic equation.

8. Bed concentration, C_b, can also be computed from

$$C_b = C_2 - (1-C_2)\ U_r\ C_2/\ U_2$$

9. Steps 4 to 8 were repeated for the convergence of C_b.

10. The value of pressure gradient, i_m, was calculated from the two force balances equations 5.12 and 5.13. Unless the chosen value of β is correct the difference in numerical value of these pressure gradients will not be equal to zero.

11. So steps 3 to 10 were repeated with new value of β until convergence was achieved for pressure gradients.

12. The overall iterative calculation was carried out for a new value of C_s and C_d and U_m. A BBC microcomputer was used for convenience and speed.

C.II Computational Procedure used to Predict i_m and C_1 for the Derived Model

The whole procedure is the same as section C.I except equations 5.7 and 5.10 are replaced by 5.35 and 5.36 and fluid shear stress for each layer are the function of their mixture density ρ_{m1} and ρ_{m2}.

Finally step 4 is replaced by 4a and 4b as follows:

4a The value of C_2 is independently measured and is equal to loose packed concentration of each coal sample. This is given in Appendix B.

4b As long as A_2 is more than or equal to AC_s/C_2 there will be no suspended particles meaning that $C_1=0$ and when A_2 is less than AC_s/C_2 the value of C_1 can be calculated from

$$C_1 = \frac{AC_s - A_2C_2}{A_1}$$

C.III Computational Procedure used to Predict i_m using Doron et al (12) Two-Layer Model

The following iterative procedure was carried out in order to predict the pressure gradient, i_m, upper layer concentration, C_1, upper layer and lower layer velocities, U_1 and U_2, and the bed depth, y_2.

1. The physical properties of the carrier fluid and the coal particles are given in Appendix B.

2. The mean slurry velocity, mean particle diameter, mean in-situ and packed solid concentration and particle hindered settling velocity were taken as a mean input variables.

3. Using an assumed value of bed dpeth, y_2, the areas, A, A_1, A_2 and perimeters, S_1, S_{12} and S_2 were computed.

4. Using an assumed value of upper layer velocity, U_1, and using a numerical analysis (Simpson rule) for calculation of C_1 from equation 6.13, the mean velocity for each layer can be calculated. This enables the shear stresses for the fluid and the particles for each layer to be calculated.

5. The value of hydraulic gradient, i_m, was calculated from equations 6.9 and 6.10 unless the chosen value of y_2 is correct the difference in the numerical value of these hydraulic gradient will not be equal to zero.

6. So step 3 to 5 were repeated with new value of y_2 until convergence was achieved for the pressure gradients.

7. The overall iterative calculations were carried out for a new value of U_m and C_s. A BBC microcomputer was used for convenience and speed.